PERFORMANCE ANALYSIS OF EVACUATED TUBE COLLECTOR AUGMENTED DOUBLE SLOPE SOLAR DISTILLER UNDER FORCED MODE

A DISSERTATION

SUBMITTED IN PARTIAL FULFILLMENT OF THE REQUIREMENTS
FOR THE AWARD OF THE DEGREE OF

MASTER OF TECHNOLOGY
(Thermal Engineering)

SUBMITTED BY
ASEEM DUBEY
2K18/THE/20

SUPERVISOR
Dr. Akhilesh Arora
Associate Professor

DEPARTMENT OF MECHANICAL ENGINEERING
DELHI TECHNOLOGICAL UNIVERSITY
Govt. of NCT of Delhi
Shahbad Daulatpur, Bawana Road, Delhi-110042

JULY 2020

DECLARATION

I hereby declare that the work which is being presented in the M. Tech dissertation entitled **"Performance analysis of Evacuated Tube Collector augmented double slope solar distiller under forced mode"** in partial fulfilment of the requirements for the award of the **Master of Technology in Thermal Engineering** and submitted to the Department of Mechanical Engineering of Delhi Technological University, Delhi is an authentic record of my work carried out during a period of 4th semester under the supervision of **Dr. Akhilesh Arora, Associate Professor, Department of Mechanical Engineering, Delhi Technological University.** The matter presented in this Project report has not been submitted by me for the award of any other degree elsewhere.

Aseem Dubey

2K18/THE/20

M. Tech (Thermal Engineering)

Department of Mechanical Engineering

Delhi Technological University

Delhi-110042, India

CERTIFICATE

I hereby certify that the Project Dissertation titled **"Performance analysis of Evacuated Tube Collector augmented double slope solar distiller under forced mode"** which is submitted by Aseem Dubey, 2K18/THE/20, Department of Mechanical Engineering, Delhi Technological University, Delhi in partial fulfilment of the requirement for the award of the degree of Master of Technology, is a record of the project work carried out by the student under my supervision. To the best of my knowledge this work has not been submitted in part or full for any Degree or Diploma to this University or elsewhere.

Place: Delhi

Date:

Dr. Akhilesh Arora

SUPERVISOR

Associate Professor

Department of Mechanical Engineering

Delhi Technological University, Delhi

ACKNOWLEDGEMENTS

I would like to place on record my deep sense of gratitude to my mentor and advisor Dr. Akhilesh Arora, Associate Professor, Department of Mechanical Engineering, Delhi Technological University for his patience, generous guidance, help, usual suggestions and continuous encouragement throughout the course of present work and for enlightening me with his immense knowledge of the subject. His cooperation and support during the entire research work were one of the main reasons I could complete this thesis with a satisfactory conclusion.

I also wish to extend my thanks to the Head of the Department of Mechanical Engineering, Prof Vipin for his regular academic discussion, encouragement, and help from time to time.

I am fortunate enough to get constant support and assistance from all the teaching as well as non-teaching staff of the Department of Mechanical Engineering which helped me in successfully completing my project work.

I owe my profound gratitude to my parents, who have been a consistent source of inspiration for me. Their love, affection, and blessings made this work possible and assisted me greatly. Finally, yet importantly I would like to extend my earnest thanks to my colleagues, for their insightful comments and constructive suggestions to improve the quality of this project work.

Aseem Dubey

ABSTRACT

It is a well-known fact that, at present, one of the foremost challenges in front of the entire world is to obtain fresh water from the natural resources of water to meet the increasing demand for freshwater for domestic as well as industrial use. The scarcity score of water is ranked high (R > 0.422) among all the Middle Eastern countries, China, Pakistan, South Africa, etc. including India. To explore the potable water, the population in these areas have to travel long, especially during summer. It is expected that by 2050, worldwide potable water demand may increase more than twice including higher energy use (20-50%) than at present ~ 350 EJ/year. India is a tropical country with about 16% of the combined population of the world, having only 4% of pure water availability with scarcity already apparent in many regions, leading to challenges for the survival of Biota. This may exaggerate further with expected population growth to 1.6 billion at the end of 2050.

The water available from rivers, lakes, and underground reservoirs contain a large number of micro-organisms which may cause health hazard to human beings. However, the available water, after distillation, may be used for domestic and industrial use. The conventional methods for distillation exist, they are energy-intensive techniques and require fast depleting sources of energy. In such circumstances, solar energy, which is the oldest form of energy available to mankind and is abundant in nature, provides the best alternative to obtain fresh water by the use of solar still.

The rate of distillate obtained from solar stills mainly depends on the operating temperature and shape and material of condensing cover. It is to be noted that the primary aim of most of the research work done in the field of solar distillation is to increase the yield of the distiller unit, which can be attained by maximizing the temperature difference between water

and the condensing cover. Hence the design parameters should be employed efficiently to attain the above-mentioned aim. Intensity and temperature are interrelated to each other. Higher intensity leads to high temperature inside the solar still and hence results in the higher temperature of water in it. It is essential that the solar radiations falling on solar still should contribute towards the enhancement of temperature of the water, especially during winter months. Temperature is the most critical climatic factor during winter.

The aim of most of the research work carried out in the field of solar distillation is to increase the yield. This can be achieved either by increasing the water temperature or by increasing the difference between water and glass cover temperature or by both. The higher water temperature can be obtained by feeding the additional thermal energy to the basin water after pre-heating it externally in the collector. Therefore, a new approach has been employed by designing a modified geometry, coupling double slope solar still with ETC in force mode. The force mode operation has various merits associated with it compared to the natural mode of operation. As per the literature survey, the performance investigation of ETC integrated double slope solar still has not been carried out. The objective of the present work is to develop a thermal model for the proposed geometry of solar still and carry out the numerical simulation to optimize the flow rate and water depth for the number of tubes connected in parallel. The effect of the diffused reflector has also been considered. Further, the performance of the system has been investigated for the water temperature attainable below the boiling point at an optimum flow rate. The effect of water depth in the basin on the output such as yield, energy efficiency, and exergy efficiency has also been investigated. Finally, the annual performance of the present design of solar still has been estimated and compared with the other designs reported in the open literature. The performance of the proposed model of solar still is found superior compared to other designs in terms of output per m^2 of surface area. At optimal flow rate, system yields 6.644 kg using 10 tubes at 0.005 m water depth.

TABLE OF CONTENTS

LIST OF FIGURES

LIST OF TABLES

NOMENCLATURE

a'	Collector efficiency factor ($Wm^{-2}K^{-1}$)
A_b	Half basin area (m^2)
A_{CT}	Area of collector receiving solar radiation.
A_g	Condensing cover area (m^2)
A_t	Tube surface area (m^2)
c_w	Water specific heat ($Jkg^{-1}K^{-1}$)
d_t	Outer diameter of tube (m)
CD	Center distance between two consecutive tubes (m)
CPL	Cost of one liter/kg of distillate (Rs. kg^{-1})
CC_Y	Carbon credit (Rs)
CF	Cash flow (Rs)
E_{in}	Embodied energy (kWh)
$E_{in,\ solar}$	Input solar energy (kWh)
E_{out}	Output energy (kWh)
EPF	Energy production factor
$\dot{Ex}$	Exergy transfer rate (W)
η_{EX}	Exergy efficiency (%)
h_{ba}	Overall h.t.c. basin to air ($Wm^{-2}K^{-1}$)
h_{bw}	Convective h.t.c. basin to water ($Wm^{-2}K^{-1}$)
h_{1w}	Total h.t.c. water to the condensing cover ($Wm^{-2}K^{-1}$)
h_{kg}	Conductive h.t.c. of condensing cover ($Wm^{-2}K^{-1}$)

h_{cw}/h_{cwg}	Convective h.t.c. water to condensing cover ($Wm^{-2}K^{-1}$)
h_{ew}/h_{ewg}	Evaporative h.t.c. water to condensing cover ($Wm^{-2}K^{-1}$)
h_{rw}/h_{rwg}	Radiative h.t.c. water to condensing cover ($Wm^{-2}K^{-1}$)
$h_{1g,\,E}$	Overall h.l.c. from east side condensing cover ($Wm^{-2}K^{-1}$)
$h_{1g,\,W}$	Overall h.l.c. from west side condensing cover ($Wm^{-2}K^{-1}$)
h_{tw}	h.t.c. tube to water ($Wm^{-2}K^{-1}$)
h_{ta}	h.l.c. tube to ambient ($Wm^{-2}K^{-1}$)
i	Interest rate
$\dot{I}$	Irreversibility rate during day time (W)
I_c (t)	Radiation over tubes (Wm^{-2})
I_E(t)	Radiation over the east condensing cover (Wm^{-2})
I_W(t)	Radiation over the west condensing cover (Wm^{-2})
K_b	Conductivity of FRP ($Wm^{-1}K^{-1}$)
L_t	Tube length
L	Latent heat (Jkg^{-1})
l_b	Thickness of solar still body
l_g	Condensing cover thickness
LCCE	Life cycle conversion efficiency (%)
$\dot{m}$	Flow rate (kgs^{-1})
M	Maintenance cost
$M_{ew,T}$	Hourly distillate yields (kgm^{-2} day^{-1})
$M_{ew,E}$	Hourly yield from east side (kgm^{-2} day^{-1})
$M_{ew,W}$	Hourly yield from west side (kgm^{-2} day^{-1})

M_{sw}	Water mass in solar still (kg)
M_{cw}	Water mass in tubes
M_Y	Annual yield (kg)
n_p	Payback time (years)
N_c	Number of ETC tubes
$p_{gi,\,E}$	Partial pressure of vapour at east side condensing cover (Pascal)
$p_{gi,\,W}$	Partial pr. of vapour at west side condensing cover (Pascal)
p_W/p_{sw}	Partial pr. of vapour at the surface of water (Pascal)
$\dot{q}_{uc}$	Energy input to solar still from ETC (W)
S_p	Selling price (Rs. kg^{-1})
t	Time (second)
T_a	Temperature of ambient (^oC)
T_b	Temperature of liner (^oC)
T_{cw}	Water temperature in the tube (^oC)
T_{gi}	Inner surface temperature of condensing cover (^oC)
T_{go}	Outer surface temperature of condensing cover (^oC)
T_{sw}	Water temperature in the basin (^oC)
UA_{net}	Annualized cost (Rs)
V_a	Wind speed (ms^{-1})

Greek symbols

α_b	Basin liner absorptivity
α_g	Absorptivity of condensing cover
α_w	Absorptivity of water

α'_{eff}	Effective absorptance–transmittance
ε_g	Emissivity of glass
ε_w	Emissivity of water
ε_{eff}	Effective emissivity
σ	Stephan - Boltzmann constant ($Wm^{-2}\ K^{-4}$)
η_{ic}	Energy efficiency of ETC
η_{is}	Energy efficiency of system
ρ_r	Reflectivity of reflector plate
γ	Intercept factor of absorber tube for reflected radiation

Subscripts

a	Ambient
b	Basin
c	Collector
g	Glass
i	Initial
w	Water
acm	Accumulated
cwi	Input point to collector
h.t.c.	Heat transfer coefficient
h.l.c.	Heat loss coefficient
osp	Outside re-circulating pipe connected to solar still

Chapter-I

General Introduction

1.1 Introduction

Water is the most abundant and important substance in nature. It is the principal component of life, health, and sanitation. More than two-thirds of the earth's surface is covered with water. A major fraction of the available water is either present as seawater or icebergs in the Polar regions. More than 97 % of the earth's water is salty; rest around 2.6% is freshwater. Less than 1% of freshwater is within human reach. The availability of potable water to meet human needs is limited worldwide and its scarcity seems most prevalent, particularly in the belt of arid regions. Scarcity scores of water are ranked high (R > 0.422) among all the Middle Eastern countries, China, Pakistan, South Africa, etc. including India [1]. To explore the potable water, the population in these areas have to travel long, especially during summer. The reports of WHO (2017), mention that about 2.1 billion humans worldwide have an inadequacy of safe water and remote arid regions are highly water-stressed and facing scarcity. Richey et al. [2] reported that globally out of 37 large aquifers, 21 possesses the scarcity of water and will worsen soon with an increase in population. Worldwide, about 80 countries have a scarcity of pure water, especially in the belt of the southern Mediterranean [3]. However, less energy-intensive plants utilize renewable energy sources to provide potable water for water-stressed

areas (MENA) and Pacific Asia. It is expected that by 2050, worldwide potable water demand may increase more than twice including higher energy use (20%-50%) than at present ~ 350 EJ/year [4]. India is a tropical country with about 16% of the combined population of the world, having only 4% of pure water availability with scarcity already apparent in many regions, leading to challenges for the survival of Biota. This may exaggerate further with expected population growth to 1.6 billion at the end of 2050. Inter-dependence of potable water and energy necessitates a requirement of self-sustainable technology to meet the need. The use of solar energy is an alternative, self-sustainable source to distillate the brackish/saline water to meet the requirement in an eco-friendly manner of small communities located remotely (requirement is less than 200 m^3/day), using a device called solar still [5]. The use of solar still to purify water for the distant communities, in particular, can be a solution to reduce water stress.

As the available freshwater is fixed on earth and its demand is increasing day by day due to the increasing population, hence there is an essential and earnest need to get fresh water from the saline/brackish water present on or inside the earth. This process of getting fresh water from saline/brackish water can be done easily and economically by solar distillation.

According to World Health Organization (WHO), the permissible limit of salinity in water is 500 ppm and for special cases up to 1000 ppm while most of the water available on earth has the salinity level up to 10,000 ppm whereas seawater normally has a salinity in the range of 35,000-45,000 ppm in the form of total dissolved salts.

Excess brackishness causes the problem of taste, stomach problems, and laxative effects. One of the control measures includes the supply of water with total dissolved solids within permissible limits of 500 ppm or less. This is accomplished by several desalination methods like reverse osmosis, electrodialysis, vapor compression, multistage flash distillation, and solar distillation, which are used for purification of water, as shown in Table 1.1.

Table 1.1. Various desalination processes [6]

S. No	Phase-change/ Thermal processes	Single-phase/ Membrane processes
1.	Multi-stage flash (MSF)	Reverse osmosis (RO) • RO without energy recovery • RO with energy recovery (ER-RO)
2.	Multiple effect boiling (MEB)	Electrodialysis (ED)
3.	Vapour compression (VC)	
4.	Freezing	
5.	Humidification/dehumidification	
6.	Solar stills • Conventional stills • Special solar stills • Cascaded type solar stills • Wick-type solar stills • Multiple-wick-type stills	

Among these, the solar stills can be used as a desalination plant for such remote settlements where briny water is the only type of moisture available, power is scarce and demand is less than 200 m^3/day. On the other hand, the setting of water pipelines for such areas is uneconomical and delivery by truck is unreliable and expensive. Since other desalination plants are uneconomical for low-capacity freshwater demand, under these situations, solar stills are viewed as a means to attain self-reliance and ensure a regular supply of water.

The World Bank adopted a policy of water privatization and full-cost water pricing. This policy is causing great distress in many third world countries, which fear that their citizens will not be able to afford for-profit water. The blue planet project is an international effort begun by

the Canadian Council to protect the world's fresh water from the growing threats of trade and privatization. During March 16-22, 2000, activists from Canada and more than a dozen other countries met in Hague to oppose the trade and privatization agenda of the second world water forum and to kick start an international network to protect water as a common resource and a basic human right. This necessitated the different approaches in terms of economic and technological efforts to cope up with this problem.

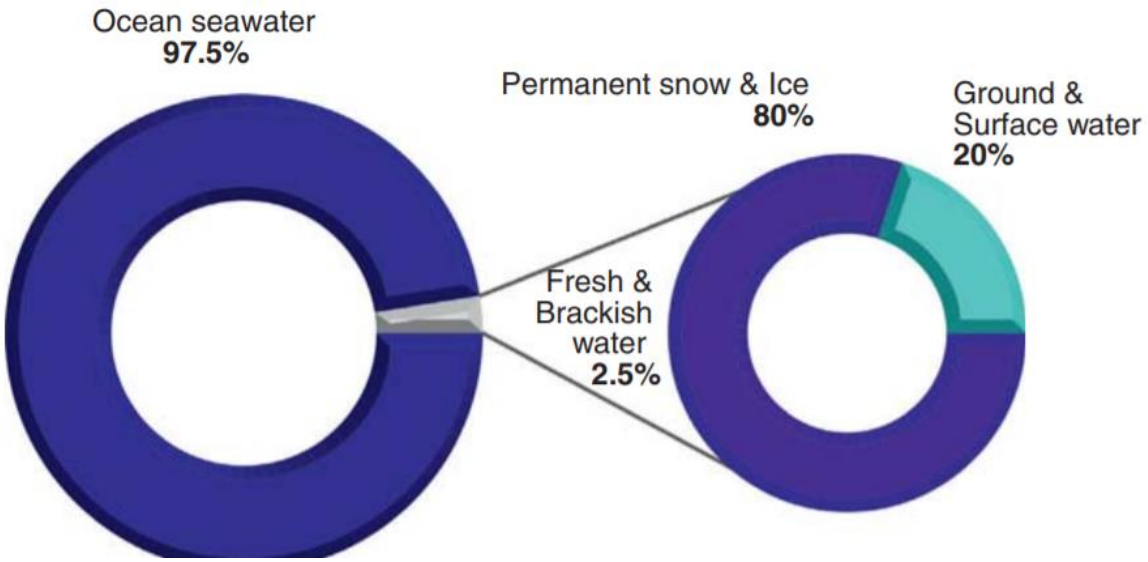

Fig. 1.1. Allocation of the world's water resources [7]

The allocation of the world's water is shown in Fig. 1.1. More than 97%, or about 1338 million km^3, of the world's water is seawater. Eighty percent of the remaining water is bound up as snow in permanent glaciers or as permafrost. Hence, only 0.5% of the world's water is readily available as low-salinity groundwater or in rivers or lakes for direct use by humans [7].

Some regions of the world are blessed with an abundance of freshwater. This includes areas with relatively low populations and easy access to surface waters, such as northern Russia, Scandinavia, central and southern coastal regions of South America, and northern North America [8]. More populated areas and areas with repaid industrialization are experiencing more water stress, particularly when located in arid regions.

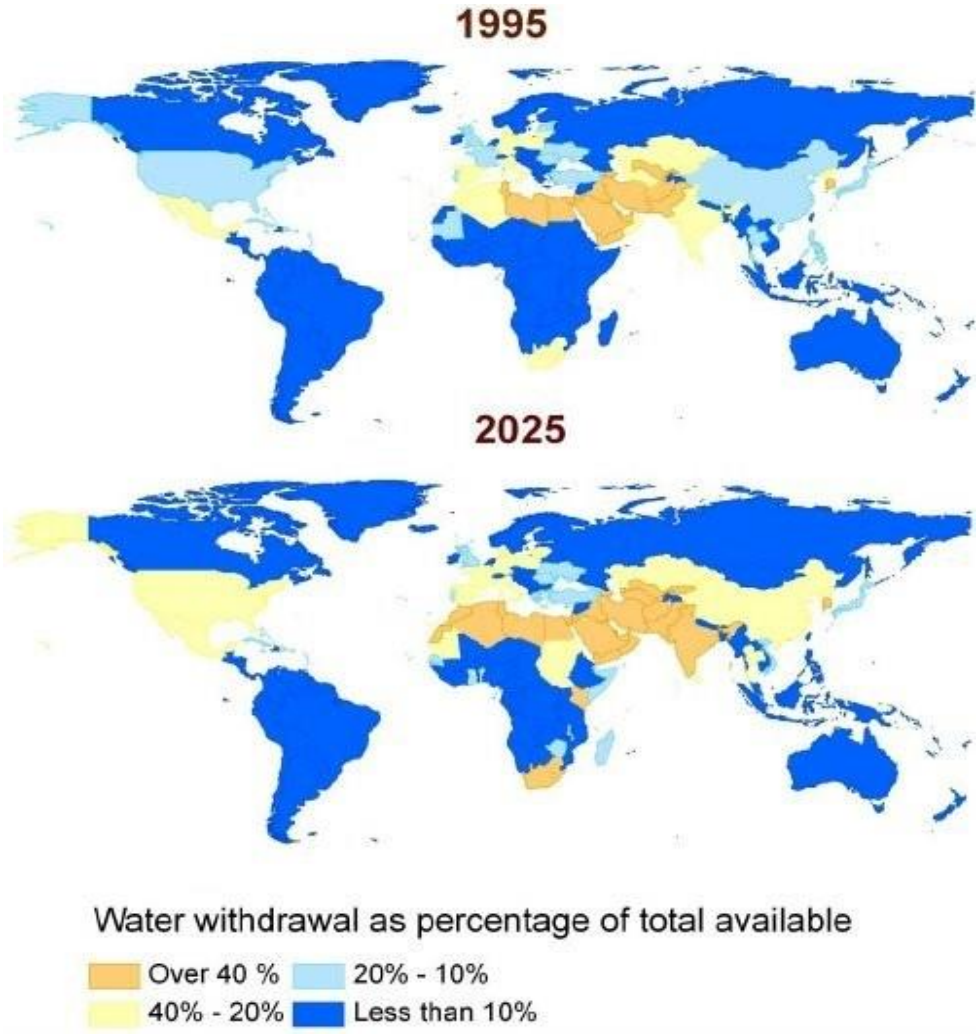

Fig. 1.2. Global water stress in 1995 and predicted for 2025 [9]

Fig. 1.2 compares the global water stress in 1995 with that predicted for 2025. The areas of the world that are not rich in water resources and that also experience un-stable and rapid population growth and industrialization will see water stress significantly increase in the future. As many as 2.8 billion people will face water stress or scarcity issues by 2025; by 2050, that number could reach 4 billion people. Water stressed areas will include the south-central United States, Eastern Europe, and Asia, while water scarcity will be experienced in the Southwestern United States; Northern, Southern, and Eastern Africa; the Middle East; and most of Asia [9].

In 2015, data received by the National Aeronautics and Space Administration (NASA)'s satellite revealed that out of 37 world's large aquifers, 21 are facing severely water-stressed [2]. With increasing population and increased demand from industry and agriculture, researchers indicate that calamity of pure drinkable water will become worsen soon. As per the reports of WHO and UNICEF [10], about 0.844 billion humans in the world have an inadequacy of fundamental drinking water service and 2.1 billion humans have an inadequacy of safely managed water.

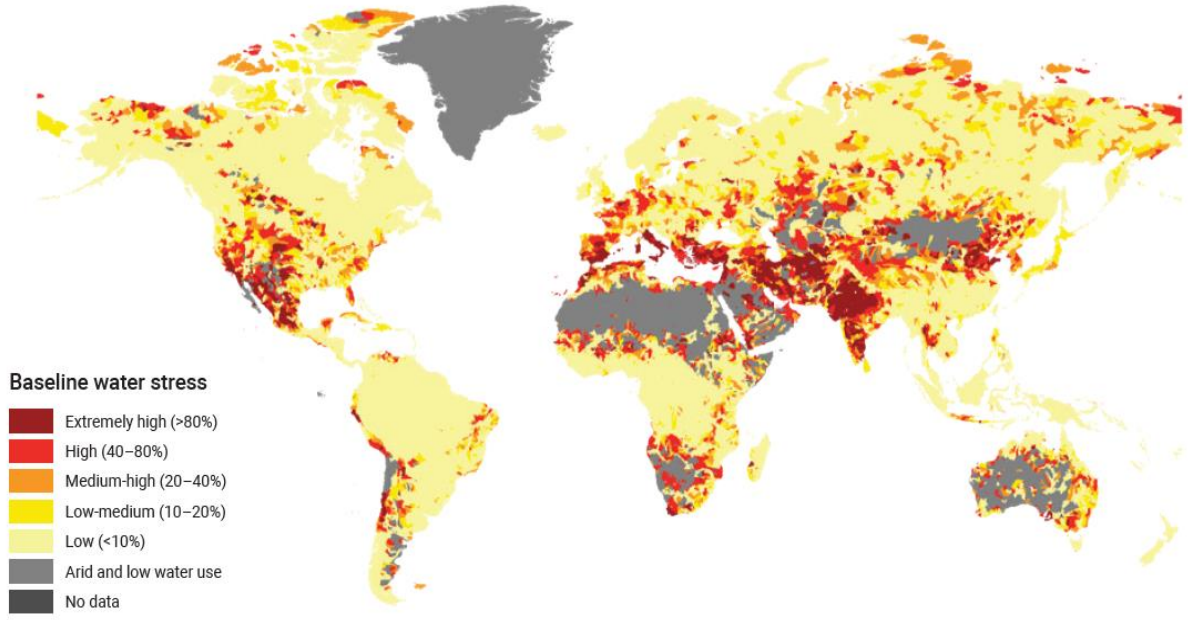

Fig. 1.3. Annual baseline water stress [11]

Fig. 1.3 shows the Water Stress Index 2019 that estimates current water stress by comparing water use to the available, renewable supply for regions around the world. Baseline water stress estimates the ratio of overall water withdrawals to available renewable water supplies. Water withdrawals include domestic, industrial, irrigation, and livestock consumptive use. Available renewable water supplies include surface and groundwater supplies and considers the impact of upstream consumptive water users [11].

Therefore, the worldwide challenge in the current era is the shortfall of safe, drinking water. Solar desalination may be the economic and effective technique for converting the brackish water into pure drinkable water.

1.1.1 Water Pollution

Human infectious diseases are among the most serious effects of water pollution, especially in developing countries, where sanitation may be inadequate or non-existent. Waterborne diseases occur when parasites or other disease-causing microorganisms are transmitted via contaminated water, particularly water contaminated by pathogens originating from excreta. These include typhoid, intestinal parasites, and most of the enteric and diarrheal diseases caused by bacteria, parasites, and viruses. Among the most serious parasitic diseases are amoebiasis, giardiasis, ascariasis, and hookworm. Some important issues arising due to water pollution are listed below [12]:

- 5 million people die every year due to water-related disease and out of this 84% are children in age group 0 - 14.
- Diarrhea is the main cause of 43% of water-related deaths.
- In the developing world, 98% of deaths are water-related.
- Poor people living in the slums often pay 5-10 times more per litre of water than wealthy people living in the same city.
- About 13.2 gallons of water per person is required daily for sanitation, bathing, and cooking needs, as well as for assuring survival.

1.1.2 Salinity of Water

The quality of groundwater has changed to an extent that the use of such water could be hazardous. An increase in overall salinity of the groundwater and/or presence of high

concentrations of fluoride, iron, nitrate, arsenic, total hardness, and few toxic metal ions have been noticed in large areas in several states of India.

Specific water quality problems include salinity (Total dissolved solids (TDS)), hardness value ($CaCO_3$), iron, zinc, manganese, fluorides, heavy metals, pH value, bacterial contamination, and pesticide/herbicide residues, etc. According to WHO guidelines [13] for drinking water quality, the water with a TDS level less than 500 ppm is generally considered safe for drinking and above 1000 ppm it becomes significantly objectionable to consume. In India, the water salinity consumption by people reaches to 1500 ppm. Most of the water available on earth as underground water has the salinity level up to 10,000 ppm. Seawater normally has a salinity in the range of 35,000-45,000 ppm in the form of total dissolved salts. India has about 53,000 habitations with salinity greater than 1500 mg/litre, most being in remote and arid areas with saline water. Salinity varies slightly from place to place around the world and varies somewhat with the seasons (affected by temperature and precipitation). The water of salinity between freshwater and seawater is called brackish.

1.2 Solar Distillation: A State of Art

The idea of saline water evaporation by using thermal energy and its subsequent condensation for freshwater production was empirically applied several centuries ago to simulate the atmospheric air humidification and dehumidification during the hydrologic cycle [14].

Many options (conventional and non-conventional) are available to distillate the brackish/saline water. Among all the non-conventional methods the most prominent method is the ‘solar distillation’ and is the oldest method to get the potable /distilled water by utilizing the solar energy which is an abundantly available natural resource in the world. Solar distillation of brackish water is an option to obtain fresh water for drinking, medicinal use, battery charging,

school, laboratories, etc. as it needs simple technology and low maintenance and it can be used anywhere with a lesser number of problems.

Solar Still is a perfect water distiller designed especially for remote areas or during power outages. Solar stills mimic the natural process when the water evaporates, it removes only pure water and leaves all contaminated behind. Solar Still was certified for arsenic removal by the National Sanitation Foundation (NSF). To use this free energy more efficiently, various solar distillation methods have been studied since the past to desalinate impure water. Swedish engineer Carlos Wilson in 1872 (worked till 1910) in Las Salinas, Chile built a plant of 64 basins (4,459 m^2) of capacity 20,000 liters /day. Based on the method of energy feed, solar distillation is broadly classified as passive distillation and active distillation with various designs reported [15-18].

1.3 Requirements for Solar Distillation

As long as the distiller is kept clean and working properly, the high quality of treated water will be very consistent regardless of the incoming water quality. The various favorable conditions for solar distillation are [19];

- Availability of salty/ brackish water if other sources are fully exploited.
- Total 3 m^3/ day or less water requirement.
- Availability of solar energy.
- Rainfall below 0.5m/year.
- High water transportation costs.
- Competing technologies that require expensive and/or unreliable supply of conventional fuel.

1.4 Advantages and Disadvantages of Solar Distillation

The major advantages and disadvantages of solar distillation are as follows [20]:

1.4.1 Advantages of Solar Distillation

- Solar distillation is a simple technology, eco-friendliness, the requirement of less skilled workers, low maintenance and low energy needs.
- It produces potable water.
- No prime movers are required to run the unit.
- Solar distillation also removes pathogens present in the water.
- Solar stills, operating on sea or brackish water, can ensure supplies of potable water.
- It can encourage cottage industries, animal husbandry, or hydroponics for food production in areas where such activities are now limited due to inadequate supplies of potable water.
- Solar distillation will permit settlement in sparsely - populated locations, thus relieving population pressures in urban areas.
- Operating cost is nearly zero and it is compact and lightweight.
- Approximately 90% feed water recovery.
- Investment is low.

1.4.2 Disadvantages of Solar Distillation

The main disadvantages of solar distillation are as follows:

- In solar distillation, a large surface area is required for the collection of solar energy.
- Distillate output mainly depends on climatic conditions.
- Difficult to transport mainly due to handling of the glass cover.
- Low daily distillate yield per m^2 of the basin area. (3 – 4 liter $day^{-1}m^{-2}$).
- Routine maintenance is required.

1.5 Factors Influencing the Performance of Solar Distillation

The effects of design and climatic parameters on solar still performance are given below:

1.5.1 Effects of Design Parameters

The design parameters of the solar still affect the performance of solar sill in the following ways:

(a) High water temperature.

Following design parameters affect the temperature of water in the solar still basin:

- Integration of collectors with the solar still basin
- High absorptivity of basin liner and collector plate
- Reducing thermal losses to ambient using good insulating materials
- High ambient temperature
- Low water depth

(b) Large temperature difference between evaporative and condensing surfaces.

The large temperature difference between the evaporative and condensing surfaces can be obtained as:

- Less absorptivity of the glass cover
- Rapid removal of heat from the outer glass cover by blowing of the wind or by other means

(c) Low vapour leakage.

- The basin of the distillation system is made watertight to avoid water leakage

1.5.2 Effects of Climatic Parameters

The climatic parameters affect the performance of solar still in the following ways:

- The higher convective heat loss from the glass surface can be achieved with the higher wind velocity and hence higher will be temperature difference between the evaporative and condensing surface.
- The output of solar still increases with the increase in the intensity of solar radiation.

1.6 Classification of Solar Distillation Systems

Depending upon the mode of operation, solar still can be classified as shown in Fig. 1.4.

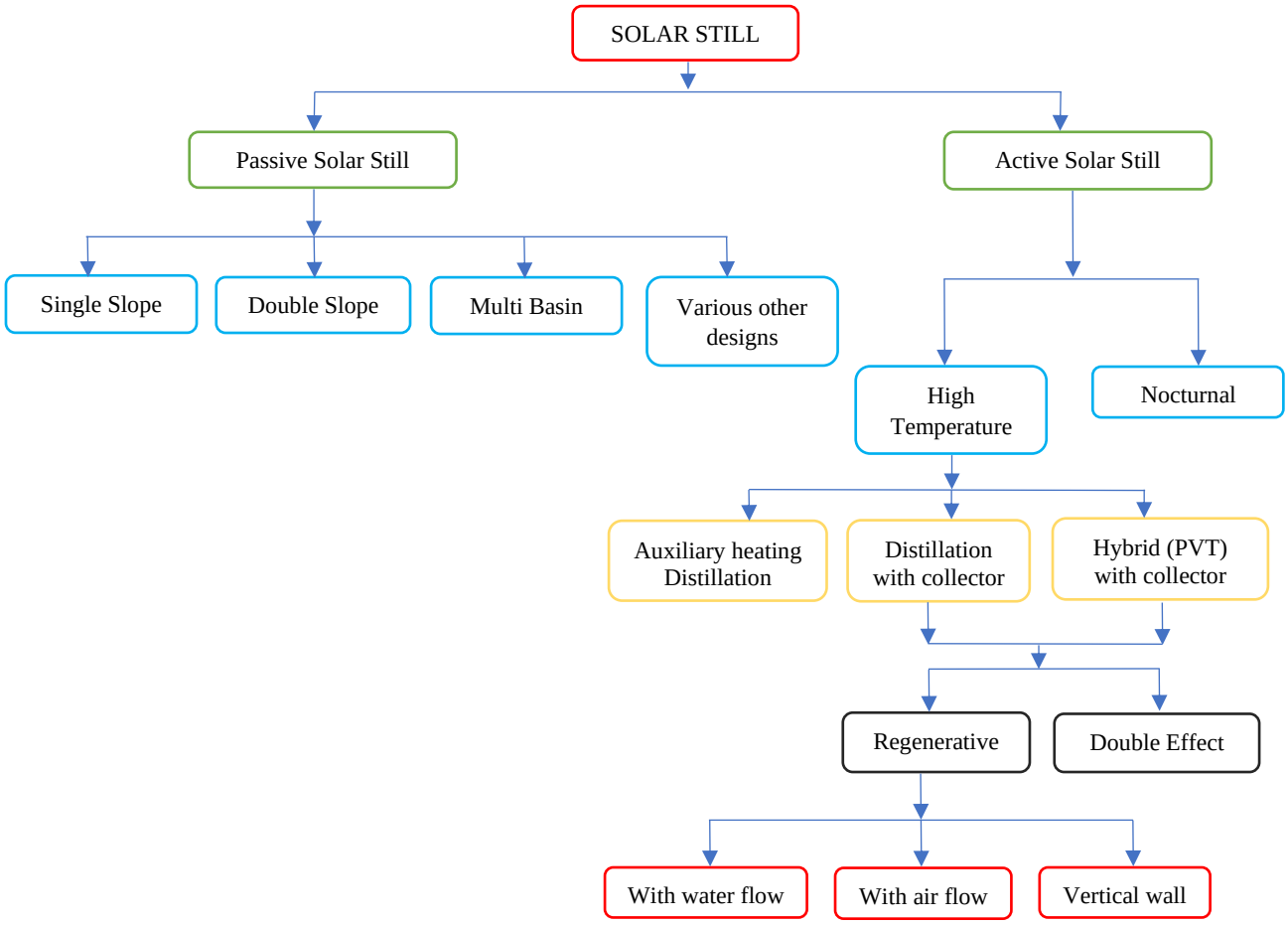

Fig. 1.4. Classification of solar distillation systems

1.6.1 Passive Solar Still

In this case, the water in the basin of the solar still is heated directly by solar radiation. Various researchers have carried out study on the passive solar still [21-24]. Most of the

researchers reported that passive solar still is a slow process of water evaporation and daily total yield is about 2.25 kg/m^2 day during summer. The operating range of temperature for a clear day and maximum solar radiation is in the range of 20ºC - 50ºC. A double slope passive solar still is shown in Fig. 1.5.

Fig. 1.5. Double slope passive solar still at I.I.T Delhi

1.6.2 Active Solar Still

The temperature of the basin water governs the evaporation rate in the solar still. The temperature of the basin water in the solar still can be heated both directly by solar radiation as well as indirectly (i.e. feeding hot water, available from solar collector or industries or power plant, etc.), and such system is known as active solar still. Double slope solar still in active mode is depicted in Fig. 1.6. The active solar distillation is mainly classified as follows:

(i) High-temperature distillation: Hot water will be fed into the basin from a solar collector/concentrator. The operating range of temperature is in the range of 50ºC - 100ºC and generally referred to as high operating distillation.

(ii) Nocturnal production: Water of the solar still is heated during the sunshine hours and most of the energy is stored in the water mass. This stored energy is then utilized for distillation during off sunshine hours.

Fig. 1.6. Double slope active solar still [25]

Various researchers have carried out study on solar distillation systems with a flat plate collector/concentrator [26-31] and using waste thermal energy from any chemical/industrial plant [32]. Tiwari et al. [33] developed the thermal model for active solar still coupled with different types of solar collectors and validated the theoretical values with experimental values for 0.05 m water depth. The study reported that solar still integrated with evacuated tube collector gives a maximum yield of 4.24 kg/m^{2}day, among all other types of solar still.

1.7 Heat Transfer in Solar Still

There are two types of heat transfer in solar distillation systems as detailed in Fig. 1.7.

1.7.1 Internal Heat Transfer

The internal heat transfer within the solar still from the water surface to the inner surface of the condensing cover consists of radiation ($\dot{q}_{rw}$), convection ($\dot{q}_{cw}$) and evaporation ($\dot{q}_{ew}$). The internal heat transfer mainly governs the transport phenomena of water vapour formed above the water surface.

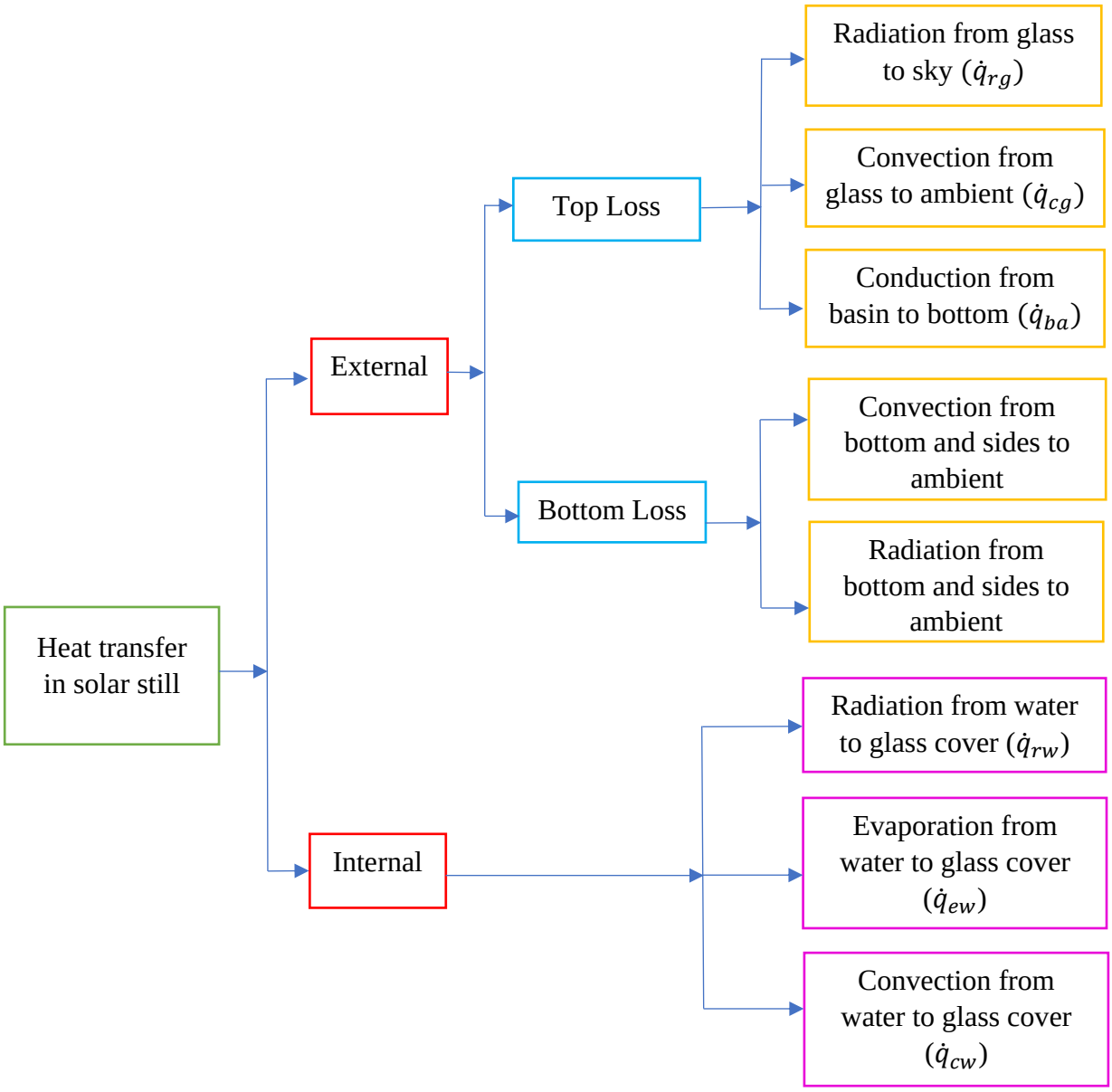

Fig. 1.7. Types of heat transfer in the solar still

All heat transfer occurs simultaneously, the evaporative heat transfer depends upon the convective heat transfer but these two are independent of radiative heat transfer. Various modes of heat transfer and energy losses in double slope solar still are shown in Fig. 1.8.

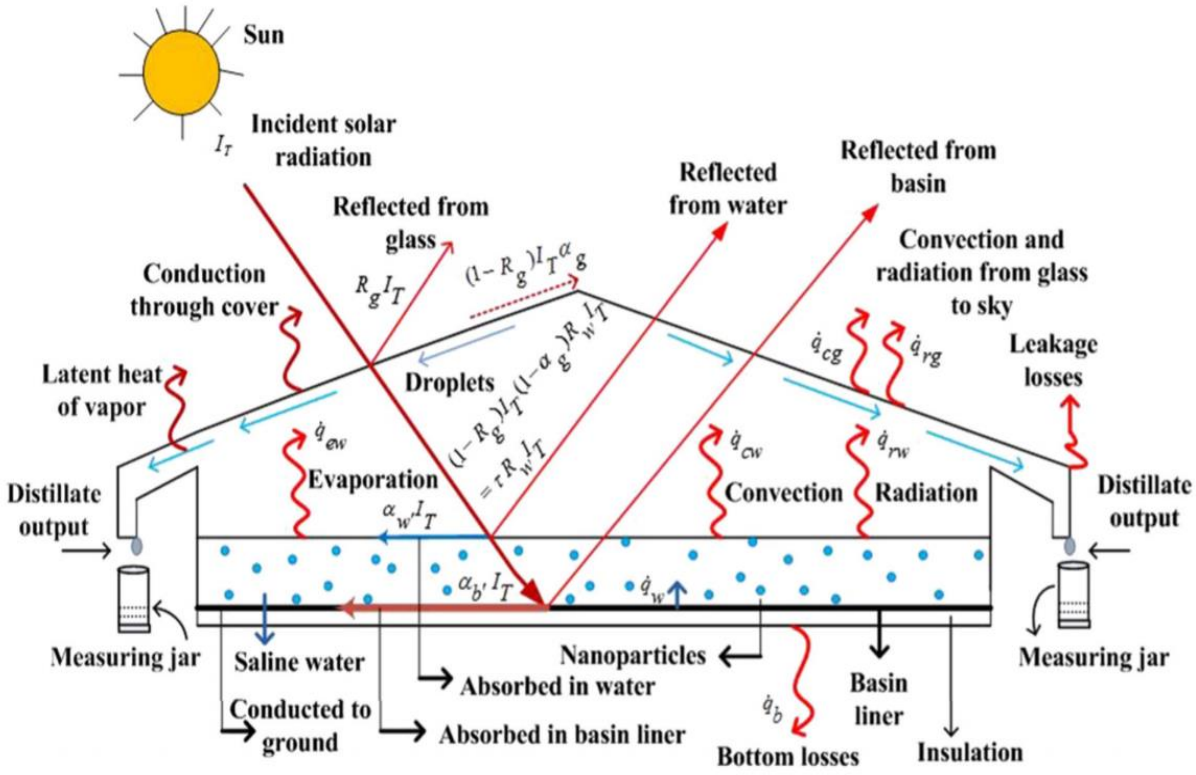

Fig. 1.8. Heat transfer and energy losses in double slope solar still

The rate of heat transfer by different modes within the solar still is expressed as [19, 34]:

1.7.1.1 Radiative Heat Transfer

The radiative heat transfer between the water surface and inner surface of the glass cover is obtained as:

$$q_{rw} = \in_{eff} \sigma[(T_w + 273)^4 - (T_g + 273)^4] \quad (1.1)$$

$$q_{rw} = h_{rw}(T_w - T_g) \quad (1.2)$$

$$h_{rw} = \in_{eff} \sigma[(T_w + 273)^2 + (T_g + 273)^2][T_w + T_g + 546] \quad (1.3)$$

Where, h_{rw} is the radiative heat transfer coefficient from the water surface to the glass cover

and $\varepsilon_{eff} = \left[\frac{1}{\varepsilon_w} + \frac{1}{\varepsilon_g} - 1 \right]^{-1}$

1.7.1.2 Convective Heat Transfer

Heat transfer occurs across humid air in the distillation unit by free convection, which is caused by the effect of buoyancy, due to the density variation in the humid fluid. This occurs due to the temperature gradient in the fluid.

The general equation of convective heat transfer from the water surface to glass cover of the solar still is given as:

$$q_{cw} = h_{cw}(T_w - T_g) \tag{1.4}$$

The convective heat transfer coefficient (h_{cw}), depends on the following parameters:

- Operating range of temperature
- The geometry of condensing cover
- Physical properties of the fluid within operating temperature

This convective heat transfer is calculated by using non-dimensional numbers. The relation of non-dimensional Nusselt number carry convective heat transfer coefficient is given as:

$$Nu = \frac{h_{cw} \cdot L_v}{K_v} = C\left(Gr\,\mathrm{Pr}\right)^n \tag{1.5}$$

or, $h_{cw} = \frac{K_v}{L_v} \cdot C\left(Gr\,\mathrm{Pr}\right)^n$

where, *Gr* and Pr are the Grashoff and Prandtl numbers, respectively, and C and n are unknown constants. The *Gr* and Pr are given by the following expressions:

$$Gr = \frac{\beta g L_v^{\,3} \rho^2 \Delta T}{\mu^2} = \frac{Buyoancy\ force}{Viscous\ force}$$

and, $\Pr = \frac{\mu C_p}{K_v} = \frac{Momentum\ Diffusivity}{Thermal\ Diffusivity}$

1.7.1.3 Evaporative Heat Transfer

The evaporative transfer coefficient (h_{ew}) can be written in terms of the convective heat transfer coefficient as:

$$\frac{h_{ew}}{h_{cw}} = \frac{L}{C_p} \times \frac{M_w}{M_a} \times \frac{1}{P_T} \tag{1.6}$$

Using Lewis relation (1922, 1933) i.e. the ratio of heat transfer coefficient to mass transfer coefficient is equal to the specific heat per unit volume at a constant pressure of the mixture and is given as:

$$\frac{h_{cw}}{h_D \rho_a C_p} = 1 \tag{1.7}$$

where h_D is the convective mass transfer coefficient (m/s) from the water surface and is given as:

$$\frac{m}{a} = h_D(\rho_w - \rho_a)$$

where m is the mass transfer rate (kg/h). Using the perfect gas equation (PV=RT', V=M/ρ) for water vapor and solving the Eq. (1.6) and Eq. (1.7) we will get

$$\frac{h_{ew}}{h_{cw}} = \frac{L}{\rho_a C_p} \times \frac{M_w}{RT'} \times \frac{1}{P_T} \tag{1.8}$$

After substituting the values of M_w, ρ_a, C_p, R, L, P_t (P_t=P_a) and T (at 50^{o}C) in the Eq. (1.8), we get

$$h_{ew} = 16.273 \times 10^{-3} \times h_{cw}$$

The rate of evaporative heat transfer is expressed as:

$$\dot{q}_{ew} = h_{ew}(T_w - T_{ci}) \tag{1.9}$$

1.7.1.4 Total Internal Heat Transfer

Total upward internal heat transfer coefficient (h_{1w}) can be written as:

$$h_{1w} = h_{rw} + h_{cw} + h_{ew} \tag{1.10}$$

The total internal energy ($\dot{q}_{1w}$) transfers from water surface to inner glass cover and can be expressed by adding the Eq (1.2), Eq (1.3) and (1.4) as:

$$\dot{q}_{1w} = h_{1w}(T_w - T_{ci}) \tag{1.11}$$

1.7.2 External Heat Transfer

The external heat transfer occurs outside the solar still by conduction, convection, and radiation which are independent of each other. This occurs from the side, bottom, and top surface of the glass cover to the environment. However, the side loss coefficient is generally neglected.

1.7.2.1 Top Heat Loss from Glass Cover

The external heat transfer from glass cover to the environment takes place by means of convection and radiation. To get the more realistic value of the external radiative heat transfer coefficient (h_{rcs}), the sink temperature is considered as the sky temperature (T_{sky}) rather than taking the ambient temperature (T_a) [35]. The sky temperature is expressed as [36];

$$T_{sky} = 0.0552 \times \left(T_a\right)^{1.5} \tag{1.12}$$

where, both the temperatures T_{sky} and T_a are in Kelvin.

Based on sky temperature, the external radiative (h_{rcs}) and convective (h_{ccs}) heat transfer coefficient may be written as:

$$h_{rcs} = \varepsilon_g \sigma \frac{\left((T_{co} + 273.15)^4 - (T_a + 273.15)^4\right)}{\left(T_{co} - T_{sky}\right)} + \varepsilon_g \frac{\Delta R}{\left(T_{co} - T_{sky}\right)} \tag{1.13a}$$

where, $\Delta R = \sigma\left((T_a + 273.15)^4 - (T_{sky} + 273.15)^4\right)$

Rate of external radiative heat transfer is given as:

$$\dot{q}_{rcs} = h_{rcs}(T_{co} - T_{sky}) \quad (1.13b)$$

The convective heat transfer coefficient from the exterior surface of the glass cover can be expressed as:

$$h_{ccs} = h_w \frac{\left(T_{co} - T_a\right)}{\left(T_{co} - T_{sky}\right)} \quad (1.14a)$$

where, h_w is the wind convective heat transfer coefficient, which depends upon the wind speed. Several correlations are available in the literature [37] and generally, h_w is determined from an expression in the form expressed as [37] :

$h_w = a + bV_a^{\,n}$

where, $a = 2.8$, $b = 3$, and $n = 1$ for $V_a < 5$m/s and, $a = 0$, $b = 6.15$, and $n = 0.8$ for $V_a > 5$m/s. The rate of external convective heat transfer from the outer surface of glass cover to ambient is given as:

$$\dot{q}_{ccs} = h_{ccs}(T_{co} - T_{sky}) \quad (1.14b)$$

The total external heat transfer coefficient (h_{2c}) between glass cover and sky can be written as:

$$h_{2c} = h_{rcs} + h_{ccs} = h_{rcs} + \frac{h_w\left(T_{co} - T_a\right)}{\left(T_{co} - T_{sky}\right)} \quad (1.15a)$$

The higher variation in the value of h_{2c} (includes radiative and convective) occurs with the variation of glass and ambient temperature. Some researchers proposed the simple correlation to predict the external heat transfer coefficient as [19];

$h_w = 2.8 + 3.0V_a$ and $h_{2c} = 5.7 + 3.8V_a$

Total heat transfer from glass cover to ambient is expressed as:

$$\dot{q}_{2c} = h_{2c}(T_{co} - T_a) \tag{1.15b}$$

1.7.2.2 Bottom Heat Loss

The loss of heat from the bottom to the environment can be written as:

$$\dot{q}_{ba} = h_{ba}(T_b - T_a) \tag{1.16}$$

where, $h_{ba} = \left[\frac{L_b}{K_b} + \frac{1}{h_{cb} + h_{rb}} \right]^{-1}$

1.7.2.3 Side Heat Loss

The loss of heat from the side ($\dot{q}_{sa}$) is insignificant as compared to bottom loss because of less quantity of water in the basin. However, it can be written as:

$$\dot{q}_{sa} = \dot{q}_{ba} \left(\frac{A_{ss}}{A_b} \right) \tag{1.17}$$

where A_{ss} is the surface area in contact with basin water

1.8 Global Status of Solar Distillation

Most of the distillation systems have been abandoned due to a very slow production rate. However, research in the area of solar distillation is limited in the following academic organizations namely IIT Delhi (INDIA); Central Arid Zone Research Institute, Jodhpur (INDIA); Sardar Patel Renewable Energy Research Institute, Anand (INDIA); Ciudad Universitaria, Coyoacán (MEXICO); The University of the Ryukyus, Nagoya University and Chuo University (JAPAN); Ben-Gurion University of the Negev, Be'er Sheva (ISRAEL); Technische Universitat Bergakademie Freiberg (GERMANY); Alexandria University (EGYPT); Jordan University of Science and Technology, Irbid (JORDAN); University of Ouargla (ALGERIA); Xian Jiao Tong University (CHINA) and University of Foggia (ITALY).

In India, the first largest solar distillation plant was installed by Central Salt and Marine Chemical Research Institute (CSMCRI), Bhavnagar to supply drinking water in Awania village (then non-electrified) and Chhachi lighthouse in 1978. The well waters in the area were found to be saline with total dissolved solids exceeding 3000 ppm (and above 5000 ppm during summer) and fluoride concentration about 6 to 8 ppm [38].

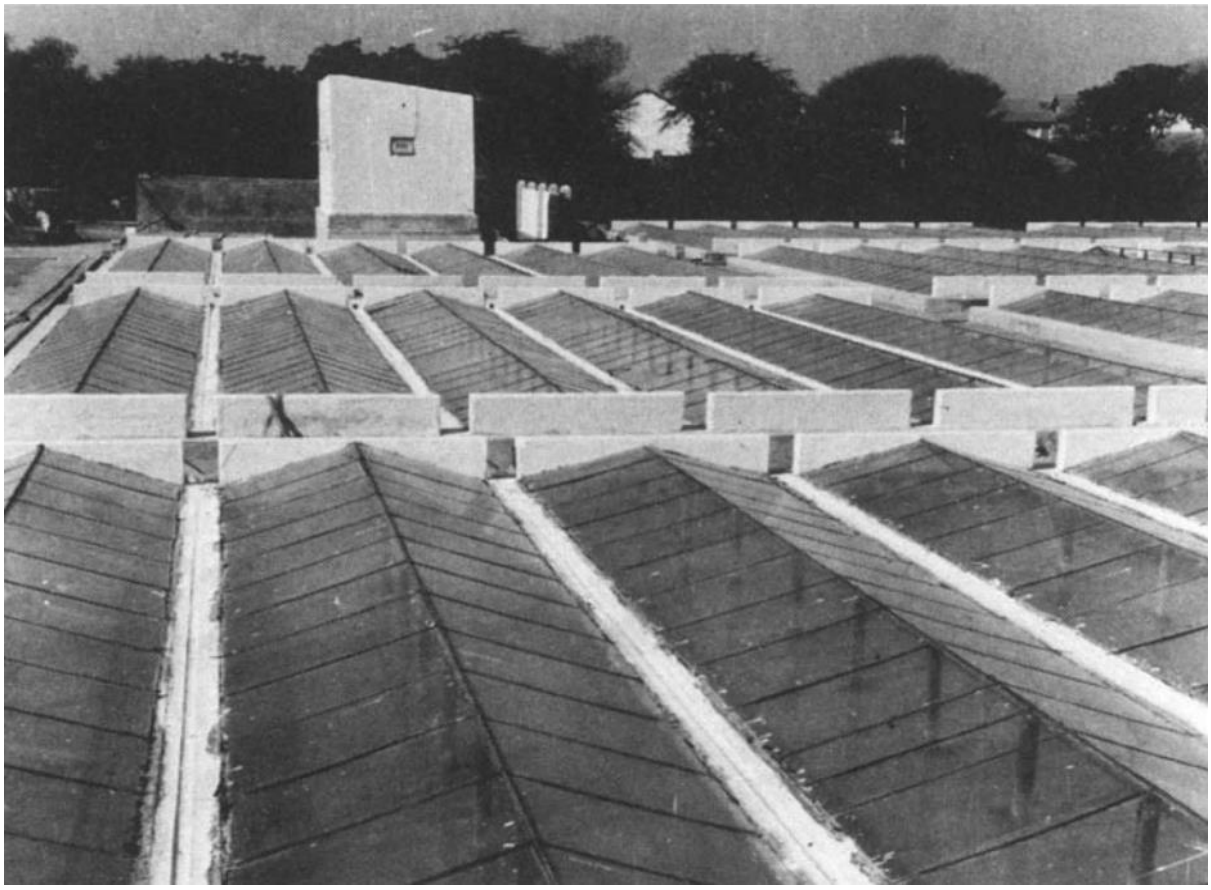

Fig. 1.9. Solar desalination plant at village Awania, Gujarat [38]

1.9 Thesis Outline

The remainder of this thesis is organized as follows:

Chapter 2: Includes an in-depth literature review designed to provide a summary of the base of knowledge already available involving the issues of interest. It presents the research works of previous investigators on solar distillation.

Chapter 3: Thermal modeling and optimization of double slope solar still augmented with ETC under forced mode are carried out. The output results are also discussed at the optimal flow rate with water depth.

Chapter 4: Exhaustive energetic and exergetic assessment of the proposed system is carried out in this chapter along with irreversibility. The effect of water depth and sessional effect outcome in terms of energy and exergy efficiency are also reported.

Chapter 5: Finally, conclusions on the performance and recommendations are made for the present design of solar still.

Chapter-II

Literature Survey

2.1 Introduction

The chapter gives an in-depth literature review on various developments and researches that happened in the field of solar distillation ever since the first known use of a solar still, to date.

2.2 Literature Survey

The green-house effect had been first discovered by the Egyptians. The use of solar energy had begun on 214-212 BC by Archimedes who made heat rays to defend the harbor of Syracuse against the Roman fleet. First solar engine by using glass lenses, supporting frame, and an airtight metal vessel containing water and air had been made by Salomon de Caux, a French engineer, and architect, in the year 1615. This arrangement produced a small water fountain when the air was heated up during operation. In the year 1774, Joseph Priestly, an English Chemist, had discovered oxygen gas through an Experiment in which sunlight was focused on mercuric oxide (HgO) inside a glass tube. The first known use of solar stills dates back to 1551 when it was used by Arab alchemists. Other scientists and naturalists used stills over the coming centuries including [39-41].

It is also believed that Sailors were the first people to duplicate the natural water cycle as shown in Fig. 2.1. They boiled seawater in a vessel using a wood fire and condensed it. They condensed the vapour in a sponge. The water squeezed out of the sponge (virtually salt-free) tasted unbeknownst. Sailors such as Sir Richard Hawkins reported that their men generated freshwater for the purpose of drinking from seawater during voyage using this technique. A primitive yet simple approach of desalination. However, the research and technological advancements in the distillation facilities paced upon the verge of the nineteenth century.

Fig. 2.1. Ancient representation of drinking water extraction from the sea

Mauchot [41] in his review, had written: "*One uses glass vessels for the solar distillation operation. According to the Arab alchemists, polished Damascus concave mirrors should be used for solar distillation*". The great French chemist used a large glass lens, mounted on supporting structures to concentrate solar energy on distillation flasks filled with content to be

distilled [40]. The use of silver or aluminum-coated glass reflectors to concentrate solar energy for distillation purposes had also been described [41].

Nebbia and Menozzi [42] had mentioned the work of Della Porta (1589) in a review of the water desalination field. About his designed solar still, he said: "*Insert green leaves into wide earthen pots full of water, so that the vapours may thicken more quickly into water. Turn all this apparatus, when it has been fully prepared, to the most intense heat of the sun's rays, for immediately, they dissolve into vapours and will fall drop by drop (i.e. the distillate which contains the essence of the green leaves, etc.) into the vessel which has been placed underneath. In the evening after sunset, remove them and fill with new herbs. Knotgrass, also commonly called "sparrow's tongue", when it has been cut up and distilled is very good for inflammation of the eyes and other affictions. A liquid produced by ground-pine which will end all convulsions if the sick man washes his limbs with it, and there are other examples too numerous to mention*". The solar still used by Della Porta has been illustrated in Fig. 2.2 and Fig. 2.3.

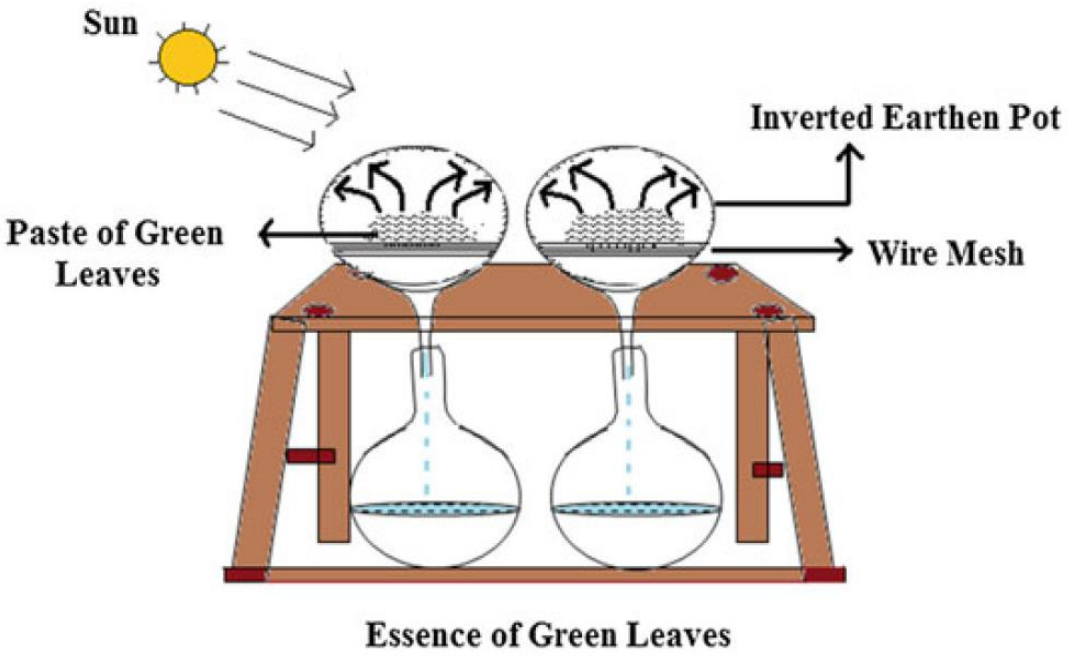

Fig. 2.2. Solar distillation apparatus used by Della Porta [42]

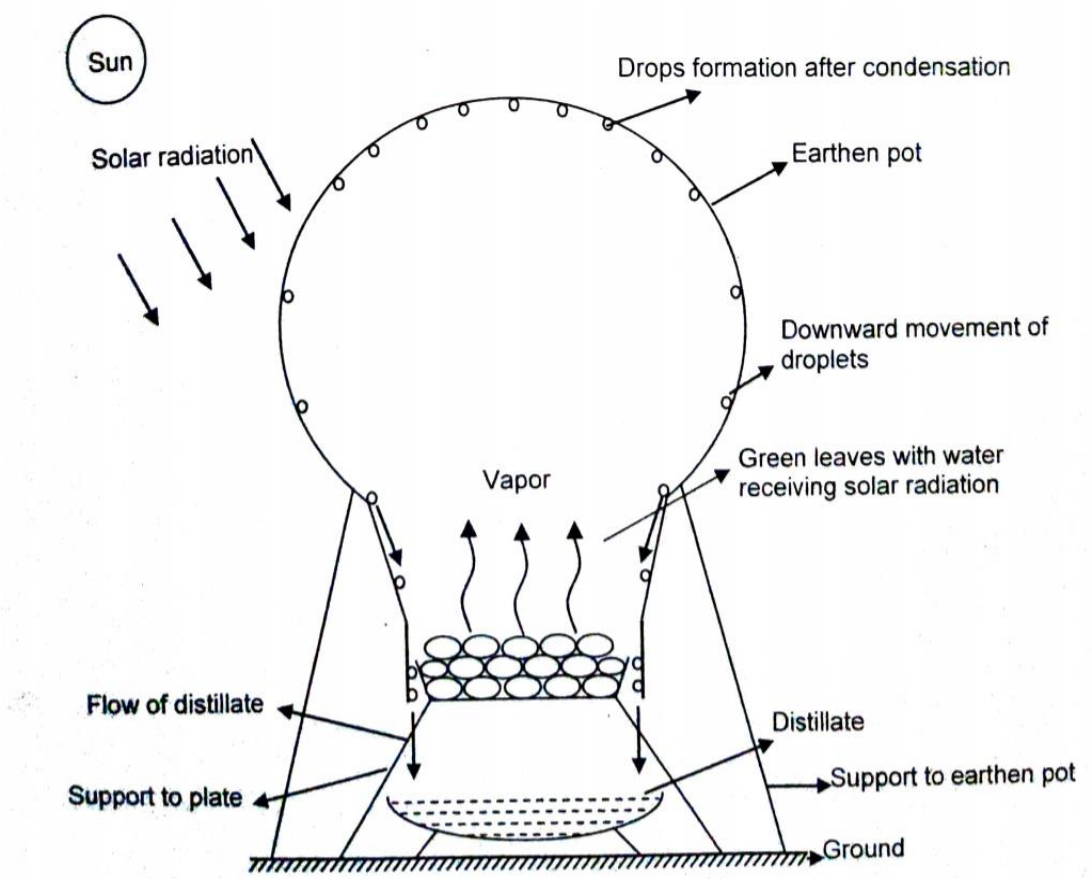

Fig. 2.3. Detailed schematic of solar still [39]

In 1870, the first American patent on solar distillation was granted to Wheeler and Evans. A famous plant built by Swedish engineer Carlos Wilson in 1872 in Las Salinas, Chile. It consisted of 64 water basins (4,459 m^2) to supply water (20,000 liters /day) to miners working in mining operations. It worked until 1910, due to the problem of accumulation of salts in the basin that needed regular cleaning [22]. The design of conventional basin type solar still formed a base for the majority of solar stills that are being built since that time. After 1878, works on solar energy slowed down because of the availability of low-cost conventional fuels.

Different designs of solar stills namely metallic reflector to concentrate solar rays used by Kush in 1920 [43], Cylindrical and parabolic reflectors [44] and spherical stills [45] were studied and reported. About 200,000 of spherical stills have been used during the world war-II to supply water in arid / desert areas, just after the war to supply fresh/potable water. During

the 1950s, interest in solar distillation was revived to develop large centralized distillation plants. However, after about 10 years, researchers around the world concluded that large solar distillation plants were too expensive to compete with fuel-fired ones. Therefore, research shifted to smaller solar distillation plants. Between, 1960-1970, 38 solar distillation plants were built in 14 countries, with capacities ranging from a few hundred to around 30,000 liters of water per day. Thereafter many pieces of research on design, fabrication methods and performance evaluation, etc. of solar distillation systems have been carried out by various scientists throughout the world.

The majority of high capacity solar still plants in India were installed by Central Salt & Marine Chemicals Research Institute (CSMCRI), Bhavnagar. Gomkale [46] studied in detail the solar distillation systems as per the Indian scenario. The pilot plant constructed at Bhavnagar in 1965 was the first large capacity plant in India with a permanent construction of basin area 350 m^2 with distillate production of 1000 liter per day. In 1977/78 a few plants were also installed for community use. The solar stills constructed in 1968 at Navinar Lighthouse for use by a small isolated group of those staying at the lighthouse. In 1983, basin type solar still of area 7500 m^2 was constructed in Lakshadweep to distillate the seawater of productivity 2000 liter per day.

Twenty years (1952 – 1973) work on solar distillation was reviewed at the University of California [5]. Talbert et al. [47] gave an excellent historical review of solar distillation. Delyannis and Delyannis [48] reviewed the work of major solar distillation plants around the world. This review also included the work of [49-51]. Gomkale [46] studied in detail the solar distillation systems as per the Indian scenario. Various investigations have also been carried out to study the impact of various techniques and how they affect the yield e.g. factors influencing the performance, effect of orientation of glass cover [52], the effect of dyes [53], use of condenser and water film cooling [54].

The various designs of Passive solar stills have been proposed and research work carried out [55-58] and for Active solar still [59-60] and on wick type solar still [61].

Garg and Mann [62], reported that productivity increases with an increase in solar radiation and ambient temperature, however, the efficiency of active solar still is more than passive, because of the higher operating temperature range. Tiwari and Madhuri [63] found that the dependence of yield on water depth is a strong function of the initial temperature of the brine in the basin of the still. Tripathi and Tiwari [64] reported the effect of water depths on the heat and mass transfer coefficients and found that the convective heat transfer coefficient between water and inner condensing cover depends significantly on the water depth.

Bouker and Harmim [65] carried out the effect of climatic conditions on the performance of solar still for the climatic conditions of Algeria and reported that the daily productivity in summer for simple double basin solar still varies from 4.01 to 4.34 $l/m^2/d$ as compared with 8.07 to 8.07 $l/m^2/d$ for a coupled double basin still in clear days. Al-Hinai et al. [66] reported that with the rise in ambient temperature from 23ºC to 33ºC, the daily yield increases by 8.2%. Tanaka and Nakatake [67], carried out the study of the effect of various factors on the productivity of multiple – effect diffusion type solar still coupled with flat plate reflector.

It is found from the literature review that more work has been carried out during the clear sky days on active and passive solar still performance. Rai and Tiwari [26] have developed a thermal model of active solar still by using Dunkle's relation [68]. EI-Sebaii [69] carried out the effect of wind speed and other parameters on the different designs of active and passive solar stills. Badran [70] carried out an experimental study of the enhancement parameters on single slope solar still and found that the performance of solar still is increased by 51 percent by combined asphalt basin liner and sprinkler. Kabbi and Nafila [71] studied the impact of temperature difference on solar still global efficiency and found that with greenhouse effect it improves solar still global efficiency and it can also be improved by attaching mirror, reflector

and concentrator to increase the intensity of solar radiation to solar distillation system and observed 20 l/d per unit area of reflector. Various aspects of passive and active solar stills have also been reported [19].

Kudish et al. [72] designed and tested a solar desalination system suitable for desalination of seawater; consisting of a solar collector coupled to an evaporation/condensation chamber made of non-corrosive polymeric materials (polymers). The carrier of thermal energy associated with the PV module may be either air or water. Once thermal energy withdrawal is integrated with the photovoltaic (PV) module, it is referred to as a hybrid PV/T system. The work on the PVT system has been reported by various researchers [73-75].

The low productivity was the main issue of passive solar stills, thus to enhance the productivity, various methods i.e. multi-stage solar still [76], use of nanofluids [77], integrated solar still with ETC, parabolic concentrator, FPC had been used for considerable improvement. Among them, FPC is becoming popular because of its less maintenance and ease of operation. The enhancement of annual performance using hybrid (PV/T) solar still was investigated and observed an increase in productivity by 350% compared to a passive one, using $4m^2$ size of series-connected PVT-FPC [78]. Dwivedi and Tiwari [25] carried out work under the natural mode on FPC integrated double slope solar still and estimated the yield about 51% higher than the uncoupled solar still. Higher yield (51%–148 %) than passive solar still was obtained using PVT, FPC, and hot air methods [79]. Feilizadeh et al. [80] reported that the optimal ratio between width and length as 0.4 for the maximum yield from a single slope distiller. Singh and Tiwari [81] carried out theoretical performance evaluation of series integrated PVT-CPC solar still and found the optimal rate of flow as 0.04 kg/s using 7 collectors to achieve outlet water collector temperature below boiling point.

Utilizing the evacuated tubes collectors in the solar distillation leads to the refinement in the performance of the system. Morrison et al. [82] reported better performance using an ETC

than FPC for high-temperature operation. Glembin et al. [83] reported a decrease in efficiency by 10% when the hourly rate of flow decreases (78 to 31 kg/m^2) using 60 parallel vacuum tubes. Dev and Tiwari [84] investigated daily yield as 3.328 with an overall energy efficiency of 30.1% during summer when a single slope distiller was charged from the ETC water heater. In the scenario of natural ETC water heater, Sato et al. [85] reported that the natural operation of ETC dis-favors the extraction of energy due to the intermixing of fluid, which takes place within the tube as hot and cold-water currents travel in opposite directions. Singh et al. [86] investigated the performance of single slope solar still augmented with ETC under natural flow in summer using 10 parallel tubes. They analytically predicted an increase in yield to 3.8 kg/day, while corresponding exergy efficiency as 2.5%. Sampathkumar et al. [87] experimented with an ETC integrated single slope solar still under natural mode using 15 tubes and found 219% higher production than obtained under the passive arrangement. Further, Kumar et al. [88] extended the work of previous researchers using the forced mode in ETC augmented single slope solar distiller and reported output as 3.9 kg/m^2/day while thermal efficiency as 33.8%. Panchal and Awasthi [89] found an increase in yield by 140%, using ETC integrated solar still under natural mode. Yari et al. [90] experimentally validated the results presented for ETC integrated single slope solar still and reported that placing semi-transparent photovoltaic modules on the solar still and coupling the basin with ETC size of 10 tubes, under natural mode yields maximum 2.3 kg.m^{-2}day^{-1} at 0.07 m water depth, which increases to 4.76 kg.m^{-2}day^{-1} using 30 tubes. Patel et al. [91] studied stepped type solar still charged using ETC water heater and reported improvement in yield ~ 24% during summer than uncoupled solar still.

Operation of ETC in forced mode has advantages over natural circulation mode namely:

a) better heat extraction from the tube.

b) no internal recirculation.

c) no stagnation in the reservoir.

d) the non-circulation area at the bottom of the tube avoided.

e) controlled water flow rate.

Recently, Jowzi et al. [92] have used a modified evacuated tube system with the attachment of an additional tube between the water tank and bottom of ETC tube to remove stagnation and found an enhancement in performance.

2.3 Research gap

From the literature survey, it is noted that investigations on ETC augmented single slope solar still have been reported. However, in the field of high-temperature distillation, no work has been reported for the double slope solar still augmented with Evacuated tube collectors (ETC) with 'N' parallel tubes under the forced mode.

2.4 Objective of the Present study

The objective of the present work is to extend the work further using double slope solar still under forced mode (a modified geometry). Hence, the performance of double slope solar still integrated with ETC under forced mode has been estimated analytically for the first time. The objectives of this research work are:

- To present a comprehensive mathematical model and carry out the performance evaluation of the system.
- To optimize the mass flow rate through the collector for optimal performance.
- Sizing of the number of tubes in terms of water depth for water temperature and yield, energy efficiency and exergy efficiency.
- To study the effect of the diffused reflector on the performance.
- To carry out the energetic and exergetic analysis.

Chapter-III

Thermal Modelling and Optimization of the System

3.1 Introduction

In this Chapter, a thermal model is developed for ETC integrated double slope solar still under forced mode. The internal heat transfer coefficients obtained by using the Dunkle model [68] are used along with other design and climatic parameters. The results are validated with previously published results with some changes in design conditions. The predicted results are obtained for water temperature, inner glass temperature, and finally distillate yield using the proposed model for different water depths. The results are obtained after developing a computer program for the proposed model in MATLAB.

The thermal model to simulate the rate of production of freshwater from seawater as a function of different meteorological parameters and specifications of the solar stills were developed by various researchers. Tiwari and Tiwari [93] carried out the indoor simulation to study the effect of condensing cover slope (15^o, 30^o, 45^o) on internal heat and mass transfer in the passive distillation unit and reported higher yield with increase in water temperature for 30^o cover inclination. Besides, there is a significant reduction in the evaporative heat transfer coefficient with an increase of inclination. The researchers [60, 94, 95] also developed the thermal models based on the energy balance equations of passive and active solar still with

different concepts, in different operating modes and validated the theoretical results with the experiments.

Operation of ETC in force mode has advantages over natural circulation mode, namely (a) better heat extraction from the tube (b) internal recirculation avoided (c) stagnation in reservoir avoided (d) the non-circulation area at the bottom of the tube avoided and (e) controlled flow rate. Kumar et al. [88] executed a theoretical analysis of ETC incorporated single slope solar distiller under forced manner and reported maximum daily yield and efficiency as 3.9 kgm^{-2} and 33.8%, respectively in summer. Panchal and Awasthi [89] found an increase in yield by 140%, using ETC integrated solar still under natural mode. Yari et al. [90] experimentally validated the results presented for ETC integrated single slope solar still and reported that placing semi-transparent photovoltaic modules on the solar still and coupling the basin with ETC size of 10 tubes, under natural mode yields maximum 2.3 $kg.m^{-2}day^{-1}$ at 0.07 m water depth, which increases to 4.76 $kg.m^{-2}day^{-1}$ using 30 tubes. Patel et al. [91] studied stepped type solar still charged using ETC water heater and reported improvement in yield ~ 24% during summer than uncoupled solar still. Theoretical performance evaluation of single and double slope solar still coupled with N numbers of PVT-CPC in series was carried out and optimum performance at an optimal flow rate of 0.04 kg/s was reported, using seven collectors at outlet water collector temperature below boiling point [81]. Recently, Jowzi et al. [92] have used a modified evacuated tube system with the attachment of an additional tube between the water tank and bottom of ETC tube to remove stagnation and found an enhancement in the performance.

3.2 System description

An ETC coupled solar distiller with double slope under forced mode with basin size of 2 m^2 is illustrated in Fig. 3.1. The basin is composed of fibre reinforced plastic (FRP), oriented E-W direction (latitude 28º35´ N and longitude 77º28´E).

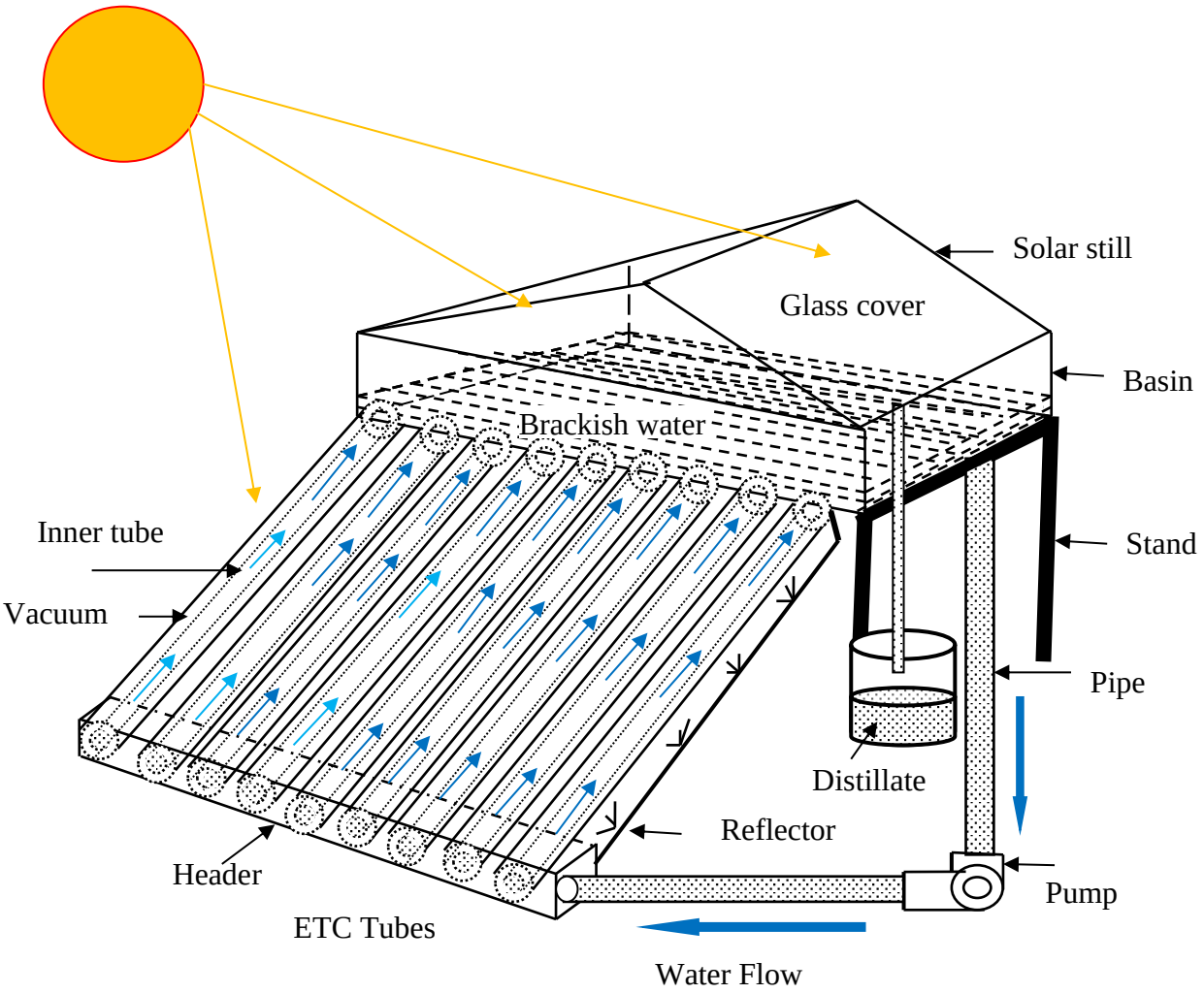

Fig. 3.1. Schematic of double slope solar still augmented with ETC under forced mode

On the top, a transparent condensing cover (made of glass) of 0.004 m thickness and 0.76 $Wm^{-1}K^{-1}$ thermal conductivity is fixed at 15º inclination from horizontal with proper sealing. Evacuated tubular collector composed of several parallel tubes of 1.4 m length and 0.07 m center spacing is inclined at 45º from horizontal, south oriented, and fixed at the bottom of the

basin. A valve is also provided to regulate the flow rate. To avoid reverse flow during the night, ETC may be cut off from solar still by providing a regulating valve in the pipeline after the pump, which also regulates flow rate as per requirement during the day. The radiations are transmitted through glass cover after reflection and absorption of some part and reach to basin water. Out of transmitted radiations, some are reflected while some percentile is absorbed by the water and remaining reaches to the basin liner. Basin water gets heated and water vapor condenses underneath the glass surface, flows down in a trough fabricated at the lower end, and finally taken in a jar kept outside using a pipe. The flow rate can be fitted after the pump.

The design specifications of the complete system are given in Table 3.1. Exhaustive performance of the complete system has been carried out using experimental climatic data recorded and given in Table 3.2 for a typical day. The initial water temperature of solar still, ETC has been taken as 23.1^{o}C along with 23^{o}C initial glass temperature and measured values of ambient temperature (23^{o}C).

Table 3.1. Parameters of ETC coupled double slope solar still distillation system

Parameters	Value	Parameters	Value
basin area	2 m^2	conductivity of glass	0.78 $Wm^{-1}K^{-1}$
glass area	1.14 m^2	glass thickness	0.004 m
thickness of basin	0.005 m	conductivity of basin	0.351 $Wm^{-1}K^{-1}$
outer dia. of tube	0.047m	tubes No.	10
tube inner dia.	0.044m	water per tube	2.25 kg
center distance between tubes	0.07m	length of tube	1.4m
pump size	12 V/ 24W	surface area of tube	0.21m^2
		connecting pipe	1/2 ” GI

Table 3.2. Measured parameters for 4th October 2010 [96]

Time	$Is_E(t)$ (Wm^{-2})	$Is_W(t)$ (Wm^{-2})	$I_c(t)$ (Wm^{-2})	T_a (^oC)	
7am	0	0	0	23	Initial water temperature of solar
8	300	180	280	25	still and ETC = 23.1^oC
9	500	300	480	28	Initial glass temperature = 23^oC
10	540	420	600	30	
11	600	520	660	31	
12	680	660	720	32	
13	600	620	680	33	
14	460	560	600	34	
15	300	470	460	33	
16	180	300	280	32	
17	120	200	180	31	
18	0	0	0	29	
19	0	0	0	27	
20	0	0	0	26	
21	0	0	0	26	
22	0	0	0	25	
23	0	0	0	25	
24	0	0	0	25	
1	0	0	0	24	
2	0	0	0	24	
3	0	0	0	23	
4	0	0	0	23	
5	0	0	0	22	
6am	0	0	0	22	

3.3 Thermal analysis

To evaluate the temperatures, yield, and performance parameters, the thermal equations are developed with the help of relations given in the Appendix. These equations are then solved with the hereunder assumptions:

(a) no vapour leakage from the system.

(b) negligible heat storage by condensing and basin material.

(c) thermophysical properties are temperature dependent.

(d) temperature drop in the connecting pipe is 2^{o}C.

(e) heat transfer coefficients (h.t.c) are evaluated based on initial water and condensing cover temperatures.

(f) basin water mass at a constant level.

(g) the system is in a quasi-steady condition during sunshine.

(h) heat loss through the frictional resistance is neglected.

(i) bending effects in the tubes/pipe are neglected.

Energy balance equations at different locales of the system are given hereunder:

3.3.1 Water mass in evacuated tubes

Following Budihardjo et al. [97], instantaneous efficiency is calculated as;

$$\eta_{ic} = \eta_o - \frac{a'(T_{cw}-T_a)}{I_c\,(t)} \tag{3.1}$$

Useful heat gain from collector tubes can be obtained as;

$$\dot{q} = I_c(t)_T \eta_{ic}$$

or

$$\dot{q} = I_c(t)\, N_c\, [0.5A_t + (CD - d_t)\gamma\rho_r . L_t]\eta_{ic} \tag{3.2}$$

Energy balance in ETC tubes using this useful heat is expressed as [88];

$$\dot{q} = [I_c\,(t)_T\, \eta_o - \alpha' A_t N_c(T_{cw} - T_a)] = M_{cw}c_w \frac{dT_{cw}}{dt} + \dot{m}c_w(T_{cw} - T_{sw}) \tag{3.3}$$

Using eqn. (3) we get:

$$\frac{dT_{cw}}{dt} + a_1.\ T_{cw} + b_1\ .T_{sw} = g_1(t) \tag{3.4}$$

where,

$$a_1 = \frac{(U_t)}{M_{cw}\ .C_w}$$

$$b_1 = -\frac{\dot{m}}{M_{cw}}$$

$$g_1(t) = \frac{I_c(t)_T\ \eta_o + \alpha' T_a\ A_t\ N_c}{M_{cw}.\ c_w}$$

$$U_t = \dot{m}.\ c_w + \alpha'\ A_t\ N_c, I_c(t)_T = I_c(t)\ N_c\ [0.5A_t + (CD - d_t)\gamma\rho_r.\ L_t]$$

3.3.2 Energy balance on east condensing cover

(i) Inner side of cover

$$\alpha_g I_E(t) A_{gE} + h_{1w,E}(T_{sw} - T_{gi,E})A_b - h_{r,EW}(T_{gi,E} - T_{gi,W})A_{gE} = h_{kg}(T_{gi,E} - T_{go,E})A_{gE} \quad (3.5)$$

(ii) Outer side of cover

$$h_{kg}(T_{gi,E} - T_{go,E})\ A_{gE} = h_{1g,E}\ (T_{go,E} - T_a)\ A_{gE} \quad (3.6)$$

3.3.3 Energy balance on west condensing cover

(i) Inner side of cover

$$\alpha_g\ I_w(t) A_{gW} + h_{1w,W}(T_{sw} - T_{gi,W})A_b - h_{r,WE}(T_{gi,W} - T_{gi,E})A_{gW} = h_{kg}(T_{gi,W} - T_{go,W})A_{gW} \quad (3.7)$$

(ii) Outer side of cover

$$h_{kg}\ (T_{gi,W} - T_{go,W})A_{gW} = h_{1g,W}(T_{go,W} - T_a)A_{gW} \quad (3.8)$$

3.3.4 Basin Liner

$$\alpha_b\ (I_E(t)A_{gE} + I_W(t)A_{gW}) = 2\ A_b\ h_{bw}(T_b - T_{sw}) + 2A_b h_{ba}(T_b - T_a)$$

or

$$T_b = \frac{\alpha_b\ (I_E(t)A_{gE} + I_W(t)A_{gW}) + 2A_b(h_{bw}T_{sw} + h_{ba}T_a)}{2A_b(h_{bw} + h_{ba})} \quad (3.9)$$

3.3.5 Basin water mass

Rearranging the energy inflow and outflow at water mass using energy balance, the instantaneous temperature of water in solar still (T_{sw}) together with collector water temperature (T_{cw}) can be expressed as [98];

$$\dot{q_{uc}} + \alpha_w\left(I_E(t)A_{gE} + I_W(t)A_{gW}\right) + 2\ h_{bw}A_b(T_b - T_{sw}) = M_{sw}\,c_w\,\frac{dT_{sw}}{dt} + h_{1w,E}A_b\left(T_{sw} - T_{gi,E}\right) + h_{1w,W}\,A_b\left(T_{sw} - T_{gi,W}\right) \quad (3.10)$$

where

$$\dot{q_{uc}} = \dot{m}\,c_w(T_{cw} - T_{cwi}) \quad (3.11)$$

With the above eqns. (3.5 to 3.8), we get the following;

$$T_{gi,E} = \frac{\alpha_g\,I_E(t)A_{gE} + h_{1w,E}T_{sw}A_b + h_{r,EW}T_{gi,W}\,A_{gE} + U_1T_aA_{gE}}{h_{1w,E}\,A_b + h_{r,EW}\,A_{gE} + U_1\,A_{gE}}$$

or

$$T_{gi,E} = \frac{R_1 + h_{1w,E}\,T_{sw}\,A_b + h_{r,EW}T_{gi,W}\,A_{gE}}{U_3} \quad (3.12)$$

where

$$U_1 = \frac{h_{kg}h_{1g,E}}{h_{kg} + h_{1g,E}}$$

$$U_3 = h_{1w,E}\,A_b + U_1\,A_{gE} + h_{r,EW}\,A_{gE}$$

$$R_1 = (\alpha_g I_E(t) + U_1T_a)A_{gE}$$

$$T_{gi,W} = \frac{\alpha_g\ I_W(t)A_{gW} + U_1T_aA_{gW} + h_{1w,W}T_{sw}A_b + h_{r,WE}T_{gi,W}A_{gW}}{h_{1w,W}A_b + h_{r,WE}A_{gW} + U_2A_{gW}}$$

or

$$T_{gi,W} = \frac{R_2 + h_{1w,W}T_{sw}A_b + h_{r,WE}T_{gi,E}A_{gW}}{U_4} \quad (3.13)$$

where

$$U_2 = \frac{h_{kg}\,h_{1g,W}}{h_{kg} + h_{1g,W}}$$

$$U_4 = h_{1w,W}A_b + h_{r,EW}A_{gW} + U_2A_{gW}$$

$R_2 = (\alpha_g\, I_W(t) + \, U_2 T_a)\, A_{gW}$

From Eqns, (3.12) and (3.13);

$$T_{gi,W} = \frac{T_{gi,E}U_3 - R_1 - h_{1w,E}T_{sw}\, A_b}{h_{r,EW}\, A_{gE}} = \frac{R_2 + h_{1w,W}T_{sw}\, A_b + h_{r,WE}T_{gi,E}\, A_{gW}}{U_4}$$

or

$$T_{gi,E}U_3U_4 - R_1U_4 - h_{1w,E}T_{sw}A_bU_4$$

$$= R_2h_{r,EW}A_{gE} + h_{1w,W}T_{sw}A_bh_{r,EW}A_{gE} + h_{r,WE}T_{gi,E}A_{gW}h_{r,EW}A_{gE}$$

or

$$T_{gi,E} = \frac{A_1 + A_2\, T_{sw}}{U} \tag{3.14}$$

and $\quad T_{go,E} = \frac{h_{kg}\, T_{gi,E} + h_{1g,E}\, T_a}{h_{kg} + h_{1g,E}}$ (3.15)

Similarly, for west side condensing cover;

$$T_{gi,W} = \frac{B_1 + B_2 T_{sw}}{U} \tag{3.16}$$

and $\quad T_{go,W} = \frac{h_{kg}\, T_{gi,W} + h_{1g,W}T_a}{h_{kg} + h_{1g,W}}$ (3.17)

where

$A_1 = R_1U_4 + R_2h_{r,EW}\, A_{gE}$ $\qquad$ $A_2 = h_{1w,E}U_4A_b + h_{1w,W}A_bh_{r,EW}A_{gW}$

$B_1 = R_2U_3 + R_1h_{r,WE}\, A_{gE}$ $\qquad$ $B_2 = h_{1w,W}U_3A_b + h_{1w,E}A_bh_{r,WE}A_{gW}$

$U = U_3U_4 - h_{r,EW}h_{r,WE}\, A_{gE}A_{gW}$

From eqn. (3.10);

$$\dot{m}c_w(T_{cw} - T_{sw}) + \, \alpha_w \left(I_E(t)A_{gE} + I_W(t)A_{gW}\right) + 2h_{bw}A_b(T_b - T_{sw}) = M_{sw}c_w \frac{dT_{sw}}{dt} +$$

$$h_{1w,E}\, A_b\left(T_{sw} - T_{gi,E}\right) + h_{1w,W}A_b\left(T_{sw} - T_{gi,W}\right)$$

or

$$\frac{dT_{sw}}{dt} - \frac{\dot{m}c_w T_{cw}}{M_{sw}c_w} + \frac{(\dot{m}c_w + 2h_{bw}A_b + h_{1w,E}A_b + h_{1w,W}A_b)}{M_{sw}c_w} T_{sw} = \frac{\alpha_w(I_E(t)A_{gE} + I_W(t)A_{gW})}{M_{sw}c_w} +$$

$$\frac{\alpha_b h_{bw}(I_E(t)A_{gE} + I_W(t)A_{gW})}{(h_{bw}+h_{ba})M_{sw}c_w} + \frac{2A_b h_{bw}^2}{(h_{bw}+h_{ba})M_{sw}c_w} T_{sw} + \frac{2A_b h_{bw} h_{ba} T_a}{(h_{bw}+h_{ba})M_{sw}c_w} + \frac{(h_{1w,E}A_1 + h_{1w,W}B_1)A_b}{UM_{sw}c_w} +$$

$$\frac{(h_{1w,E}A_2 + h_{1w,W}B_2)A_b}{UM_{sw}c_w} T_{sw}$$

or

$$\frac{dT_{sw}}{dt} - \frac{\dot{m}T_{cw}}{M_{sw}} + \frac{1}{M_{sw}c_w}\left[\dot{m}c_w + \frac{2h_{bw}h_{ba}A_b}{(h_{bw}+h_{ba})} + h_{1w,E}A_b\left(\frac{U-A_2}{U}\right) + h_{1w,W}A_b\left(\frac{U-B_2}{U}\right)\right] T_{sw} =$$

$$\frac{1}{M_{sw}c_w}\left\{\left[\left(\alpha_w + \frac{\alpha_b h_{bw}}{h_{bw}+h_{ba}}\right)\left(I_E(t)A_{gE} + I_W(t)A_{gW}\right)\right] + \frac{2A_b h_{bw} h_{ba} T_a}{(h_{bw}+h_{ba})} + \frac{(h_{1w,E}A_1 + h_{1w,W}B_1)A_b}{U}\right\}$$

$$\frac{dT_{sw}}{dt} + a_2 . T_{cw} + b_2 . T_{sw} = g_2(t) \qquad (3.18)$$

where

$$a_2 = -\frac{\dot{m}}{M_{sw}}$$

$$b_2 = \frac{\dot{m}.c_w + U_{Leff}}{M_{sw}c_w}$$

$$g_2(t) = \frac{(\alpha\tau)_{eff2} I_{seff} + U_L T_a + h_{1weff}}{M_{sw}c_w}$$

$$U_L = \frac{2h_{bw}h_{ba}A_b}{(h_{bw}+h_{ba})} \quad U_{Leff} = U_L + h_{1w,E}A_b\left(\frac{U-A_2}{U}\right) + h_{1w,W}A_b\left(\frac{U-B_2}{U}\right)$$

$$(\alpha\tau)_{eff2} = \left(\alpha_w + \frac{\alpha_b h_{bw}}{h_{bw}+h_{ba}}\right)$$

$$I_{s,eff} = \left(I_E(t)A_{gE} + I_W(t)A_{gW}\right)$$

$$h_{1w,eff} = \frac{(h_{1w,E}A_1 + h_{1w,W}B_1)A_b}{U}$$

The relations to evaluate various heat transfer coefficient, the properties are given in Appendix.

Solving eqns. (3.4) and (3.18). After multiplying Eqn. (3.18) by γ and adding with eqn. (3.8), and solving after multiplying e^{ct} one gets;

$$\frac{d}{dt}(T_{cw} + \gamma T_{sw})\, e^{ct} = \{g_1(t) + \gamma g_2(t)\}\, e^{ct} \qquad (3.19)$$

Further considering $(a_1 + \gamma a_2) = c;\ (b_1 + \gamma b_2) = \gamma c$ and resolving the above equation one get;

$$a_2\gamma^2 + (a_1 - b_2)\gamma - b_1 = 0 \tag{3.20}$$

One can get $\gamma = \frac{-(a_1-b_2)\pm\sqrt{(a_1-b_2)^2+4a_2.b_1)}}{2a_2}$

This gives us two roots i.e. γ^+ and γ^- corresponding values of c^+ and c^-

Further, with the hereunder assumptions;

(a) The time interval is very small.

(b) T_{cwi} and T_{swi} are the temperatures at $t = 0$.

(c) No flow of water through ETC during off-sunshine hours.

On solving the equation (3.19) we get;

$$(T_{cw} + \gamma^+ T_{sw}) = \frac{\left\{\overline{g_1(t)}+\gamma^+\overline{g_2(t)}\right\}}{c^+}\left(1 - e^{-c^+t}\right) + (T_{cwi} + \gamma^+ T_{swi})\, e^{-c^+t} \tag{3.21a}$$

$$(T_{cw} + \gamma^- T_{sw}) = \frac{\left\{\overline{g_1(t)} + \gamma^-\overline{g_2(t)}\right\}}{c^-}(1 - e^{-c^-t}) + (T_{cwi} + \gamma^- T_{swi})\, e^{-c^-t} \tag{3.21b}$$

Solving eqn. (3.21), we get following

$$T_{sw} = \frac{1}{(\gamma^+-\gamma^-)}\left[\overline{g_1(t)}\left\{\frac{\left(1-e^{-c^+t}\right)}{c^+} - \frac{(1-e^{-c^-t})}{c^-}\right\} + \overline{g_2(t)}\left\{\frac{\gamma^+\left(1-e^{-c^+t}\right)}{c^+} - \frac{\gamma^-(1-e^{-c^-t})}{c^-}\right\} + \right.$$

$$\left. T_{cwi}\left(e^{-c^+t} - e^{-c^-t}\right) + T_{swi}\left(\gamma^+e^{-c^+t} - \gamma^-e^{-c^-t}\right)\right] \tag{3.22}$$

and

$$T_{cw} = \frac{1}{(\gamma^+-\gamma^-)}\left[\overline{g_1(t)}\left\{\frac{\gamma^+(1-e^{-c^-t})}{c^-} - \frac{\gamma^-\left(1-e^{-c^+t}\right)}{c^+}\right\} + \gamma^+\gamma^-\overline{g_2(t)}\left\{\frac{(1-e^{-c^-t})}{c^-} - \right.\right.$$

$$\left.\left.\frac{\left(1-e^{-c^+t}\right)}{c^+}\right\} + T_{cwi}\left(\gamma^+e^{-c^-t} - \gamma^-e^{-c^+t}\right) + \gamma^+\gamma^-T_{swi}\left(e^{-c^-t} - e^{-c^+t}\right)\right] \tag{3.23}$$

Hourly distillate yield and efficiency may be obtained as [25];

$$m_{ew,\ E} = \frac{h_{ew,E}\left(T_{sw}-T_{gi,E}\right)\times 3600}{L}$$

$$m_{ew,W} = \frac{h_{ew,W}\left(T_{sw} - T_{gi,W}\right) \times 3600}{L}$$

Total hourly yield $= m_{ew,T} = m_{ew,E} + m_{ew,W}$ (3.24)

3.4 Performance parameters

3.4.1 Daily yield

Daily yield can be attained as;

$$\eta_{daily,overall} = \frac{\sum_1^{24} m_{ew}.L}{\sum_1^{24}(I_c(t).A_a + I_s(t)\,A_g) \times 3600} \times 100 \quad (3.25)$$

3.4.2 Energy efficiency

$$\eta_{i,overall} = \frac{m_{ew,T}.L}{(I_c(t).A_t.N_c + I_E(t)A_{gE} + I_W(t)A_{gW})3600} \times 100 \quad (3.26)$$

3.4.3 Exergy efficiency

Exergetic efficiency (%) for the system can be put down as [99];

$$\varepsilon = 1.072\,\eta_{i,overall} \times \left\{1 - \left(\frac{T_a+273}{T_{sw}+273}\right)\right\} \quad (3.27)$$

3.5 Methodology

The experimental data of Ghaziabad, India (NCR Delhi) on a typical day has been used. The measured radiations on both the condensing cover of solar still oriented E-W, on collector surface inclined at 45° to due south and ambient temperature reported have been considered for further assessment of the integrated system in forced mode.

The initial water temperature of solar still, ETC has been taken as 23.1°C along with 23°C initial glass temperature and measured values of ambient temperature (23°C). In order to evaluate the temperatures at various points, yield, energy efficiency, etc., equations given in sections 3 and 4 are executed using MATLAB program and using design parameters with the help of thermophysical properties appended in Appendix. Temperatures of water,

glass covers, basin obtained at the verge of an hour become entry temperature in the next round of calculation. The piping loss of 2^{o}C has been considered at the inlet of ETC.

3.6 Results and Discussion

In this section, the results of numerical simulations are shown in Figs. 3.2 - 3.8 to optimize the flow rate and water depth for water temperature ~ 98.5 from the end of a collector using 10 - 40 parallel tubes. The performance of the system with water depth at an optimal flow rate using climatic data of a typical month is presented in Figs. 3.9 - 3.14.

3.6.1 Validation of the thermal model

There is no work reported in the open literature of ETC integrated double slope solar stills. Therefore, to validate the present model, eqns. 3.1 to 3.4 are executed with a combination of equations of single slope solar still reported by Kumar et al. [88] to obtain the final eqns. 3.22 and 3.23 of water and glass temperature. The proposed thermal model is used to conclude the hourly water, glass temperature and the yield using the proposed model with modification as applied to the ETC integrated single slope solar still augmented under forced mode. The results so obtained using the proposed model are correlated with those reported by Kumar et al. [88] for the typical day for the same climatic conditions, using 10 tubes, 0.03m depth, and 0.001kg/s flow rate. The predicted results are shown in Fig. 3.2 and found in good agreement. The proposed model predicts marginally higher water and glass cover temperature with a ~ 5% increase in yield than predicted by Kumar et al. [88], due to the accounting of reflected radiations in the term $I_c(t)_T$ used in eqn. (3.2). From the validation, it can be concluded that the model developed for ETC integrated double slope solar still under forced way using eqns. (3.1 - 3.23) can be successfully applied to investigate the performance of the present geometry.

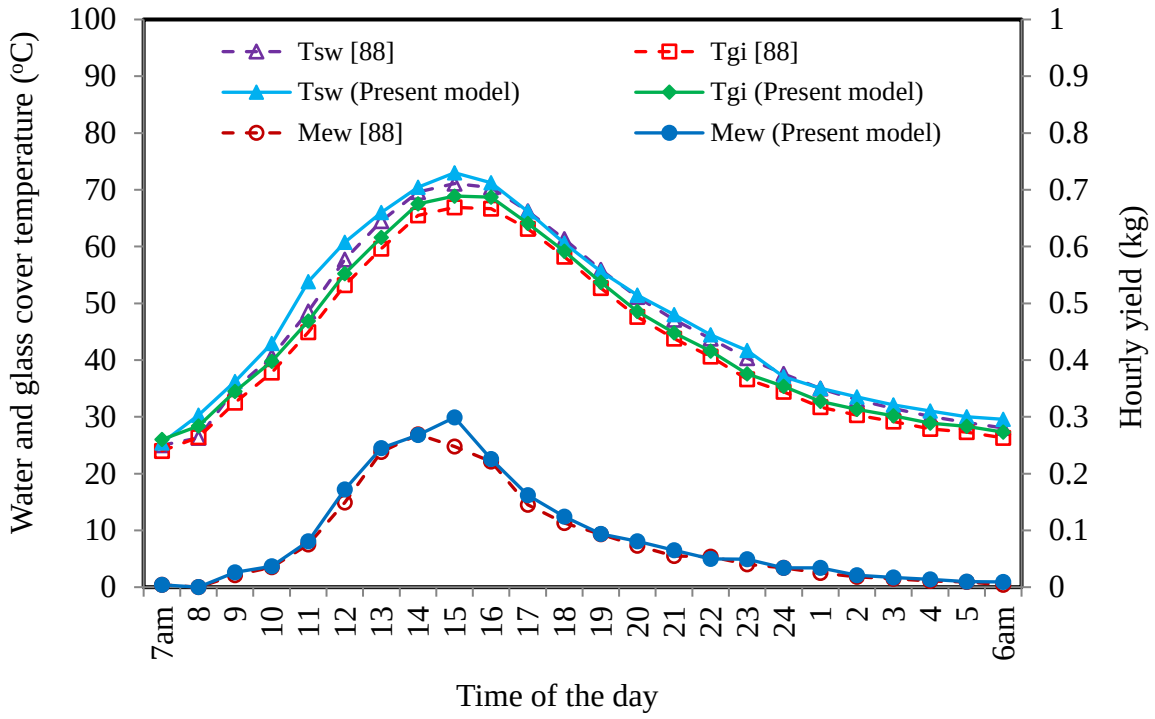

Fig. 3.2. Validation of thermal model at 0.03 m basin water depth, 0.001 kg/s flow rate and 10 vacuum tubes

3.6.2 Flow rate optimization

The optimal flow rate affects the outlet temperature and output attainments of the system. The dissimilar outlet temperature of water at the end of ETC tube, with the change of flow rate and depth of basin water, is shown in Fig. 3.3. Higher the depth, the higher the quantity of mass in the basin. It is noticed that as the flow rate decreases, outlet temperature from tube increases and hits maximum at 13:00 hrs. Variation of temperature attainable for flow rate range ~ 0.05 - 0.07 kg/s remains almost the same. This is due to a trivial change in the heat removal factor beyond this range. It is also observed that with an increase in basin water depth to 0.015 m (30 kg water mass), hourly temperatures attainable are lower than obtained at a lower water depth of 0.005 m (10 kg water mass) till 15:00 hrs and reciprocal thereafter at low sunshine hours. During low sunshine, the flow rate effect is negligible, as low solar energy is accessible for absorption by the water (flowing in the tube).

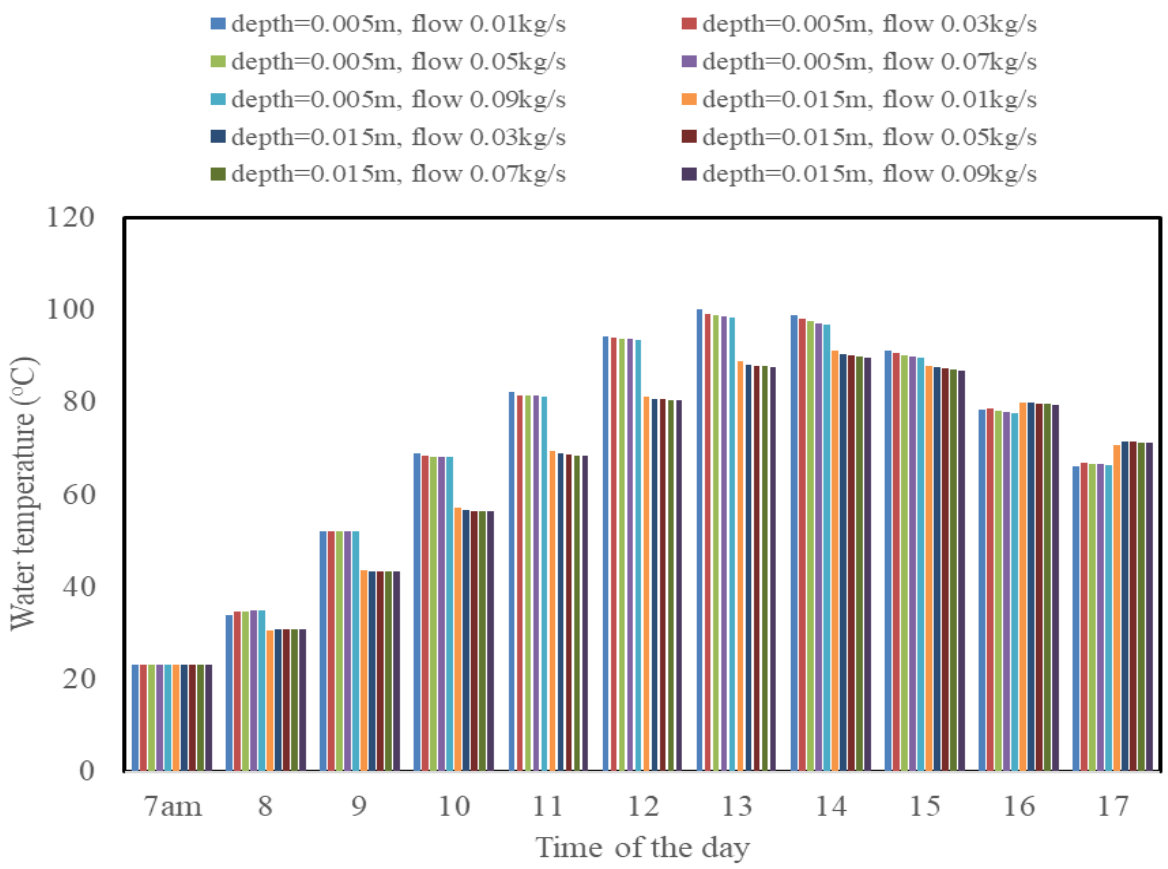

Fig. 3.3. Effect of mass flow rate and basin water depth on collector outlet temperature

The combined effect of variation of the number of ETC tubes (10 - 30), water depth (0.005 - 0.025 m) and flow rate (0.01 - 0.09 kg/s) on the maximum temperature attainable at the collector outlet (T_{cw}) is further evaluated and shown in Fig. 3.4. It is found that each combination produces a different outlet water temperature. The temperature ~ 98.5°C is observed with a combination of 10 tubes, 0.005 m depth, and rate of flow between ~ 0.06 - 0.07 kgs^{-1}. However, with 20 and 30 tubes, a higher temperature (> 100°C) is observed irrespective of the flow rate through the pump. This is due to a decreased rate of flow/tube with an increment in the number of parallel tubes, which increases the outlet water temperature. This reveals that combination with a higher number of ETC tubes attracts a higher depth of water in the basin so that the final temperature of basin water remains below the boiling point. Therefore, the system is further simulated for water depth with

ETC consisting of 20/30 tubes to obtain typical water depth between 0.005 - 0.025 m.

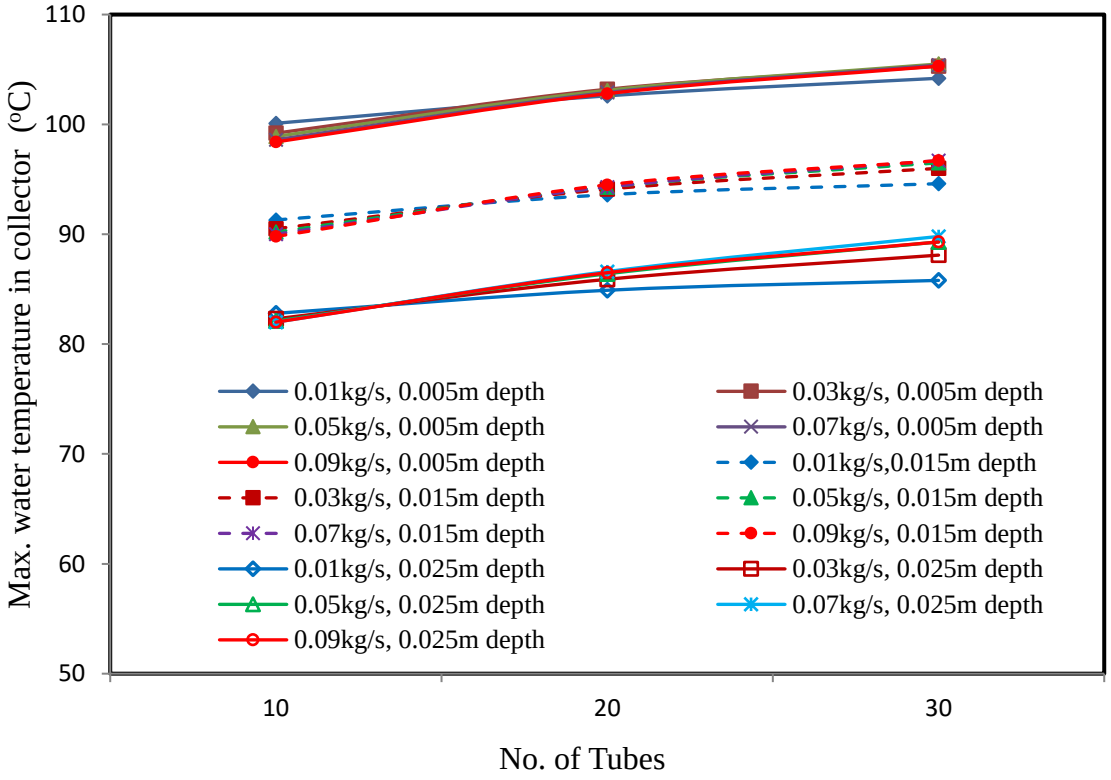

Fig. 3.4. Effect of number of tubes, water depth and flow rate on the maximum water temperature in the collector (T_{cw})

The effect of ETC size and rate of flow on daily yield, overall energy, and exergy efficiency is depicted in Fig. 3.5 - 3.6. It is noticed that as the tubes number increases, daily yield increases with a decrement in efficiencies, however, the percentage increase/decrease further depends on the rate of flow through the pump.

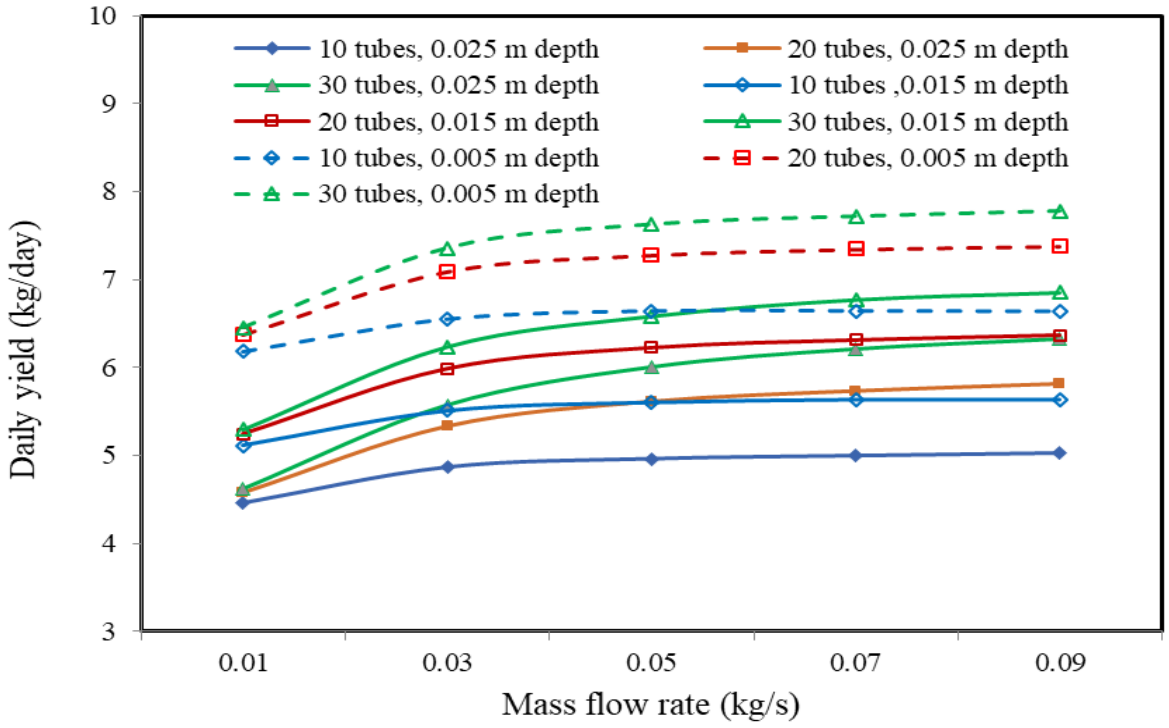

Fig. 3.5. Effect of ETC size and flow rate on the daily yield with water depth

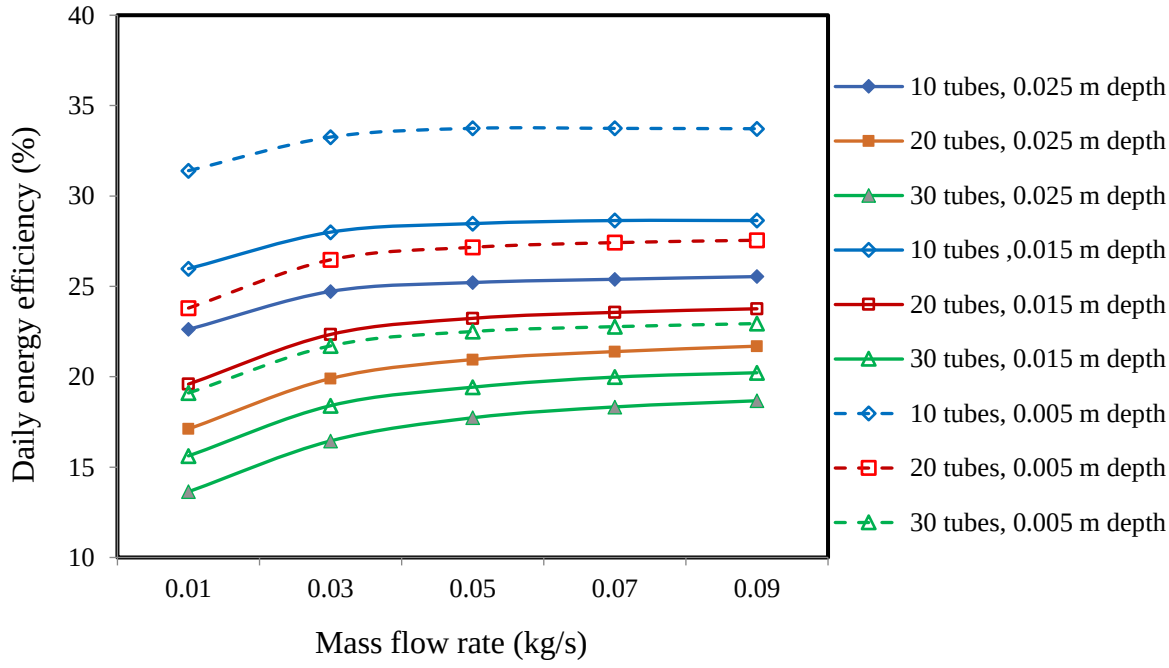

Fig. 3.6a. Effect of ETC size and flow rate on the energy efficiency with depth of water

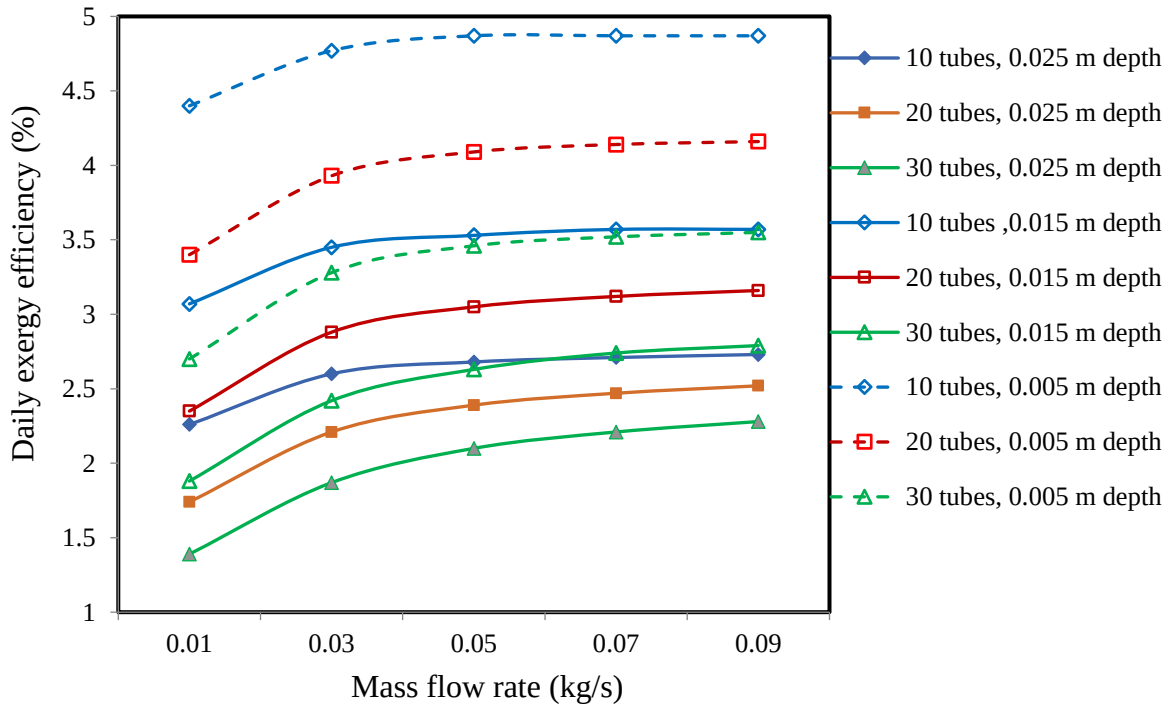

Fig. 3.6b. Effect of ETC size and flow rate on the exergy efficiency with depth of water

To optimize the system for the number of tubes, mass flow rate, and water depth for use in the high-temperature application (~ 90.0 - 99.0°C), the energy balance equations are further simulated with the variation of the number of tubes (10 - 30), flow rate (0.01 - 0.24 kgs^{-1}) and depths. The variation of results obtained is depicted in Fig. 3.7 - 3.8. It is observed that to achieve maximum temperature (≈ 98.5°C) using 10, 20 and 30 tubes, the minimum depth of basin water shall be maintained as 0.005m (10 kg), 0.010m (20 kg), and 0.0125m (25 kg), respectively. The daily yield and efficiency increase exponentially with the faster rate with an increase in flow rate (0.001 to 0.005 kg/s/tube) and then reaches to the maximum value for ~ 0.006 - 0.007 kg/s/tube and then start decreasing with increase in flow rate. No appreciable change in results are observed between ~ 0.006 - 0.007 kg/s/tube flow rate. At smaller flow rates, heat loss increases due to higher temperature, however, it reduces the amount of total energy absorbed. Yield and efficiency increase due to an increase in heat removal and collector efficiency factors as flow rate increases [100]. The decrease in

yield and efficiency with an increase in flow rate > 0.007 kg/s/tube is due to unstable collector outlet temperatures causing an increase in heat loss at a higher flow rate. It reveals that total flow rate through the pump for optimal performance with ETC size of N_c tubes may be maintained as $0.006\times N_c$ kg/s and found in the range reported [101].

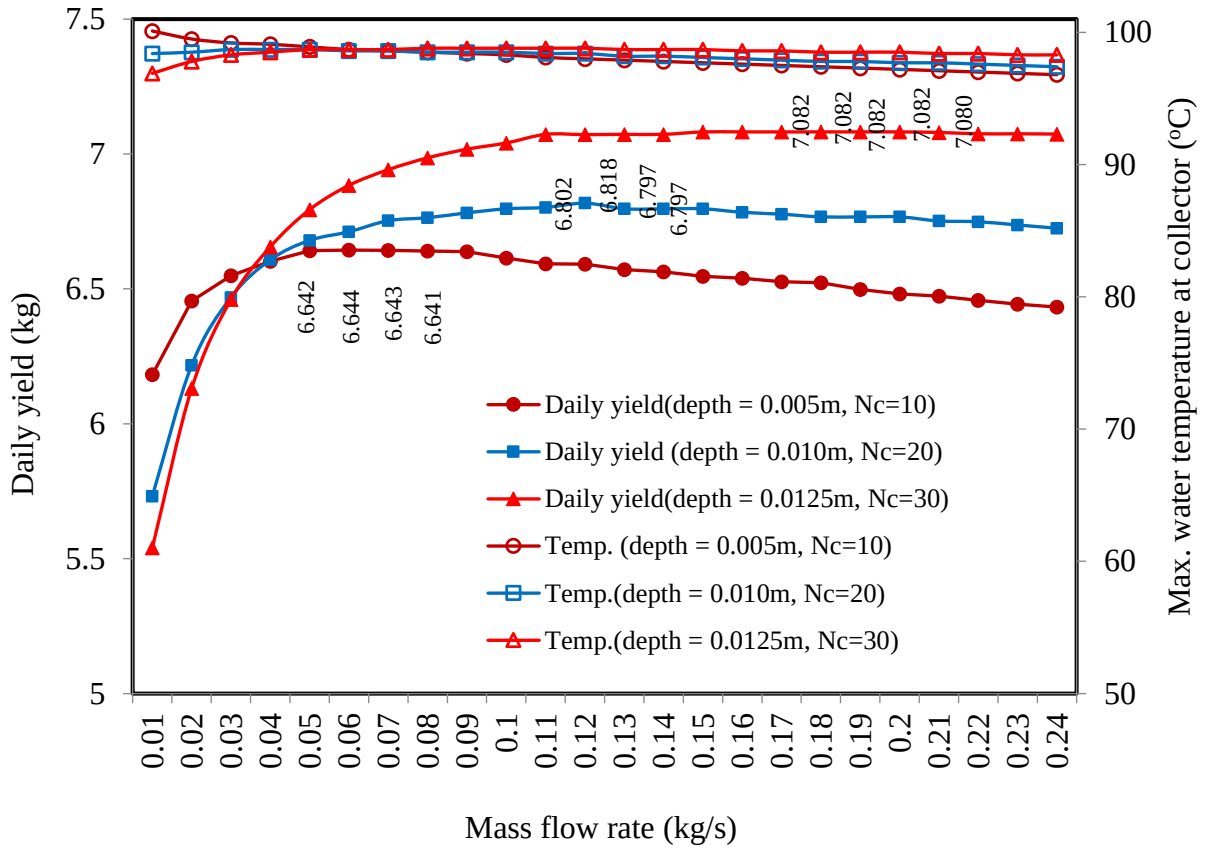

Fig. 3.7. Variation of daily yield and maximum outlet water temperature with mass flow rate and depth of water

Maximum yields of 6.644 kg, 6.618 kg and 7.082 kg while maximum energy efficiencies ~ 33.8%, 25.4% , 20.9% and exergy efficiencies ~ 4.9%, 3.6% and 2.99% are found at 0.06 kgs^{-1} (0.006 kg/s/tube), 0.12 kgs^{-1} (0.006 kg/s/tube) and 0.018 kgs^{-1} (0.006 kg/s/tube) flow rate using 10, 20 and 30 ETC tubes respectively. It is found that at the optimal flow rate, respective yields are ~ 2.64% and ~ 6.62% higher using ETC size of 20

and 30 tubes compared to ETC with 10 tubes. However, respective energy and exergy efficiencies decrease significantly by ~ 24.6% and ~ 38.6%.

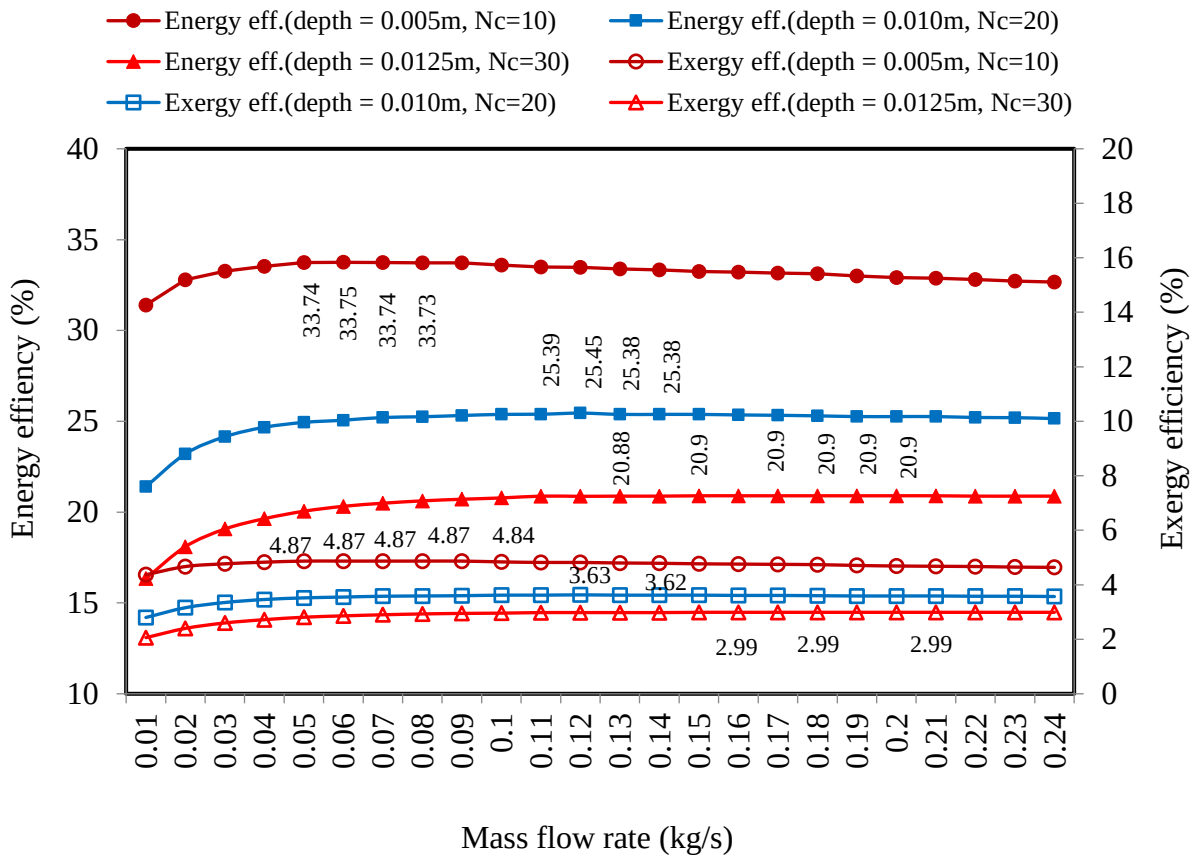

Fig. 3.8. Variation of energy and exergy efficiencies with mass flow rate and depth of water

3.6.3 Performance at optimum flow

Changes in temperatures (hourly) of water in the basin, collector, glass cover, ambient, solar radiation on a typical day at an optimal flow rate (~ 0.006 kg/s/tube) using 10 tubes for given water depth (0.005 m) are depicted in Fig. 3.9. The temperature of basin water is found 2 - 3^{o}C lower than the collector outlet temperature due to mixing with basin water.

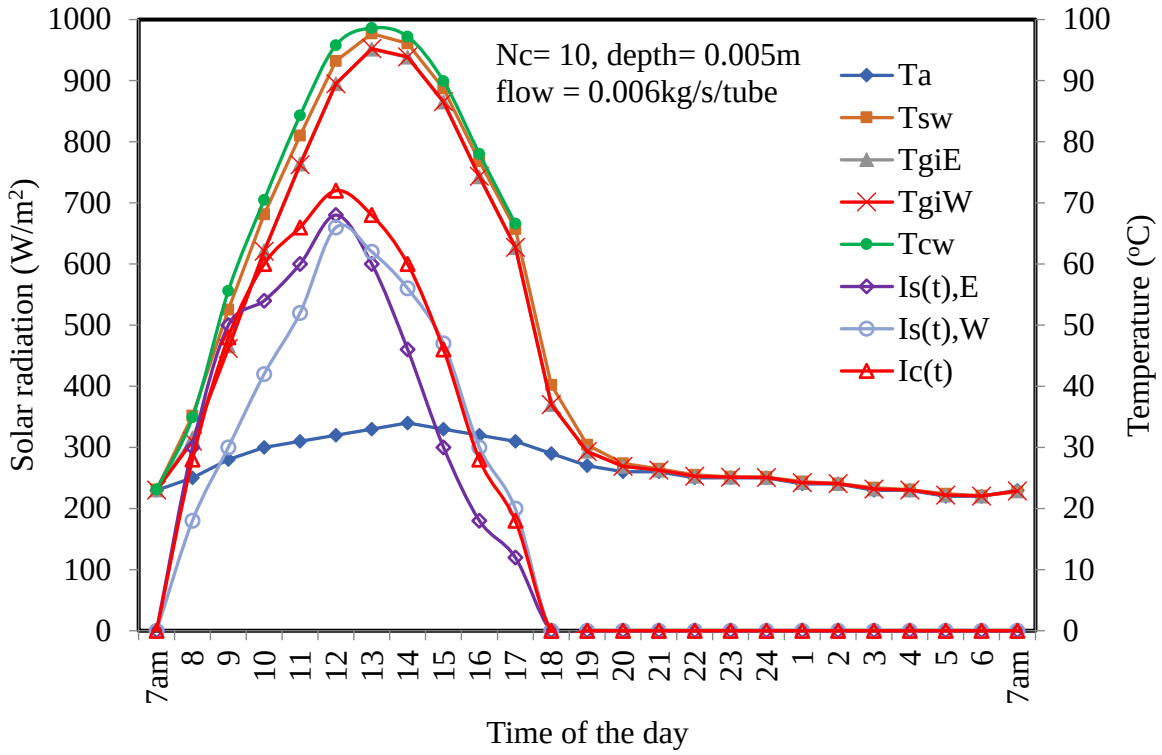

Fig. 3.9. Hourly variation of water and glass cover temperature at optimal flow rate using 10 tubes

Further, the variation of hourly yield and heat transfer coefficients is shown in Fig. 3.10 for a typical day at optimal conditions. It is observed that maximum yield is obtained at around 13:00 hrs., and maximum evaporative heat transfer coefficient at 14:00 hrs whereas maximum radiation occurs at 12:00 hrs. This is due to the dependence of yield on the evaporative heat transfer coefficient (h_{ew}), the difference in T_{sw}-T_{gi} as well as on the time lag between evaporation and condensation. The convective (h_{cw}) and radiative (h_{rw}) h.t.c. contributes to losses and found much lower than evaporative values as anticipated.

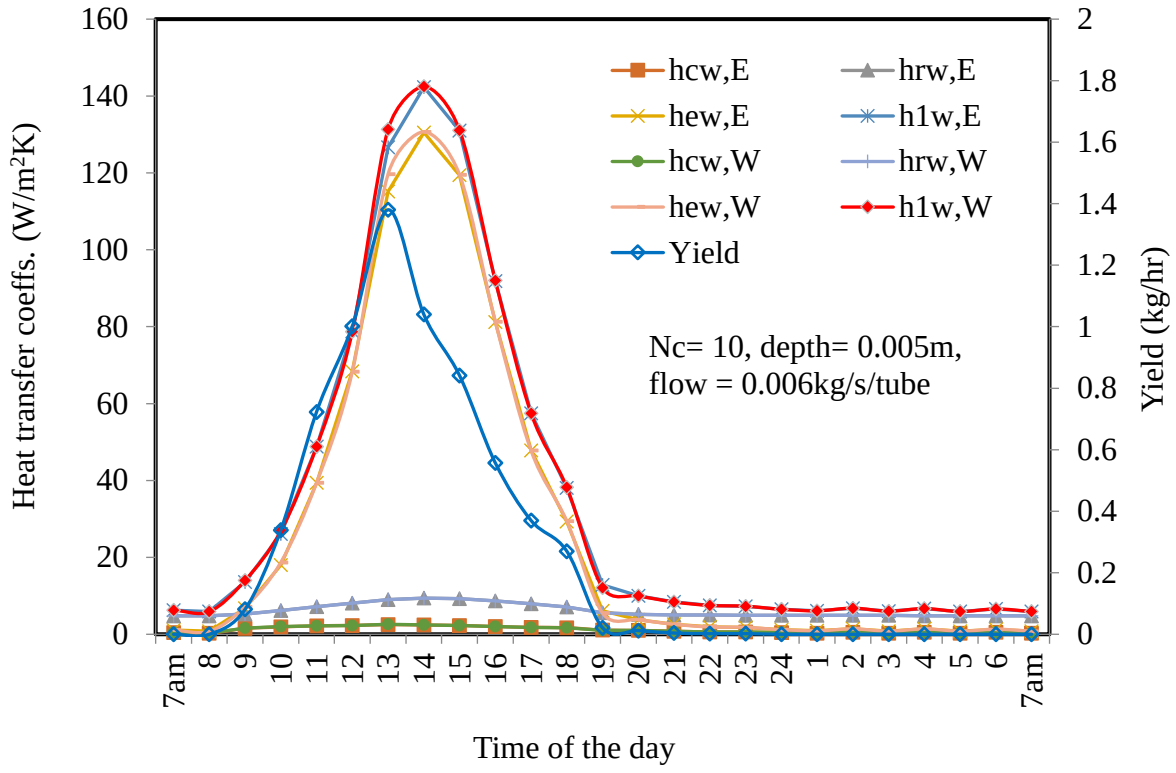

Fig. 3.10. Hourly variation of yield and heat transfer coefficients at optimal flow rate using 10 tubes

3.6.4 Effect of water depth at optimum flow

Variation of hourly yield at an optimal flow rate with water depth using 10 tubes is analyzed and depicted in Fig. 3.11. The hourly yield also depends on the accessibility of solar radiation and the comparative total percentage output at sunshine hours is found to be higher when the quantity of basin water mass is kept lower. The increased basin mass attributes to more sensible storage during the day, which decreases the temperature of basin water reducing the difference between water (T_{sw}) and glass cover (T_{gi}). During off sunshine hours, the reverse phenomena is due to increased thermal energy storage associated with an increase in basin thermal mass, which leads to a higher difference between T_{sw} and T_{gi}. The percentage decrease in day time yield is evaluated in the range of ~ 95.0 - 67.0%, while off sunshine yield increases in the range of ~ 5.0% - 33.0% with an increase in basin water depth from 0.005m (10 kg) to 0.030m (60 kg). It can be noticed

that with further increase in water depth, 0.05m onward (100 kg basin water mass), the cumulative output during day time decreases than obtained during off sunshine hours irrespective of the number of ETC tube integration as shown in Fig. 3.12. This is because of increased thermal storage of water with increasing depth in the basin, which is used during night time yield.

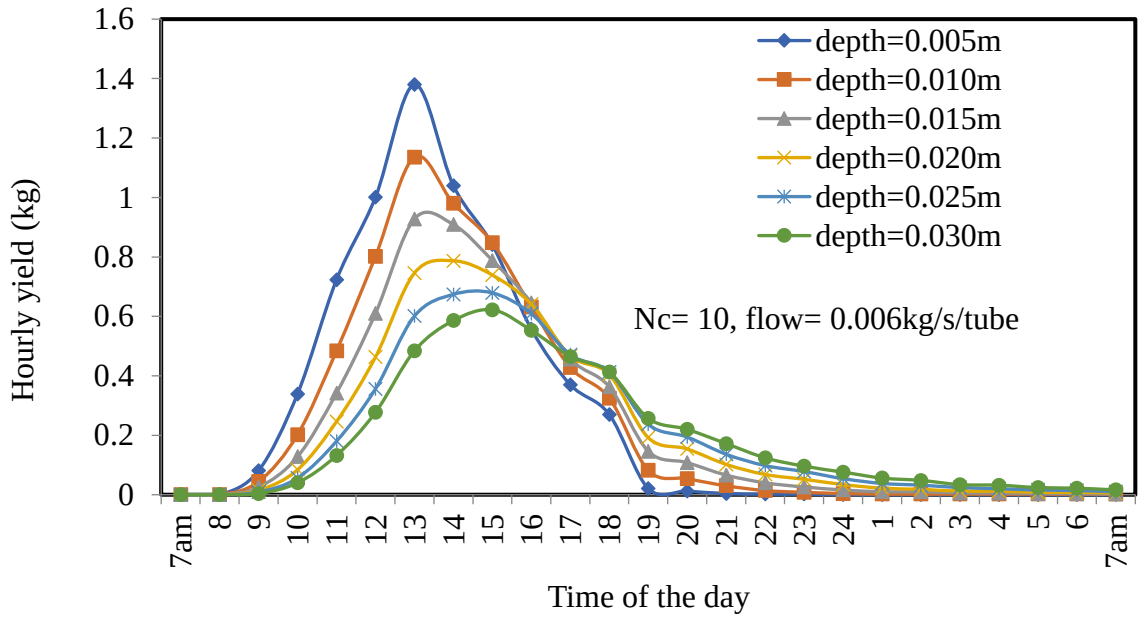

Fig. 3.11. Hourly variation of yield with depth of water at optimal flow rate using 10 tubes

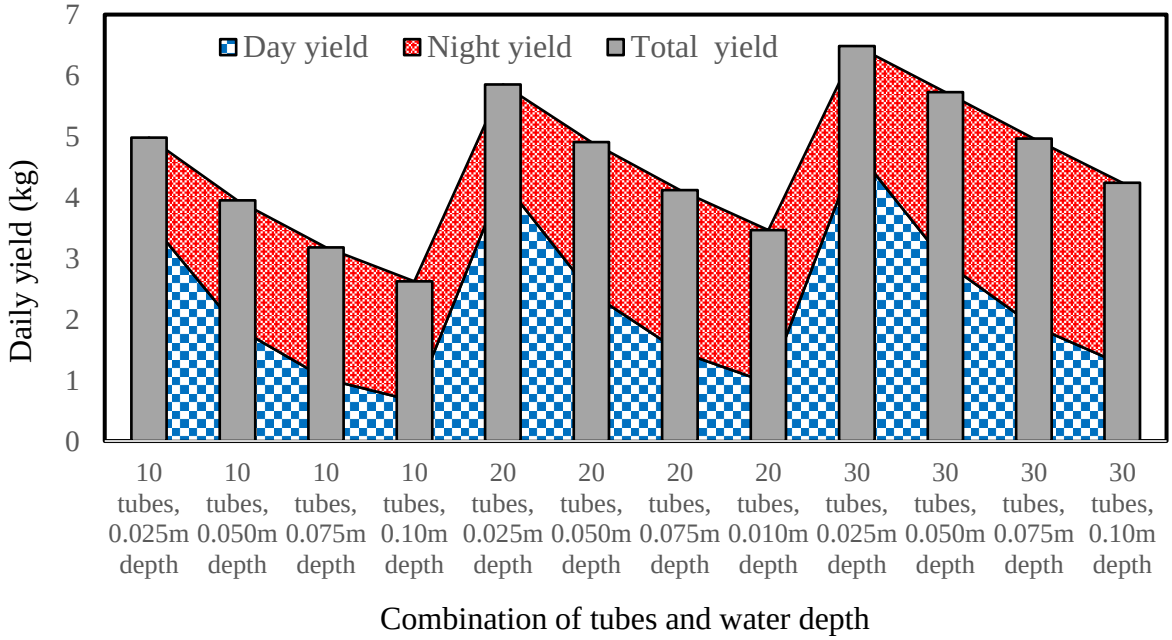

Fig. 3.12. Variation of yield with depth of water at flow rate of 0.006 kg/s/tube

Effect of variable basin water depth ~ 0.005 - 0.030m (i.e. 10.0 - 60.0 kg water) on the daily performance of solar distiller incorporated with ETC (10 tubes) maintaining the optimal flow rate of 0.006 kg/s/tube is shown in Fig. 3.13. The decrease in daily yield is in the range of ~ 6.644 - 4.753 kg, with an increase in the water depth.

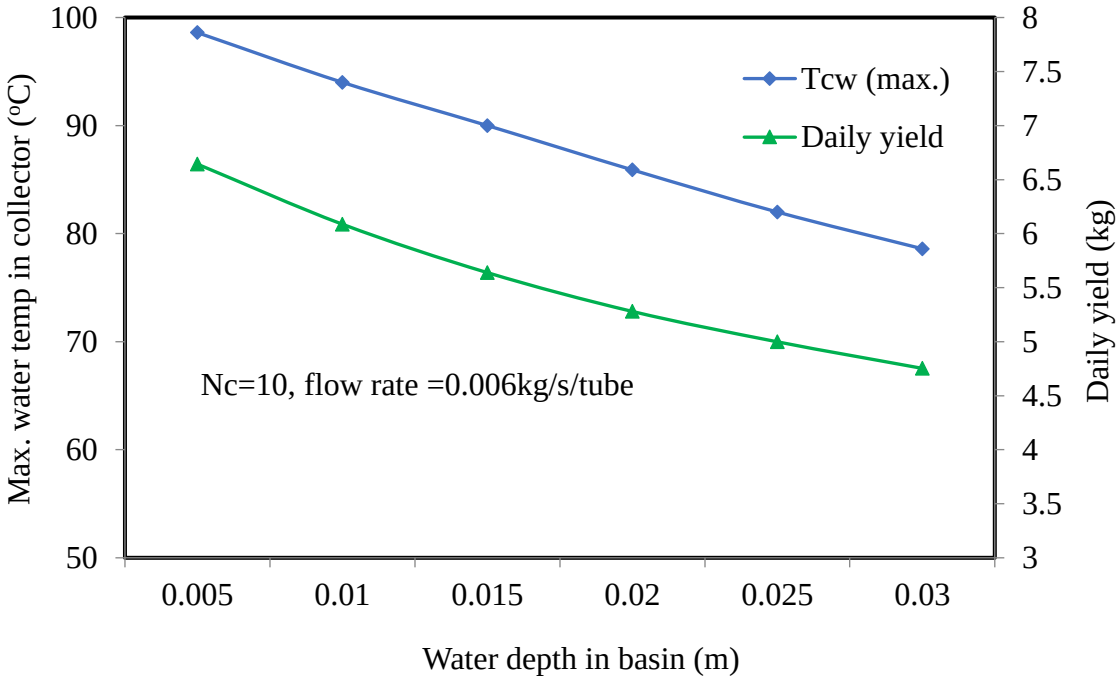

Fig. 3.13. Hourly variation of yield with depth of water at optimal flow rate using 10 tubes

3.6.5 Effect of interception of reflected radiation by the diffuse reflector

The diffuse reflector is aluminum or white painted plate of low cost placed below the tubes to reflect perpendicular radiation incident through interspacing between the tubes. The reflected radiations are received at the back (on the half surface area). Various designs of the reflector are used to increase the performance of the system as well as to reduce the cost. The effect of the reflector on the present design is analyzed and shown in Fig. 3.14. An ETC integrated solar still without reflector plate produces less yield (~ 5.764 kg), energy efficiency (~28.76%) and exergy efficiency (~3.87%), while the system with 0.72 reflectivity-absorptivity yields ~ 6.644 kg with an energy efficiency of ~ 33.74 %, and exergy efficiency

~4.9%. It is found that using the reflector with 80% interception of the reflected radiation (90%), daily yield, energy, and exergy efficiencies are enhanced (~15.0%, 15.0%, and 24% respectively) in comparison to the system without a reflector.

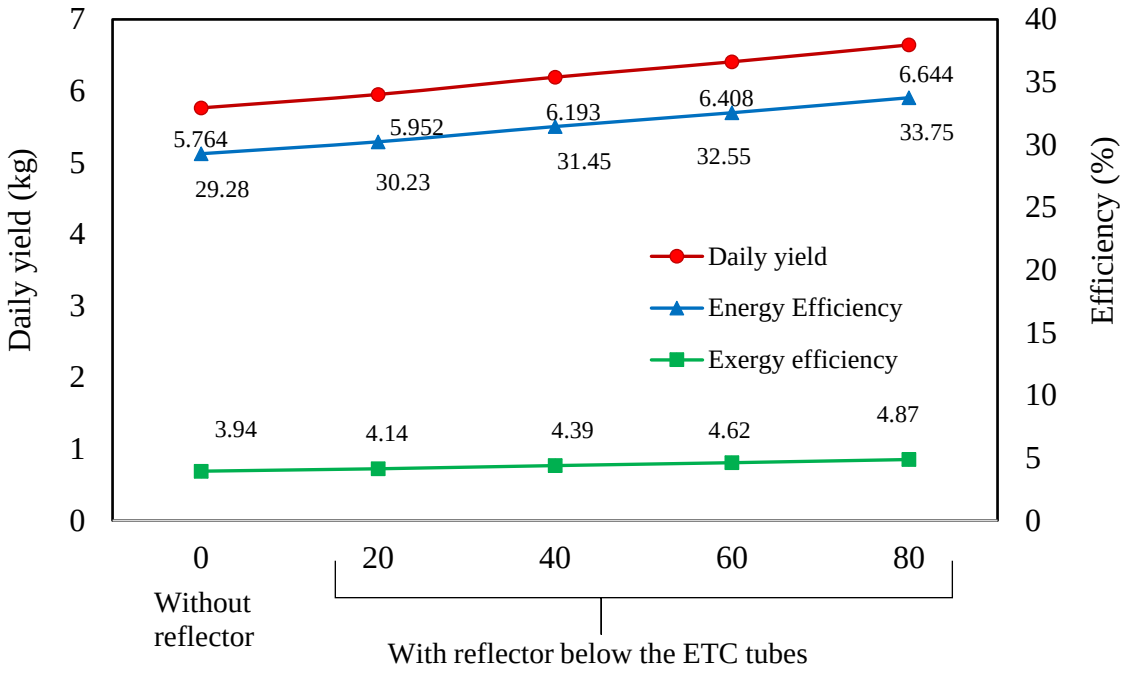

Fig. 3.14. Effect of diffuse reflector on performance at optimal flow rate using 10 tubes

3.7 Conclusions

Based on the performance evaluation carried out post thermal analysis, the following conclusions have been drawn for the modified geometry solar distiller.

(i) The optimal flow rate ranges in ~ 0.006-0.007 kg/s/tube for the prime performance irrespective of parallel tubes integrated with the system. Daily yield, energetic, and exergetic efficiencies are obtained as ~ 6.644 kg, ~ 33.74%, and ~ 4.9% respectively at water depth 0.005m, using 10 tubes at an optimal flow rate.

(ii) Higher yield is obtained with an increment in the number of tubes. It is found that at the optimal flow rate, the system with 20 and 30 tubes yield higher (2.64% and 6.62%)

than that of the ETC with 10 tubes for water temperature ~ 98.5^{o}C attainable at the collector. However, respective energy and exergy efficiencies decrease significantly by ~ 24.6% and ~ 38.6%. Though the increase in the number of tubes yields more, for the marginal gain, the higher investment is dis-favorable.

(iii) With an increment in the depth of water, day time yield decreases, and night time yield increases. At an optimal flow rate, a decrease in daily yield is in the range of ~ 6.644 - 4.753 kg, decrement in energy and exergy efficiencies is found to be in the range of 33.74 - 24.1% and ~ 4.9% - 2.4% respectively, with an increase in water depth from 0.005 - 0.030 m.

(iv) The use of a diffused reflector enhances performance. Comparative daily yield, energy, and exergy efficiencies are enhanced by ~ 15.0%, 15.0%, and 24%, respectively with the use of reflector with 90% reflectivity and tubes with 80% interception.

In the subsequent chapter IV, exhaustive energetic and exergetic performance evaluation of the ETC integrated double slope solar still is carried out.

Chapter-IV

Energetic and Exergetic Performance

4.1 Introduction

In this chapter, an Energy and Exergy analysis of ETC integrated solar still under forced mode has been carried out. The general approach for comparing the performance of different designs of solar stills in different climatic conditions is based on energy efficiency, and in use since the past. The energy analysis is governed by the first law of thermodynamics and provides the knowledge of interexchange without its use in different sections of the system. Cooper [102] presented that the efficiency of ideal solar still of about 60 percent is the upper limit. Experimental work with high-efficiency solar still has shown that in practical installations it is highly unlikely that efficiencies much greater than 50 percent would be attained. Malick et al. [34] reported the maximum energy efficiency of conventional solar still is 30%, which further depends on climatic conditions.

Rosen [103] presented that the results of energy analysis can indicate the main inefficiency within the wrong side of the system because of various limitations. Exergy is a strong instrument to identify the causes, locations, and magnitude of the system inefficiencies. Besides, it provides a precision measurement of how the solar still approaches the ideal. The exergy analysis based on the quality of energy of the thermal system enables us to identify the

sources of irreversibility and inefficiencies to reduce the losses, achieve the maximum resource utilization and capital savings. The exergy-based performance analysis of a system overcomes the limitations of an energy-based analysis.

In recent years, many engineers /researchers have recognized the use of exergy analysis in thermal design as a powerful tool for the evaluation of the thermodynamic systems. Exergetic analysis usually predicts the thermodynamic performance of an energy system and provides a clearer view of energy losses in the system by providing a qualitative and quantitative study of different losses. Several kinds of losses (exergy destruction, lost work, friction, irreversible heat) occur due to irreversibility. Exergy is generally not conserved as energy, it gets destroyed in the system. The exergy efficiency of the system is a true measure of its actual performance since it approaches the ideal and identifies the area of improvement in the system. The exergy transfer can be associated with mass, with work interaction, and with heat interaction, however in solar energy; the exergy transfer takes place with the mass flow and heat interaction.

Dincer [104] highlighted the importance of the exergy as:

- It is a primary tool in best addressing the impact of energy resource utilization on the environment.
- It is an effective method of using the conservation of mass and conservation of energy principles together with the second law of thermodynamics for the design and analysis of energy systems.
- It is a suitable technique for furthering the goal of more efficient energy resource use, for exergy enables us to locate and determine the waste and losses in the system.
- It is an efficient technique revealing whether or not and by how much it is possible to design more efficient energy systems by reducing the inefficiencies in existing systems.
- It is a key component in obtaining sustainable development.

Generally, when the performance of any system is discussed, it revolves around the energy consumption viewpoint. However, energy is conserved, follows the first law of thermodynamics and its conversion does not affect the quantity of energy. During conversions, the quality of energy gets degraded, and this degradation of quality is accounted for as exergy. Exergy is based on the quality and amount of the maximum work potential available in energy concerning to surrounding environmental conditions and follows thermodynamically the second law. There are very limited studies on the exergetic evaluation of solar desalination systems in the literature. Fujisawa and Tani [105] carried out the annual exergy-based evaluation of PV/T hybrid collector and predicted higher output than obtained from an individual PV module or liquid flat plate collector. Lourdes and Carlos [106] carried out the exergy analysis of a solar multi-effect distillation system (SOL-14 plant) located in the Almeria solar research center in southeastern Spain. Sow et al. [107] reported the energetic and exergetic analysis of a triple effect distiller driven by solar energy. This work quantifies the power consumption per unit mass of pure water. He obtained exergetic efficiencies between 19% - 26% for the triple effect system, 17% - 20% for a double effect system, and less than 4% for a single effect system. Hepbasli [108] carried out a key review on exergetic analysis and assessment of renewable energy resources for a sustainable future for solar collectors, solar cooker, solar drying, solar desalination, solar thermal power plants, and hybrid PV thermal solar collector. Torchia–Núñeza et al. [109] analyzed the theoretical exergetic performance for a low depth basin solar still and found exergy efficiencies of the liner, water, and solar still as 12.9%, 6.0%, and 5.0%, respectively. Further, Kumar and Tiwari [99] developed an analytical model and investigated a decrease in exergy efficiency by 36.7% with a decrease in basin liner absorptivity (0.9-0.6). Singh et al. [96] reported the annual energy efficiency as 17.4% from a PV/T integrated double slope still while exergy efficiency as 2.3%. The daily energy and exergy efficiencies on a typical day of summer are found to be 33.8%, and 2.6% respectively,

whereas 27.1% and 1.93% during winter for ETC integrated single slope solar still under forced mode [88]. Ranjan et al. [110] carried out an exergy and energy evaluation on a single slope. It was spotted that the exergy efficiency is smaller than the energy efficiency. They found that the exergy destruction rate in the still components is dependent on the rate of incident insolation with evaluated values equal to 9.7, 62.5, and 386 W/m^2 for the glazing, the water, and the bottom trough, respectively. Deniz [111] reported that FPC coupled single slope solar still attained maximum exergy efficiency as 2.76%. Recently, Hedayati et al. [102] carried out the exergy-based assessment of a double-slope solar still incorporated with base PCM and coupled with a PV-T collector. They reported an increase in yield by 10.6% and the exergy efficiency by 27.0% (summer) and 2.0% (winter), respectively, with an enhancement of flow rate (range 0.001-0.01 kg/s).

In this Chapter, the energetic and exergetic analysis of the system carried out. The analysis is based on experimental climatic data observed round the year 2010 on the respective surface of solar still and collector. Numerical simulation is executed to estimate energy, exergy, fractional exergy, and irreversibility using resource strategies at the optimum flow condition.

4.2 Systematic analysis

Energy and exergy conversion of any system determine its effective utilization during its lifespan. To check the performance, the following parameters are evaluated. The instant energy and exergy efficiencies of an integrated entity can be written as hereunder.

4.2.1 Energy efficiency

The energy efficiency of the solar still is the ratio of energy recovered from the yield to the original energy input from the Sun. The energy efficiency is either based on the overall system together or using solar still alone, accounting total energy fed to the distiller. Therefore,

the overall energy efficiency of the system and solar still alone can be expressed by following eqns. 4.1 and 4.2, respectively.

$$\eta_{i,overall} = \frac{m_{ew,T}\,.\,L}{(I_c\,(t)\,.A_c.+\,I_E(t)A_{gE} + I_W(t)A_{gW})\;3600} \times 100 \quad (4.1)$$

$$\eta_{i,solar\ still} = \frac{m_{ew}\,.\,L}{(\dot{q}_{uc} + I_s(t)\,A_g) \times 3600}\ \times 100 \quad (4.2)$$

Where $q_{uc} = \dot{m}\, c_w(T_{cwo} - T_{cwi})$

4.2.2 Exergetic analysis

According to the second law of thermodynamics, heat can't be completely converted to work cyclically and some part of heat supplied by the system is necessarily rejected to the sink. The maximum part of input energy that can be converted to work is called the available energy and energy rejected to the surrounding is called unavailable energy. Therefore,

Heat supplied (energy) = Available energy (exergy) + unavailable energy (anergy)

Following the exergy matrix presented by various researchers [109-110], the analytical expressions for the exergy associated with different elements of the integrated entity are as under;

The exergy efficiency can be evaluated by employing the general rule hereunder;

$$\eta_{EX} = \frac{Exergy\ out\ from\ component}{Exergy\ Input\ to\ component} = 1 - \frac{\dot{Ex}_{destruction}\ \text{in the component}}{Exergy\ input\ to\ component} \quad (4.3a)$$

$$\eta_{EX} = \frac{\dot{E}\,x_{evap}}{\dot{E}\,x_{in}} = 1 - \frac{\dot{E}\,x_{dest}}{\dot{E}\,x_{in}} \quad (4.3b)$$

The exergy efficiency of the overall system and solar still alone can be written as:

$$\eta_{i,EX,overall} = \frac{h_{ew}\,(T_w - T_g)\,A_b \times \left[1 - \left(\frac{T_a}{T_w}\right)\right]}{[0.933 I_c\,(\mathrm{t})\,A_c + 0.933 I_s\,(\mathrm{t})(A_{gE} + A_{gW})] + W_p} \times 100 \quad (4.4)$$

$$\eta_{iEX,solar\ still} = \frac{h_{ew}(T_w - T_g)A_b \times \left[1 - \left(\frac{T_a}{T_w}\right)\right]}{[\dot{E}x_{c,ETC} + 0.933 I_s\,(\mathrm{t})(A_{gE} + A_{gW})] + W_p} \times 100 \quad (4.5)$$

Daily energy/exergy efficiency can be obtained by taking cumulative values of parameters expressed in eqns. (4.1-4.5).

Patela [112] presented an expression to evaluate the exergy of the sun's radiation I_s (t) concerning the environment as given under:

$$\dot{Ex_{Sun}} = \left(1 - \frac{4}{3} \times \left(\frac{T_a}{T_s}\right) + \frac{1}{3} \times \left(\frac{T_a}{T_s}\right)^4\right) I_s\,(\mathrm{t}) \approx 0.933 I_s\,(\mathrm{t}) \tag{4.6}$$

Total solar exergy input $(\dot{E}x_{in,S})$ on the surface of integrated solar still can be expressed as:

$$\dot{Ex}_{in,S} = 0.933\left[I_s\,(\mathrm{t})\,(A_{gE} + A_{gW}) + I_c(t)A_c\right] \tag{4.7}$$

Exergy transfer between the source (T_{sw}) and the sink (T_a) temperature, can be expressed as:

$$\dot{Ex} = \dot{q}\ \left(1 - \frac{T_a}{T_{sw}}\right) \tag{4.8}$$

4.2.3 Irreversibility

Actual work done in a process is always less than idealized work available in a reversible process. The difference between the two is called irreversibility. In general, the irreversibility can be written in the process/components as under [110];

Irreversibility ($\dot{I}$) = Input exergy - output exergy- accumulated exergy

$$\sum \dot{E}\, x_{in} - \sum \dot{E}\, x_{out} = \sum \dot{E}\, x_{dest}$$

With an increase in the difference in temperature (T_{sw} – T_a) for a local/global environment, the exergy output will be higher. Exergy transfer between the various elements of the integrated unit is pictorially shown in Fig. 4.1.

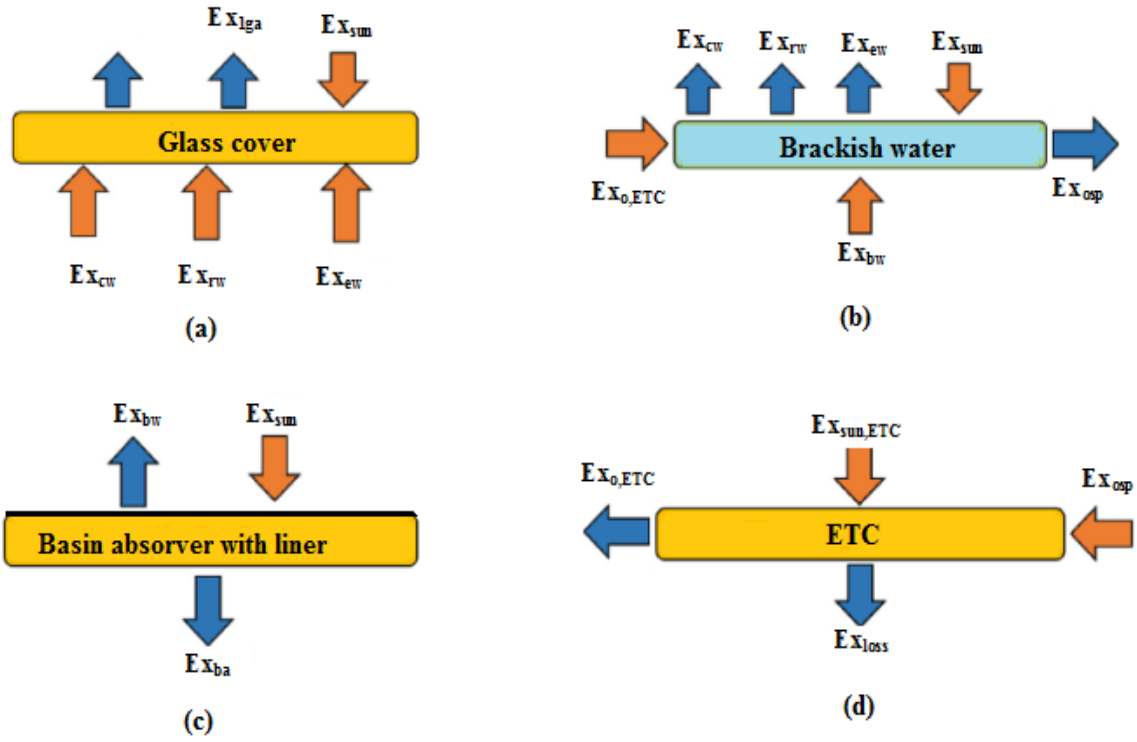

Fig. 4.1. Pictorial representation of exergy transfer in various components

4.2.4 Exergy analysis in the various components

4.2.4.1 Basin liner

The input energy/exergy is the total of solar energy/exergy on the surface of a solar still, the ETC, and used by the pump. A component of basin exergy ($\alpha_b^{'}\,\dot{E}x_{sun}$) is used to raise the water temperature ($\dot{E}x_{bw}$), some is lost to ambient ($\dot{E}x_{ba}$) and remaining destroyed ($\dot{I}_b$):

(a) Exergy absorbed by liner = $\alpha_b'\,\dot{E}x_{sun}$ (4.9a)

(b) Exergy transfer from liner to the ambient is:

$$\dot{E}x_{ba} = h_{ba}\,(T_b - T_a)\,A_b\,\left(1 - \frac{T_a}{T_b}\right) \tag{4.9b}$$

(c) Exergy transfer from liner to the basin water is only during sunshine hours and can be expressed as:

$$\dot{E}x_{bw} = h_{bw}\,(T_b - T_{sw})\,A_b\,\left(1 - \frac{T_a}{T_b}\right) \tag{4.9c}$$

(d) Irreversibility in the basin liner can be written as:

$$\dot{I}_b = \alpha'_b \, \dot{Ex}_{sun} - (\dot{Ex}_{bw} + \dot{Ex}_{ba}) \quad (4.9d)$$

4.2.4.2 Basin water

(a) Solar exergy fed to water mass = $\alpha'_w \, \dot{E}x_{sun} + \dot{E}x_{bw} + \dot{E}x_{c,Etc}$ (4.10a)

(b) Total interior exergy transfer from water - glass cover ($\dot{E}x_{1wg}$) can be given as:

$$\dot{E}x_{1wg} = \dot{E}x_{ewg} + \dot{E}x_{cwg} + \dot{E}x_{rwg} \quad (4.10b)$$

where

$$\dot{E}x_{ewg} = h_{ew}(T_{sw} - T_{gi}) \, A_b \left(1 - \frac{T_a}{T_{sw}}\right) = \dot{m}_w L \left(1 - \frac{T_a}{T_{sw}}\right),$$

$$\dot{E}x_{cwg} = h_{cw} \left(T_{sw} - T_{gi}\right) A_b \left(1 - \frac{T_a}{T_{sw}}\right),$$

and

$$\dot{E}x_{rwg} = h_{rw}(T_{sw} - T_{gi}) A_b \left(1 - \frac{4}{3} \times \left(\frac{T_a}{T_{sw}}\right) + \frac{1}{3} \times \left(\frac{T_a}{T_{sw}}\right)^4\right)$$

where $\dot{E}x_{ewg}$, $\dot{E}x_{cwg}$ and $\dot{E}x_{rwg}$ are the components of associated exergy due to the respective mode of energy transfer from water to the interior glass cover.

(c) Exergy accumulated (day time) in the basin water can be written as:

$$\dot{E}x_{acm} = M_w \, c_w \left[\left(T_{sw} - T_{sw,i}\right) - T_a \, Ln \frac{T_{sw}}{T_{sw,i}}\right] \quad (4.10c)$$

The total accumulated exergy of the day is utilized for night distillation.

(d) Exergy associated with recirculated water at the outlet of solar still.

$$\dot{E} \, x_{osp} = \dot{m} \, C_w \, [(T_{sw} - T_a) - T_a \, Ln \frac{T_{sw}}{T_a}] \quad (4.10d)$$

(e) Irreversibility rate in basin water during day:

$$\dot{I}_w = \left(\alpha'_w \, E \, \dot{x}_{sun} + \dot{E}\dot{x}_{bw} + \dot{Ex}_{oETC}\right) - \left(\dot{Ex}_{acm} + \dot{E}x_{1wg} + \dot{E}x_{osp}\right) \quad (4.10e)$$

4.2.4.3 Glass cover

The glass cover helps in the condensation and rejecting heat to the ambient. There is a marginal variation of glass cover temperature on both sides (East and West). Therefore, an average of both surfaces has been accounted while doing the exergetic estimation.

(a) exergy absorbed = $\alpha_g' \, \dot{E}x_{sun} + \dot{E}x_{1wg}$ (4.11a)

(b) external exergy transfer associated can be evaluated as:

$$\dot{E}x_{1ga} = h_{1ga} \left(T_g - T_a\right) A_g \left(1 - \frac{T_a}{T_g}\right) \quad (4.11b)$$

$$h_{1ga} = 5.7 + 3.8 \; V_a$$

(c) Irreversibility rate in glass cover during the day can be estimated as:

$$\dot{I}_g = \alpha_g' \; E \; \dot{x_{sun}} + \dot{E} x_{1wg} - \dot{E} x_{1ga} \quad (4.11c)$$

4.2.4.4 Collector

Following Jafarkazemi [113], exergy associated with ETC is hereunder:

(a) Exergy input to ETC can be expressed as:

$$\dot{E}x_{iETC} = 0.933 I_c \, (\mathrm{t}) \, A_c \; + \; \dot{E}x_{osp} \quad (4.12a)$$

(b) Exergy feed from collector to basin water $\dot{E}x_{o,ETC}$ can be written as:

$$\dot{E}x_{o,ETC} = \dot{m} \; C_w \left[(T_{sw} - T_a) - T_a Ln \frac{T_{sw}}{T_a}\right] \quad (4.12b)$$

(c) Exergy gain by water during circulating through ETC tubes can be calculated as:

$$\dot{E}x_{c,ETC} = \dot{m} \, C_w \left[(T_{cwo} - T_{cwi}) - T_a Ln \frac{T_{cwo}}{T_{cwi}}\right] \quad (4.12c)$$

(d) Irreversibility rate in ETC can be expressed as:

$$\dot{I}_{ETC} = \dot{E} \; x_{iETC} - E \; x_{c,ETC} \quad (4.12d)$$

4.3 Results and discussion

The system is simulated at an optimal flow rate, using 10 tubes and basin water depth as 0.005m. Equation (4.10b) is used to estimate the exergy fluxes associated with internal energy transfer. The modes of internal exergy flux are evaluated during diurnal and shown in Fig. 4.2. The respective exergy flux shows the dependency on temperature difference and found as ~ 50.6, ~ 2.1, and ~ 4.3 W/m^2, respectively. From the outputs, it's clear that water temperature has a notable effect on the increase of the evaporative exergy and that the temperature difference (T_{sw}-T_{gi}) affected the values and their trend. The trends are found in accordance with reported by Ranjan et al. [110].

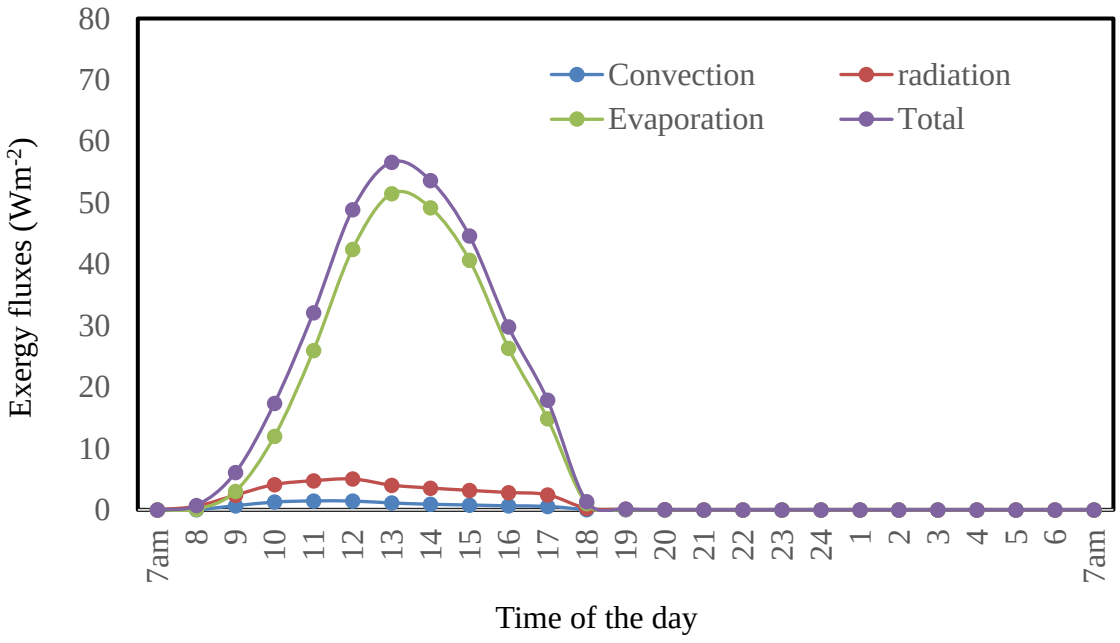

Fig. 4.2. Variation of internal exergy fluxes in different modes

Exergy fractions influence the yield and the change of three modes (i.e. evaporation, convection, and radiation) of internal fractions with water temperature is shown in Fig. 4.3. The evaporative exergy fraction affects the yield, whereas convective and radiative fractions play a negligible impact on productivity. With an enhancement in water temperature, evaporative fraction exergy increases in the range of 0.2 - 0.9, whereas convective and

radiative fraction decreases significantly. When the basin water temperature is at a peak, the evaporative exergy fraction exhibits higher value, whereas convective and radiative fractions exhibit the lowest value. With a decrease in temperature of the water, the radiative and convective flux increases, while evaporative flux decreases, with reduced available exergy. The higher the evaporative exergy fraction, the higher will be the distillate yield and hence exergy efficiency will increase.

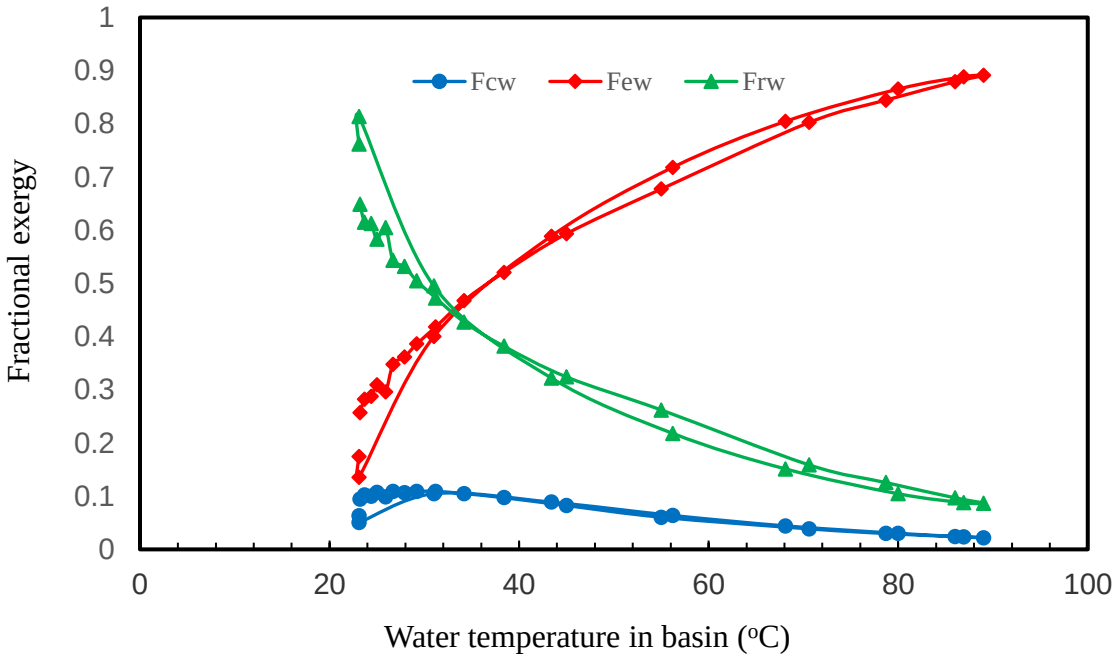

Fig. 4.3. Variation of fractional exergy transfer in different modes within solar still

Figure 4.4 shows the change of instant exergy associated and exergy efficiency of the various components of the system derived using equations referred in section 4.2. It is observed that exergy transportation from liner to the water is negative after 14:00 hrs. This is due to comparatively lower liner temperature than basin water and the associated exergy transfer from water to the basin at low sunshine hours because of high-temperature water feed from the collector end. The range of instant exergy efficiency of the collector during day time is noticed as 0.0% - 45.0%. Whereas, overall instant exergy efficiency of solar still accounting useful exergy output in the form of distillate is estimated in the range of 0.0% - 8.4%.

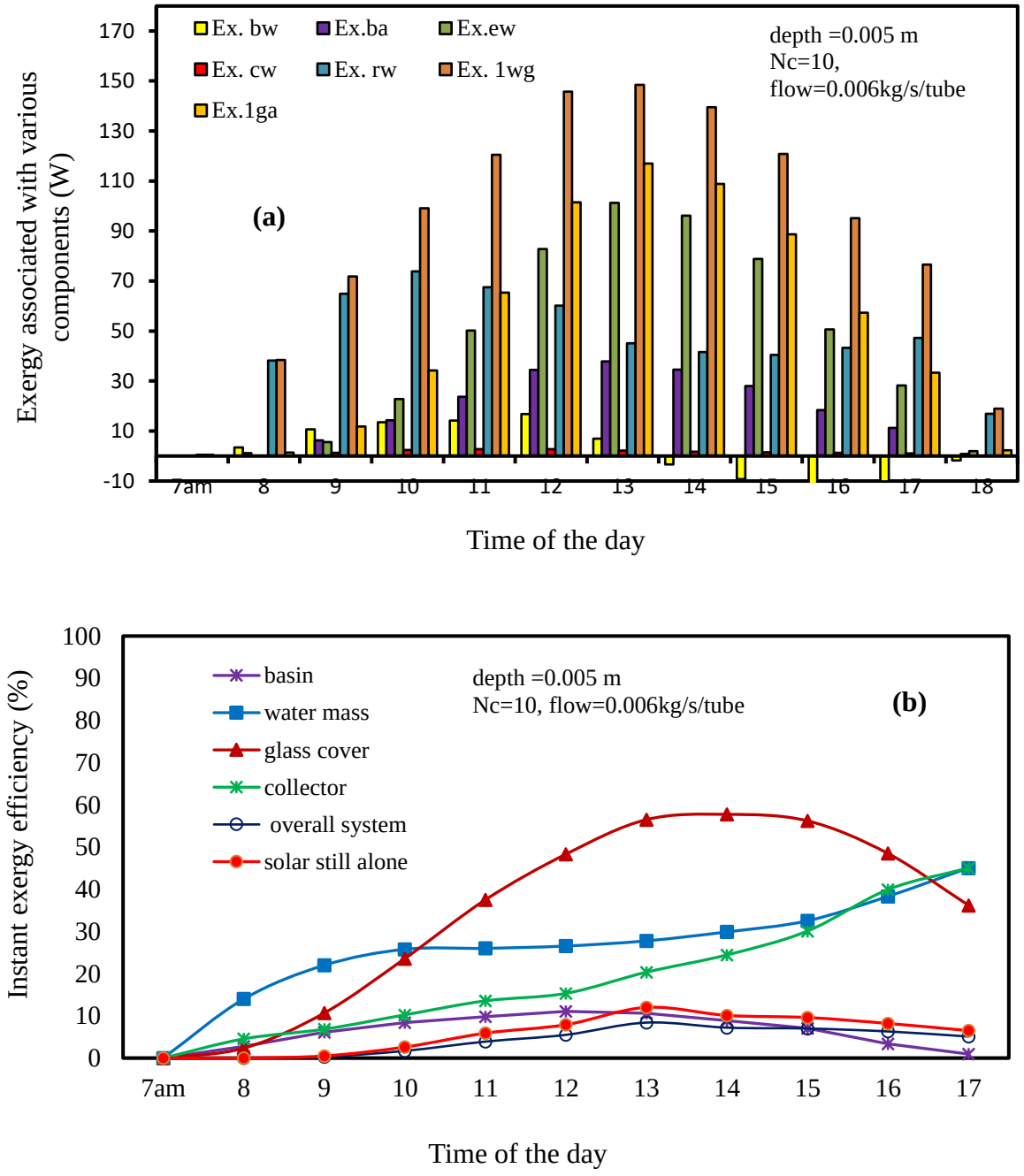

Fig. 4.4. Variation of (a) instant exergy transfer and (b) exergy efficiency of various components

The effect of water depth on instant overall energy and exergy efficiencies during day time is depicted in Fig. 4.5 and observed that the efficiencies are a function of water depth, since a decrease in water temperature leads to a decrease in temperature difference ($T_{sw} - T_{gi}$) with an enhancement of depth, resultantly decreasing the evaporative fractional exergy transfer

and increase in irreversibility. It is further noticed that exergy efficiency is lower than energy efficiency and both decrease with an enhancement of water depth due to higher irreversibility associated with enhancement of thermal storage. A decrease in respective daily efficiencies (energy/exergy) is found in the range of 33.8 - 25.2% and 4.9 - 2.7%, with an enhancement of water depth (0.005 - 0.025 m) due to higher thermal inertia effect with storage water.

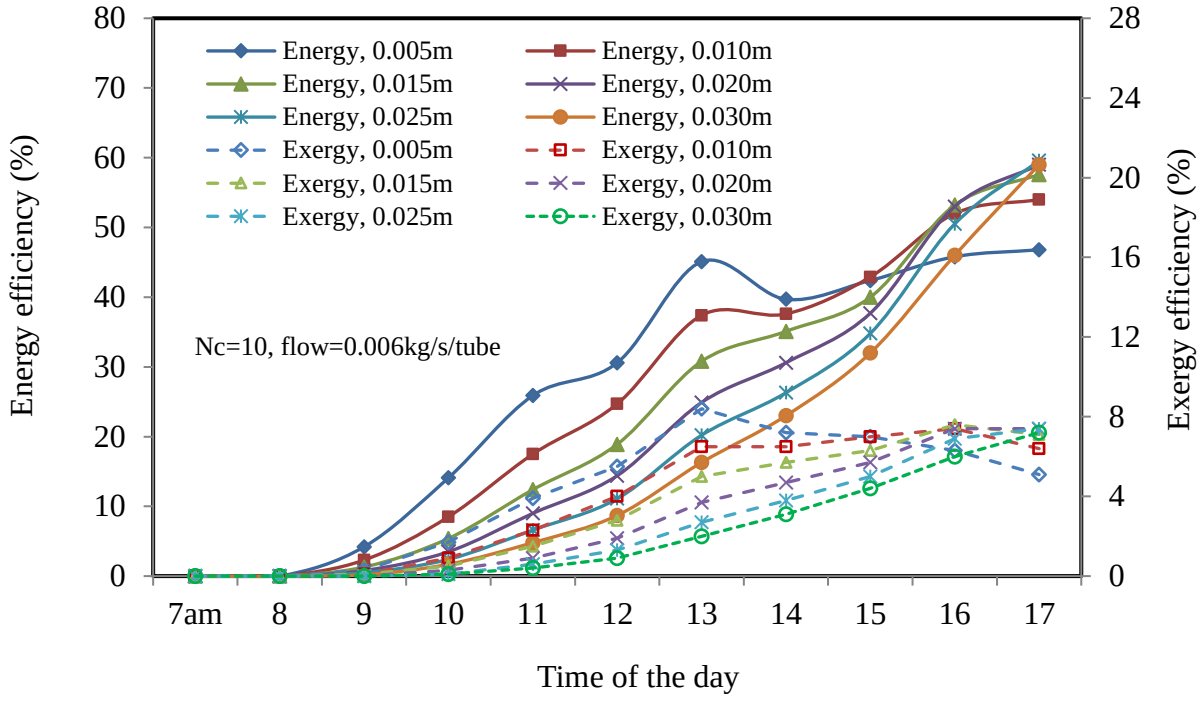

Fig. 4.5. Effect of water depth on overall instant energy and exergy efficiencies

The overall energy/exergy efficiency is observed nearly zero between 7 – 9 am to decrease low yield and low water temperature in the morning hours. As can be seen from the figure that the decrease of energy and exergy efficiency during low sunshine hours is the function of water depth possibly due to a decrease in water temperature while circulating through the ETC collector in the evening hours, which increases the value of term (T_a/T_w).

The effect of water depth on exergy efficiency associated with individual components of the integrated system is shown in Fig. 4.6. There is an insignificant increase in water exergy efficiency with an increase in water depth, due to a total increase in the convective and

radiative fractional exergy compared to the decrease in evaporative fraction as well as reduced exergy input due to decrease in water temperature. The daily exergy efficiency of the liner, water mass, glass cover, collector, overall system, and solar still alone are found as ~ 8.12, ~ 30.1, ~ 41, ~ 18, 4.9, and ~ 7.1%, respectively at 0.005m water depth at optimal conditions. It has been observed that when the exergy input rate is higher than irreversibility, both irreversibility and exergy efficiency increase.

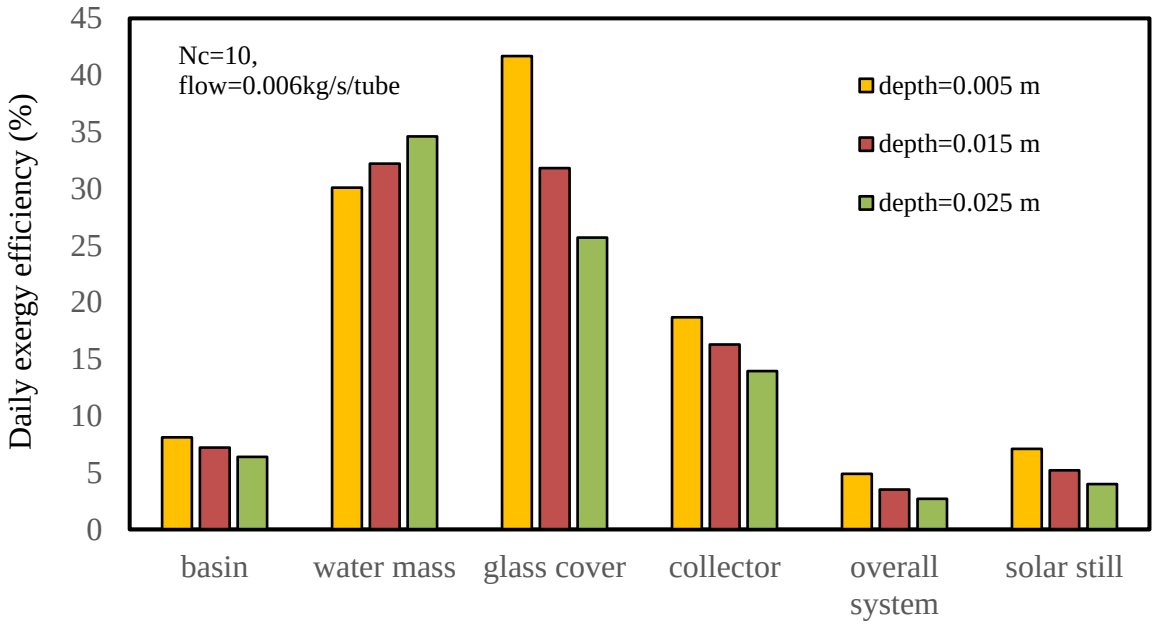

Exergy efficiency of various components of integrated solar still

Fig. 4.6. Daily exergy efficiency of various elements with water depth

Effect of variable basin water depth ~ 0.005 - 0.030m (i.e. 10.0 - 60.0 kg water) on the daily performance of solar distiller incorporated with ETC (10 tubes) maintaining the optimal flow rate of 0.006 kg/s/tube is shown in Fig. 4.7. The decrease in daily yield is in the range of ~ 6.644 - 4.753 kg. The decrement in overall energy and exergy efficiencies of the system ranged within 33.74 - 24.1%, and ~ 4.9-2.4% respectively, with an increase in the water depth.

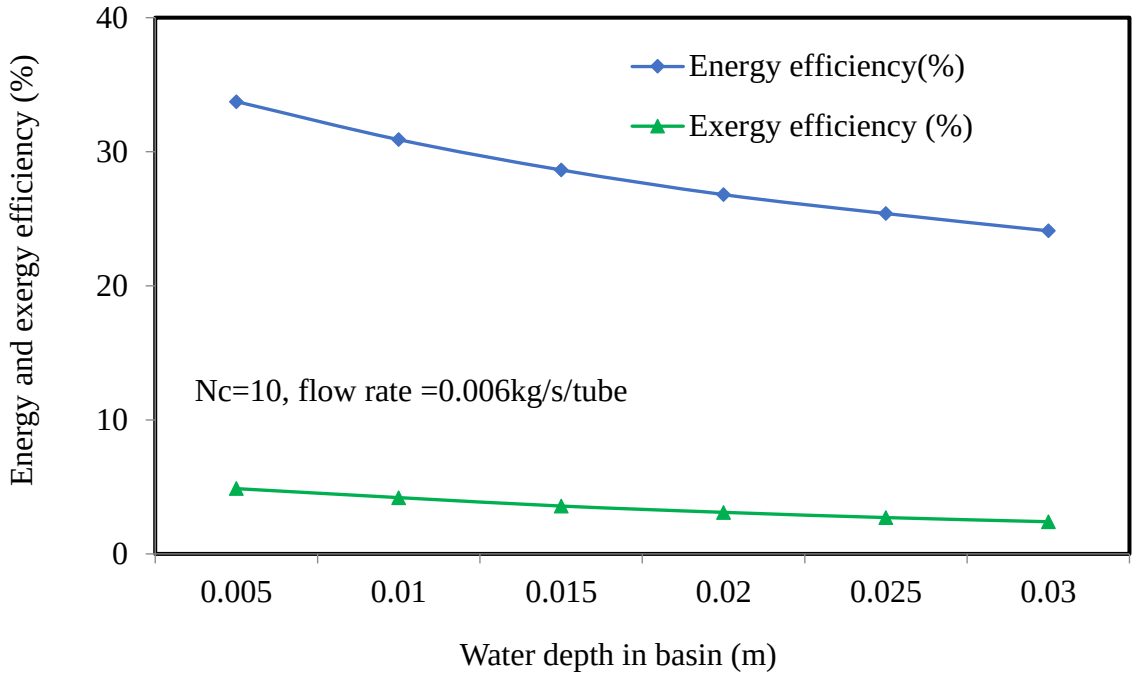

Fig. 4.7. Hourly variation of yield with depth of water at optimal flow rate using 10 tubes

The extent of the irreversibility of the various devices of the solar still at a typical flow rate is depicted in Fig. 4.8. The largest sequential rates of irreversibility during the day time are those of the liner ($\dot{I}_b$), water $(\dot{I}_w)$, and glass cover (I_g). It is further noticed that with the increase in radiation intensity, irreversibility increases due to a low difference in temperature between the entities and environment. The highest irreversibility rates are found as ~ 412, ~ 302, and ~ 98 W at liner, water, and glass cover, respectively. Higher irreversibility at the liner is due to a low heat transfer rate from liner to water as well as to the surrounding. The irreversibility of basin liner can be reduced by using a liner made up of material, tending an instant rise in the temperature to a higher degree. Further, improvement by designing a glass cover of nearly zero heat capacity, the irreversibility of water mass can be reduced due to an increase in inter exergy transfer, but these aspects are a matter of further investigations.

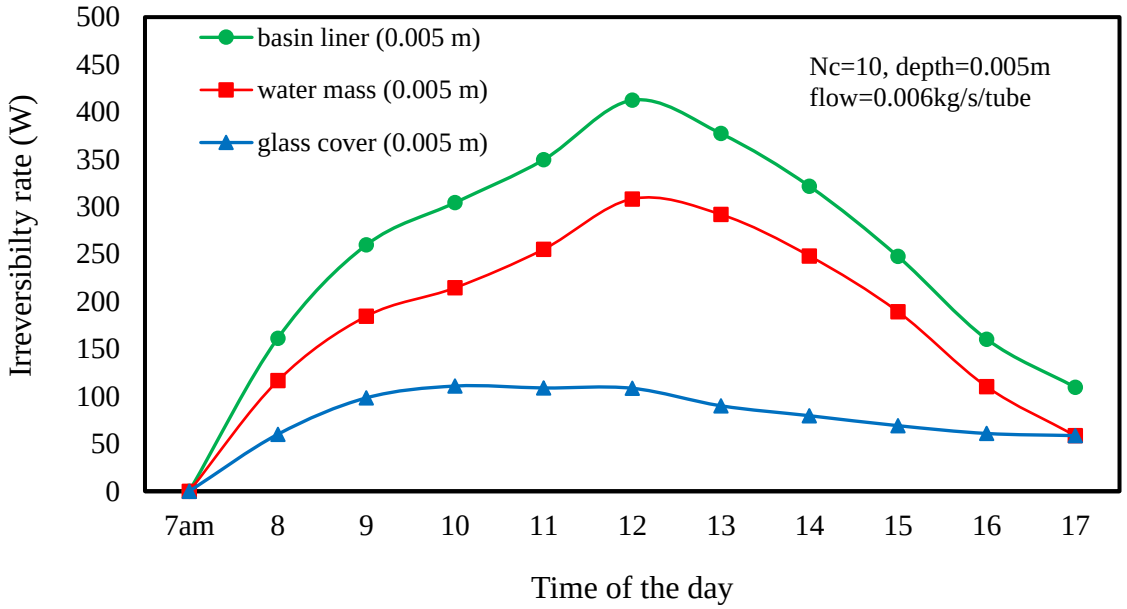

Fig. 4.8. Effect of water depth on the irreversibility of various components of solar still

Fig. 4.9. depicts the performance of the present design of integrated solar still compared to other geometries of active double slope solar stills reported under similar climatic conditions to check the performance viability of the system at water depth ~ 0.025 m (50 kg basin water mass). It is noticed that though the total daily yield obtained from the present design is lower than reported, system energy and exergy efficiencies are significantly higher. The higher yield in other designs is due to the large collection area of FPC used. Therefore, the comparative analysis based on per unit collection surface area of solar energy is evaluated and found that present design yields ~ 1.66 kgm^{-2} distillate with energy and exergy efficiencies as ~ 24.1 % and ~ 2.8%, respectively, substantially higher than other configurations. This is due to the integration of high-performance ETC collectors with solar still. The results reveal that the use of the present geometry of solar still is viable to use for distillate production with a smaller surface area.

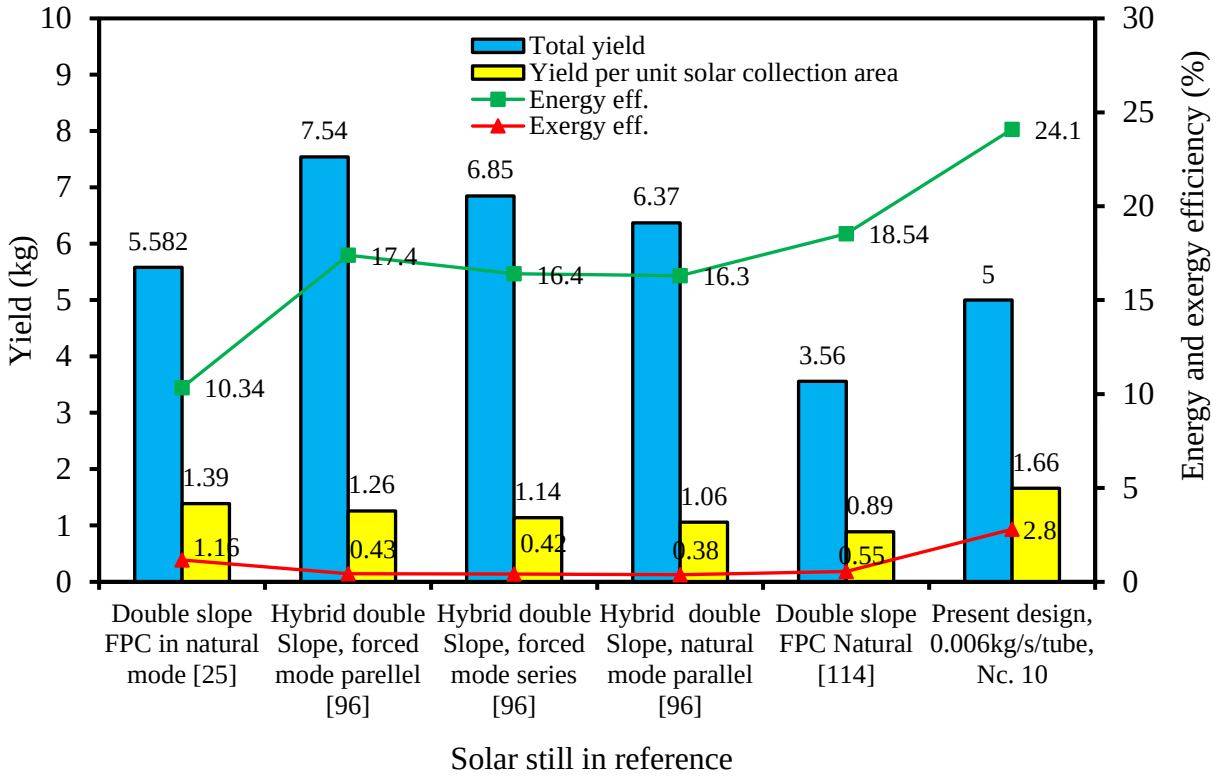

Fig. 4.9. Comparative yield, energy, and exergy efficiency of some designs of double slope active solar still for ~ 0.025 m basin water depth (~ 50 kg mass)

Evaluation of annual output is estimated and variation of monthly yield, energy, and exergy efficiency on a typical day of each month obtained using the climatic data for the year 2010 are depicted in Fig. 4.10. The annual yield ~ 1627 kg in a year is estimated with annual energy and exergy efficiency as ~ 29.5% and ~ 4.2% respectively when the system operates at 0.005m water depth at optimal flow rate with 10 tubes coupled with the collector.

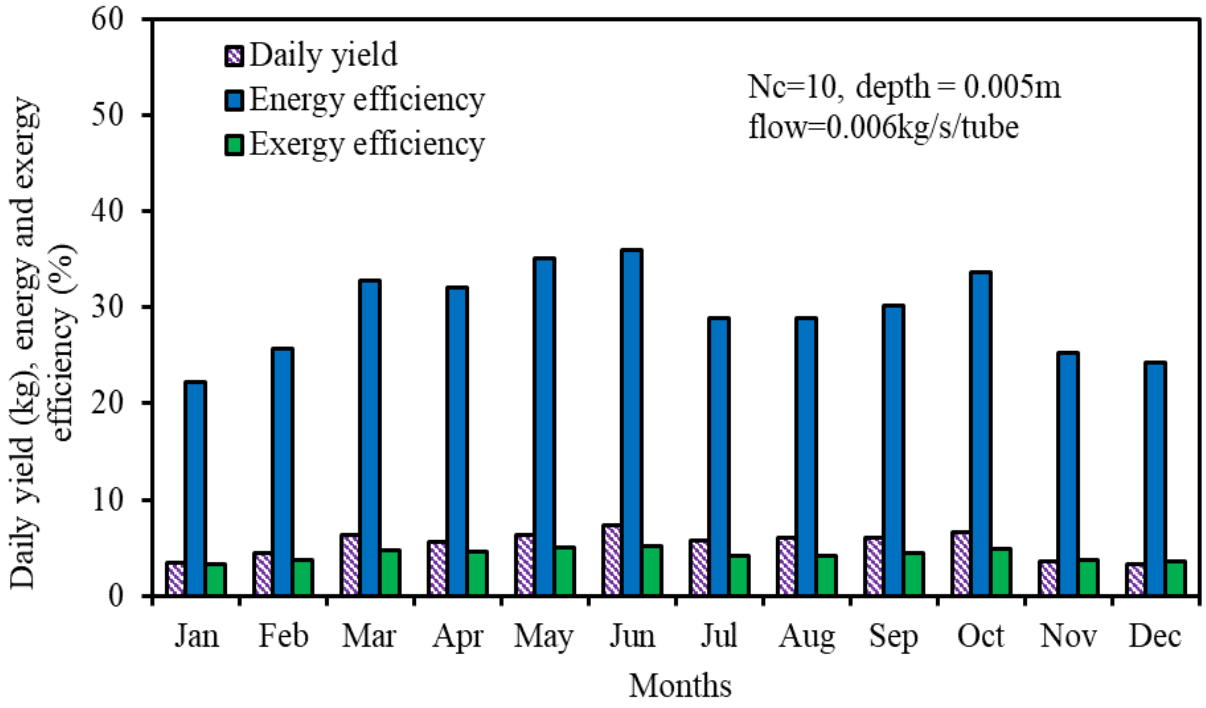

Fig. 4.10. Monthly yield, energy and exergy efficiencies from the solar still for typical parameters

4.4 Conclusions

Based on the aforementioned performance evaluation, the conclusions drawn for the modified geometry of solar distiller are hereunder.

(i) The optimal rate of flow is 0.006 kg/s/tube, irrespective of the number of vacuum tubes connected with ETC. At optimal flow rate system yields ~ 6.644 kg/day with overall energy and exergy efficiencies as ~ 33.8 and ~ 4.9%, respectively. With an increase in the number of tubes, yield increases but the energy and exergy efficiencies drop significantly.

(ii) Daily energy and exergy efficiencies are noticed to decrease in the range of 33.8% - 25.2% and 4.9% - 2.7%, respectively, with an increase in water depth from 0.005 to 0.025m. Evaporative exergy flux is found as ~50.6 W/m^2 and dominates over the convective (~ 2.1 W/m^2) and radiative (~ 4.3 W/m^2) fluxes.

(iii) With an increment in the depth of water, energy and exergy efficiencies are found to be in the range of 33.74 - 24.1% and ~ 4.9% - 2.4% respectively, with an increase in water depth from 0.005-0.030 m.

(iv) Comparative analysis based on per unit collection surface area of solar energy is evaluated and found that present design yields ~ 1.66 kg/m^2 distillate with energetic and exergetic efficiencies as ~ 24.1 % and ~ 2.8%, respectively which is substantially higher than the other designs.

The next Chapter V presents the overall conclusions drawn from the present work and suitable recommendations, suggestions for future work.

Chapter-V

Conclusions and Recommendations

5.1 Conclusions

Based on the present study and findings, the following conclusions are made:

(i) The optimal flow rate ranges ~ 0.006-0.007 kg/s/tube for the optimal performance irrespective of parallel tubes integrated with the system. Daily yield, energetic, and exergetic efficiencies obtained are ~ 6.644 kg, ~ 33.74%, and ~ 4.9% respectively at water depth 0.005m, using 10 tubes at an optimal flow rate.

(ii) Higher yield is obtained with an increment in the number of tubes. It is found that at the optimal flow rate, the system with 20 and 30 tubes yield higher (2.64% and 6.62%) than the ETC size of 10 tubes. However, respective energy and exergy efficiencies decrease significantly by ~ 24.6% and ~ 38.6%.

(iii) Though the increase in the number of tubes yields more, for the marginal gain, the higher investment is dis-favorable.

(iv) At an optimal flow rate, a decrease in daily yield is in the range of ~ 6.644 - 4.753 kg, decrement in energy and exergy efficiencies is found to be in the range of 33.74 24.1% and ~ 4.9%-2.4% respectively, with an increase in water depth from 0.005 - 0.030 m.

(v) The use of a diffused reflector enhances performance. Comparative daily yield, energy, and exergy efficiencies are enhanced by ~ 15.0%, 15.0%, and 24%, respectively with the use of reflector with 90% reflectivity and tubes with 80% interception.

(vi) Comparative analysis based on per unit collection surface area of solar energy is evaluated and it is found that present design yields ~ 1.66 kg/m^2 distillate with energetic and exergetic efficiencies as ~ 24.1% and ~ 2.8%, respectively substantially higher than other designs.

(vii) The annual productivity of yield, energy and exergy are estimated as ~ 1627 kg, ~1131 kWh, and ~ 152 kWh, respectively.

5.2 Recommendations

The study carried out in this dissertation can be extended and future investigators can explore other aspects, which include:

(i) The experimental study on the ETC integrated Double slope solar still can be carried out to know the deviation from the numerical work.

(ii) Performance evaluation of the system can be carried out using different designs of ETC tubes.

(iii) A study can be carried out with an increase in ETC tubes and using a heat exchanger with a fluid of high boiling point.

REFERENCES

[1] Pugsley, A., Zacharopoulos, A., Mondol, J.D., & Smyth, M. (2016). Global applicability of solar desalination. Renewable Energy, 88, 200–219.

[2] Richey, A.S., Thomas, B.F., Lo, M.H., Reager, J.T., Famiglietti, J.S., Voss, K., Swenson, S., & Rodell, M. (2015). Quantifying renewable groundwater stress with GRACE. Water Resources Research, 51(7), 5217–5238.

[3] Fiorenza, G., Sharma, V.K., & Braccio, G. (2003). Techno-economic evaluation of a solar powered water desalination plant. Energy Conversion and Management, 44(14), 2217–2240.

[4] Rajagopalan, B., & Brown, C. (2012). Chapter 15 - State of the resource: Quantity, in: Managing Water under Uncertainty and Risk. The United Nations World Water Development Report 4, UNESCO, United Nations Educational, Scientific and Cultural Organization, Paris, 381-395.

[5] Howe, E.D., & Tleimat, B.W. (1974). Twenty Years of work on solar distillation at the University of California. Solar Energy, 16(2), 97-105.

[6] Kalogirou, S.A. (2005). Seawater desalination using renewable energy sources. Progress in Energy and Combustion Science, 31(3), 242–281.

[7] Micale, G., Cipollina, A., & Rizzui, L. (2009). Seawater Desalination for Freshwater Production. In: Seawater Desalination, Green Energy and Technology, Springer, Heidelberg, Germany.

[8] National Research Council, Committee on Advancing Desalination Technology, Desalination, A National perspective. The National Academies Press, Washington, D.C., 2008.

[9] Hossain, F., Degu, A.M., Yigzaw, W., Burian, S., Niyogi, D., Shepherd, J.M., & Pielke Sr, R. (2012). Climate Feedback–Based Provisions for Dam Design, Operations, and Water Management in the 21st Century. Journal of Hydrologic Engineering, 17(8), 837-850.

[10] WHO/UNICEF/JMP, (2017). Progress on drinking water, sanitation and hygiene: 2017 update and SDG baselines. Geneva: World Health Organization (WHO) and the United Nations Children's Fund (UNICEF).

[11] WRI (World Resources Institute), (2019). WRI Aqueduct website. www.wri.org/aqueduct.

[12] UNICEF/WHO, (2008). Progress on drinking water and sanitation: special focus on sanitation.

[13] Samee, M.A., Mirza, U.K., Majeed, T., & Ahmad, N. (2007). Design and performance of a simple single basin solar still. Renewable and Sustainable Energy Reviews, 11(3), 543-549.

[14] Tsilingiris, P.T. (2007). The influence of binary mixture thermo physical properties in the analysis of heat and mass transfer processes in solar distillation systems. Solar Energy, 81(12), 1482-1491.

[15] Delyannis, E. (2003). Historic back ground of desalination and renewable energies. Solar Energy, 75(5), 357–366.

[16] Tiwari, G.N., Singh, H.N., & Tripathi, R. (2003). Present status of solar distillation. Solar Energy, 75(5), 367–373.

[17] Mathioulakis, E., Belessiotis, V., & Delyannis, E. (2007). Desalination by using alternative energy: Review and state-of-the-art. Desalination, 203(1), 346–365.

[18] Sampathkumar, K., Arjunan, T.V., Pitchandi, P., & Senthilkumar, P. (2010). Active solar distillation - A detailed review. Renewable and Sustainable Energy Reviews, 14(6), 1503–1526.

[19] Tiwari, G.N., & Tiwari, A.K. (2007). Solar distillation practice in water desalination systems. Anamaya Publication Ltd, New Delhi, India.

[20] Dwivedi, V.K., & Tiwari, G.N. (2008). Annual energy and exergy analysis of single and double slope solar stills. Trends in applied science research, 3(3), 225-241.

[21] Bloemer, J.W., Irwin, J.R., Eibling, J.A., & Lof, G.O.G. (1965). A practical basin type solar still. Solar Energy, 9(4), 197-200.

[22] Delyannis, A., & Delyannis, E. (1983). Recent solar distillation developments. Desalination, 45(2), 361-369.

[23] Yadav, Y.P., & Tiwari, G.N. (1987). Monthly comparative performance of solar stills of various designs. Desalination, 67, 565-578.

[24] Clark, J.A. (1990). The steady-state performance of a solar still. Solar Energy, 44(1), 43-49.

[25] Dwivedi, V.K., & Tiwari, G.N. (2010). Experimental validation of thermal model of a double slope active solar still under natural circulation mode. Desalination, 250(1), 49-55.

[26] Rai, S.N., & Tiwari, G.N. (1983). Single basin solar still coupled with flat plate collector. Energy Conversion and Management, 23(3), 145-149.

[27] Fernandez, J., & Chargoy, N. (1990). Multi-stage, indirectly heated solar still. Solar Energy, 44(4), 43-49.

[28] Lawrence, S.A., & Tiwari, G.N. (1990). Theoretical evaluation of solar distillation and natural circulation with heat exchange. Energy Conversion and Management, 30(3), 205-213.

[29] Zaki, G.M., Al-Turki, A., & AI-Fatani, M. (1992). Experimental investigation on concentrator assisted solar stills. International Journal of Solar Energy, 11(3-4), 193-199.

[30] El-Sebaii, A.A., Yaghmour, S.J., Al-Hazmi, F.S., Faidah, Adel S., Al-Marzouki, F.M., & Al-Ghamdi, A.A. (2009). Active single basin solar still with a sensible storage medium. Desalination, 249(2), 966-706.

[31] Badran, O.O., & Al-Tahainesh, H.A. (2005). The Effect of coupling flat-plate collector on the solar still productivity. Desalination, 183(1-3), 137-142.

[32] Tleimat, B.W., & Howe, E.D. (1966). Nocturnal production of solar distillers. Solar Energy, 10(2), 61-66.

[33] Tiwari, G.N., Dimri, V., Singh, U., Chel, A., & Sarkar, B. (2007). Comparative thermal performance evaluation of an active solar distillation system. International Journal of Energy Research, 31(15), 1465–1482.

[34] Malik, M.A.S., Tiwari, G.N., Kumar, A., & Sodha, M.S. (1982). Solar distillation, Oxford UK, Pergamon press, 8-17.

[35] Sharma, V.B., & Mullick, S.C. (1991). Estimation of heat transfer coefficients, the upward heat flow and evaporation in solar still. Journal of Solar Energy Engineering, 113(1), 36-41.

[36] Swinbank, W.E., (1963). Long-wave radiation from clear skies. Quarterly Journal of the Royal Meteorological Society, 89(381), 339-348.

[37] Mustacchi, C., & Vincenzo, C. (1978). Solar desalination - Design, performance and economics. Sogesta Institute of Dichimica Applicate, Rome.

[38] Natu, G.L., Goghari, H.D., & Gomkale, S.D. (1979). Solar distillation plant at Awania, Gujarat, India. Desalination, 31(1-3), 435-441.

[39] Della Porta, G.B. (1589). Magiac naturalis libri XX, Napoli.

[40] Lavoisier, A.L. (1862). Oeuvres de Lavoisier, son excellence leministre de I'instruction publique et de cultes, 3, Takle 9.

[41] Mouchot, A. (1869). La Chaleur Solavie et ses Applications, Gauthier – Villars, paris.

[42] Nebbia, G., & Mennozi, G. (1966). A short history of water desalination, Acque Dolac Dal Mare, II Inchiesta internazionole, in proceeding of International Symposium, pp. 129, Milano.

[43] Sfeir, A.A., & Guarracina, G. (1981). Ingenierie des Systemes Solaires, Applications Habitat, Technique et. Documentation, Paris.

[44] Abbot, C.G. (1938). Solar distilling apparatus, U S Patent No. 2, 141, 330.

[45] Telkes, M. (1945). Solar distiller for life rafts, US Office Technical Service, Report No. 5225 IT, OSRD, Final Report to National Defense Resarch Communication,11.2-11.24.

[46] Gomkale, S.D. (1988). Solar distillation as a means to provide Indian villages with drinking water. Desalination, 69(2), 171-176.

[47] Talbert, S.G., Eibling, J.A., & Lof, G.O.G. (1970). Manual on solar distillation of saline water. R&D Progress Report No. 546, US Department of the Interior.

[48] Delyannis, A., & Delyannis, E.A. (1973). Solar distillation plant of high capacity. Proceedings of 4th International Symposium on Fresh Water from Sea, 4, 487.

[49] Delyannis, A.A. (1965). Solar stills provide an island's inhabitants with water. Sun at Work, 10(1), 6-8.

[50] Delyannis, A., & Piperoglou, E. (1968). The Patmos solar distillation plant: technical note. Solar Energy, 12(1), 113-114.

[51] Delyannis, A., & Delyannis, E.A. (1970). Solar Desalting. Journal of Chemical Engineering, 19, 136-140.

[52] Singh, A.K., Tiwari, G.N., Sharma, P.B., & Khan, E. (1995). Optimization of orientation for higher yield of solar still for a given location. Energy Conversion and Management, 36(3), 175-181.

[53] Rajvanshi, A.K. (1981). Effect of various dyes on solar distillation. Solar Energy, 27(1), 51-65.

[54] Hijleh, B.A., & Mousa, H. (1997). Water film cooling over the glass cover of a solar still including evaporation effect. Energy, 22(1), 43-48.

[55] Cipollina, A., Sommariva., & Giorgio, M. (2005). Efficiency increase in thermal desalination plants by matching thermal and solar distillation: theoretical analysis. Desalination, 183(1-3), 127-136.

[56] Cooper, P.I. (1969). Digital simulation of transient solar still process. Solar Energy, 12(3), 313-331.

[57] El-Sebaii, A.A. (1998). Parametric study of a vertical solar still. Energy Conversion and Management, 39(13), 1303-1315.

[58] Hamdan, M.A., Musa, A.M., & Jubran, B.A. (1999). Performance of solar still under Jordan climatic conditions. Energy Conversion and Management, 40(5), 495-503.

[59] Kumar, S., & Tiwari, G.N. (1998). Optimization of collector and basin areas for a higher yield for active solar stills. Desalination, 116(1), 1-9.

[60] Tripathi, R., & Tiwari, G.N. (2006). Thermal modelling of passive and active solar stills for different depth of water by using concept of solar fraction. Solar Energy, 80(8), 956-967.

[61] Minasian, A., & Al-Karaghouli, A.A. (1995). An improved solar still: the wick basin type. Energy Conversion and Management, 36(3), 213-217.

[62] Garg, H.P., & Mann, H.S. (1976). Effect of climatic, operational and design parameters on the year-round performance of single sloped and double sloped solar still under Indian and arid zone condition. Solar Energy, 18(2), 159-163.

[63] Tiwari, G.N., & Madhuri. (1987). Effect of water depth on daily yield of the still. Desalination, 61(1), 67-75.

[64] Tripathi, R., & Tiwari, G.N. (2005). Effect of water depth on internal heat and mass transfer for active solar distillation. Desalination, 173(2), 187-200.

[65] Boukar, M., & Harmim, A. (2001). Effect of climatic conditions on the performance of a simple basin solar still: A comparative study. Desalination, 137(1-3), 15–22.

[66] Al-Hinai, H., Al-Nassri, M.S., & Jubran, B.A. (2002). Effect of climatic, design and operational parameters on the yield of a simple solar still. Energy Conversion and Management, 43(13), 1639–1650.

[67] Tanaka, H., & Nakatake, Y. (2005). A simple and highly productive solar still: a vertical multiple-effect diffusion-type solar still coupled with a flat-plate mirror. Desalination, 173(3), 287-300.

[68] Dunkle, R.V. (1961). Solar water distillation: the roof type solar still and a multi effect diffusion still. International developments in heat transfer A.S.M.E Proceedings of International Heat Transfer, 5, 895-902.

[69] El-Sebaii, A.A. (2004). Effect of wind speed on active and passive solar stills. Energy Conversion and Management, 45(7-8), 1187-1204.

[70] Badran, O.O. (2007). Experimental study of the enhancement parameters on a single slope still productivity. Desalination, 209(1-3), 136-143.

[71] Kabbi, A., & Nafila, S., (2007). Impact of temperature difference (water-solar collector) on solar still global efficiency. Desalination, 209(1-3), 298-305.

[72] Kudish, A.I., Evseeva, E.G., Walter, G., & Thomas, P. (2003). Simulation study on a solar desalination system utilizing an evaporator/condenser chamber. Energy Conversion and Management, 44(10), 1653-1670.

[73] Garg, H.P., Agarwal, R.K., & Joshi, J.C. (1994). Experimental study on a hybrid photovoltaic thermal solar water heater and its performance prediction. Energy Conversion and Management, 35(7), 621-633.

[74] Chow, T.T., (2003). Performance analysis of photovoltaic–thermal collector by explicit dynamic model. Solar Energy, 75(2), 143-152.

[75] Kumar, S., & Tiwari, A. (2008). An experimental study of hybrid photovoltaic thermal (PVT) active solar still. International Journal of Energy Research, 32(9), 847-858.

[76] Reddy, K.S., & Sharon H. (2017). Energy–environment–economic investigations on evacuated active multiple stage series flow solar distillation unit for potable water production. Energy Conversion and Management, 151, 259–285.

[77] Bait, O., & Si-Ameur, M. (2018). Enhanced heat and mass transfer in solar stills using nanofluids: A review. Solar Energy, 170, 694–722.

[78] Kumar, S., & Tiwari, A. (2010). Design, fabrication and performance of a hybrid photovoltaic/thermal (PV/T) active solar still. Energy Conversion and Management. 51(6), 1219–1229.

[79] Etawil, M.A., & Omara, Z.M. (2014). Enhancing the solar still performance using solar photovoltaic, flat plate collector and hot air. Desalination 349, 1-9.

[80] Feilizadeh, M., Soltanieh, M., Karimi Estahbanati, M.R., Jafarpur, K., & Ashrafmansouri, S.S. (2017). Optimization of geometrical dimensions of single-slope basin-type solar stills. Desalination, 424, 159-168.

[81] Singh, D.B., & Tiwari, G.N. (2017). Performance analysis of basin type solar stills integrated with N identical photovoltaic thermal (PVT) compound parabolic concentrator (CPC) collectors: A comparative study. Solar Energy, 142, 144-158.

[82] Morrison, G.L., Budihardjoa, I., & Behnia, M. (2005). Measurement and simulation of flow rate in a water-in-glass evacuated tube solar water heater. Solar Energy, 78(2), 257–267.

[83] Glembin, J., Rockendorf, G., & Scheuren, J. (2010). Internal thermal coupling in direct-flow coaxial vacuum tube collectors. Solar Energy, 84(7), 1137–1146.

[84] Dev, R., & Tiwari, G.N. (2012). Annual performance of evacuated tubular collector integrated solar still. Desalination and Water Treatment, 41(1-3), 204–223.

[85] Sato, A.I., Scalon, V.L., & Padilha, A. (2012). Numerical analysis of a modified evacuated tubes solar collector. International Conference on Renewable Energies and Power Quality (ICREPQ'12).

[86] Singh, R.V., Kumar, S., Hasan, M.M., Khan, M.E., & Tiwari, G.N. (2013). Performance of a solar still integrated with evacuated tube collector in natural mode. Desalination, 318, 25–33.

[87] Sampathkumar, K., Arjun, T.V., & Senthikumar, P. (2013). The experimental investigation of a solar still coupled with an evacuated tube collector. Energy Sources, 35(3), 261–270.

[88] Kumar, S., Dubey, A., & Tiwari, G.N. (2014). A solar still augmented with an evacuated tube collector in forced mode. Desalination, 347, 15–24.

[89] Panchal, H.N., & Awasthi, A. (2016). Theoretical modelling and experimental analysis of solar still integrated with evacuated tubes. Heat and Mass Transfer, 53, 1943–1955.

[90] Yari, M., Mazareh, A.E., & Mehr, A.S. (2016). A novel cogeneration system for sustainable water and power production by integration of a solar still and PV module. Desalination, 398, 1–11.

[91] Patel, J., Markam, B.K., & Maiti, S. (2019). Potable water by solar thermal distillation in solar salt works and performance enhancement by integrating with evacuated tubes. Solar Energy, 188, 561–572.

[92] Jowzi, M., Veysi, F., & Sadeghi, G. (2019). Experimental and Numerical Investigations on the Thermal Performance of a Modified Evacuated Tube Solar Collector: Effect of the Bypass Tube. Solar Energy, 183, 725–737.

[93] Tiwari, A.K., & Tiwari, G.N. (2005). Effect of the condensing cover slope on internal heat and mass transfer in distillation: an indoor simulation. Desalination, 180(1), 73-88.

[94] Kumar, S., & Tiwari, G.N. (1996). Estimation of convective mass transfer in solar distillation system. Solar Energy, 57(6), 459–464.

[95] Sartori, E. (1996). Solar still versus solar evaporator: a comparative study between their thermal behaviors. Solar Energy, 56(2), 199–206.

[96] Singh, G., Kumar, S., & Tiwari, G.N. (2011). Design, Fabrication and Performance Evaluation of a Hybrid Photovoltaic Thermal (PVT) double slope active solar still. Desalination, 277, 399–406.

[97] Budihardjo, I., Morrison, G.L., & Behnia, M. (2007). Natural circulation flow through water-in-glass evacuated tube solar collector. Solar Energy, 81(12), 1460–1472.

[98] Duffie, J.A., & Beckman, W.A. (2006). Solar engineering of thermal processes. New Jersey: Hoboken- Wiley.

[99] Kumar, S., & Tiwari, G.N. (2011). Analytical expression for instantaneous exergy efficiency of a shallow basin passive solar still. International Journal of Thermal Sciences, 50(12), 2543–2549.

[100] Sukhatme, S.P. (1985). Solar Energy: Principal of thermal energy collection, Tata McGraw Hill, New Delhi.

[101] Shah, L.J., & Furbo, S. (2004). Vertical evacuated tubular-collectors utilizing solar radiation from all directions. Applied Energy, 78, 371–395.

[102] Hedayati-Mehdiabad, E., Sarhadd, F., & Sobhnamayan, F. (2020). Exergy performance evaluation of a basin-type double-slope solar still equipped with phase-change material and PV/T collector. Renewable Energy, 145, 2409-2425.

[102] Cooper, P.I. (1972). The maximum efficiency of single-effect solar stills. Solar Energy, 15, 205-217.

[103] Rosen, M.A., & Dincer, I. (2003). Exergy methods for assessing and comparing thermal storage systems. International Journal of Energy Research, 27(4), 415-430.

[104] Dincer, I. (2002). The role of exergy in energy policy making. Energy Policy, 30(2), 137–149.

[105] Fujisawa, T., & Tani, T. (1997). Annual exergy evaluation on photovoltaic-thermal hybrid Collector. Solar Energy Materials and Solar Cells, 47(1-4), 135–148.

[106] Lourdes, G.R., & Carlos, G.C. (2001). Exergy analysis of the SOL-14 plant. Desalination, 137(1-3), 251–258.

[107] Sow, O., Siroux, M., & Desmet, B. (2005). Energetic and exergetic analysis of a triple effect distiller driven by solar energy. Desalination, 174(3), 277–286.

[108] Hepbasli, A. (2008). A key review on exegetic analysis and assessment of renewable energy sources for sustainable future. Renewable and Sustainable Energy Reviews, 12, 593–661.

[109] Torchia-Nunez, J.C., Porta-Gandara, M.A., & Cervantes-de Gortari, J.A. (2008). Exergy analysis of a passive solar still. Renewable Energy, 33(4), 608–616.

[110] Ranjan, K.R., Kaushik, S.C., & Panwar, N.L. (2016). Energy and exergy analysis of passive solar distillation systems. International Journal of Low-Carbon Technologies, 11(2), 211–221.

[111] Deniz, E. (2016). Energy and exergy analysis of flat plate solar collector–assisted active solar distillation system. Desalination and Water Treatment, 57(51), 24313–24321.

[112] Patela, R. (2003). Exergy of undiluted thermal radiation. Solar Energy, 74(6), 469–488.

[113] Jafarkazemi, F., Ahmadifard, E., & Abdi, H. (2016). Energy and exergy efficiency of heat pipe evacuated tube solar collectors. International Journal of Thermal Sciences, 20(1), 327-335.

[114] Sethi, A.K., & Dwivedi, V.K. (2013). Exergy analysis of double slope active solar still under forced circulation mode. Desalination and Water Treatment. 51(42), 7394-7400.

APPENDIX

Thermophysical properties can be estimated as [86];

$$c_w = 4226 - 3.224T + 0.057T^2 - 0.0002656T^3 \quad \text{(A-1)}$$

$$L = 2.506 \times 10^6 - 3.639 \times 10^3 T + 0.2678T^2 - 8.103 \times 10^{-3} T^3 - 2.079 \times 10^{-5}\, T^4 \quad \text{(A-2)}$$

$$p_{gi} = \exp\left(25.317 - \frac{5144}{T_{gi}+273}\right) \quad \text{(A-3)}$$

$$p_{sw} = \exp\left(25.317 - \frac{5144}{T_{sw}+273}\right) \quad \text{(A-4)}$$

Internal h.t.c. can be estimated as [68];

$$h_{cw} = 0.884\left[\left(T_{sw} - T_{gi}\right) + \frac{\left(P_{sw} - P_{gi}\right)\left(T_{sw}+273\right)}{268.9\times10^3 - P_{sw}}\right]^{\frac{1}{3}} \quad \text{(A-5)}$$

$$h_{ew} = 0.016273 \times h_{cw} \times \frac{\left(P_{sw} - P_{gi}\right)}{\left(T_{sw} - T_{gi}\right)} \quad \text{(A-6)}$$

$$h_{rw} = \varepsilon_{eff}.\sigma\left[(T_{sw}+273)^2 + \left(T_{gi}+273\right)^2\right]\left[T_{sw} + T_{gi} + 546\right] \quad \text{(A-7)}$$

$h_{1w,E} = h_{cw,E} + h_{ew,E} + h_{rw,E}$, $h_{ba} = [L_b/K_b + 1/2.8]^{-1}$, $h_{kg} = k_g/l_g$ and $h_b = k_b/l_b$

$$\varepsilon_{eff} = \left[\frac{1}{\varepsilon_g} + \frac{1}{\varepsilon_w} - 1\right]^{-1}$$

The overall external h.t.c from the top glass surface, the bottom of the basin or other such surfaces can be expressed as [117];

$$h_{1gE} = h_{1gW} = 5.7 + 3.8V_a \quad \text{(A-8)}$$

and radiative h.t.c. between east and west surfaces can be expressed as;

$$h_{r,EW} = 0.34\sigma\left[\left(T_{gi,E}+273\right)^2 + \left(T_{gi,W}+273\right)^2\right]\left[T_{gi,E} + T_{gi,W} + 256\right]$$

LIST OF PUBLICATIONS

The present research work has been reported in the following international publications/ communications;

1. High temperature distillation using N-parallel evacuated tube collector integrated with double slope solar still in force mode, **Journal of Thermal Science and Engineering Applications, ASME** (Accepted, https://doi.org/10.1115/1.4047941).
2. Energetic and Exergetic study of dual slope solar still coupled with evacuated tube collector under forced mode, **Journal of Thermal Engineering, Yildiz Technical University Press** (Under review).